THEORETICAL INVESTIGATION OF MOLECULE

ADSORPTION AND DISSOCIATION MECHANISMS

ON THE SILICON SURFACE

By

QING ZHU

Bachelor of Materials Science and Engineering
University of Science and Technology of China
Hefei, China
2005

Submitted to the Faculty of the
Graduate College of the
Oklahoma State University
in partial fulfillment of
the requirements for
the Degree of
DOCTOR OF PHILOSOPHY
December, 2009

THEORETICAL INVESTIGATION OF MOELULE

ADSORPTION AND DISSOCIATION MECHANISMS

ON THE SILICON SURFACE

Dissertation Approved:

Dr. N. Materer
_____
Dissertation Adviser

Dr. J. Gelder
_____

Dr. A. Apblett
_____

Dr. J. White
_____

Dr. J. Mintmire
_____

A. Gordon Emslie
_____
Dean of the Graduate College

ACKNOWLEDGMENTS

TABLE OF CONTENTS

LIST OF SYMBOLS AND ABBREVIATIONS

h	Planck's constant
H_{SOC}	Spin-Orbit Coupling coefficient
ΔF	the slope difference of two different Potential Energy Surfaces
μ	reduced mass
P_{sh}	spin crossing probability
k	rate constant
k_b	Boltzmann's constant
HF	Hartree-Fock
RHF	Restricted Hartree-Fock
UHF	Unrestricted Hartree-Fock
ROHF	Restricted Open-shell Hartree-Fock
DFT	Density Functional Theorem
MP	Møller–Plesset
MP2	Møller–Plesset second-order Perturbation
CC	Coupled Cluster
CCSD	Coupled Cluster with Singly and Doubly excitation
CISD	Configuration Interaction with Singly and Doubly excitation
SCF	Self Consistent Field
MCSCF	Multi-Configurational Self Consistent Field

CASSCF	Complete Active Space Self Consistent Field
MRMP	Multi-Reference Perturbation
MRMP2	Multi-Reference Moller-Plesset second-order Perturbation
DMC	Diffusion Monte Carlo
B3LYP	Becke's 3-parameter nonlocal-exchange functional with the correlation functional of Lee-Yang-Parr
UPS	Ultraviolet Photoelectron Spectroscopy
XPS	X-ray Photoelectron Spectroscopy
STM	Scanning Tunneling Microscopy
AES	Auger Electron Spectroscopy
HREELES	High Resolution Electron Energy Loss Spectroscopy
NEXAFS	Near-Edge X-ray Absorption Fine Structure
QCP	Quantum Capping Potential
Si_9H_{12}	Si single dimer cluster
$Si_{15}H_{16}$	Si double dimer cluster
$Si_{21}H_{20}$	Si triple dimer cluster
$Si_{33}H_{28}$	Si five dimer cluster
$Si_{23}H_{24}$	Si single dimer V-trench cluster
$Si_{39}H_{32}$	Si double dimer V-trench cluster
$Si_{55}H_{40}$	Si triple dimer V-trench cluster
TS	Transition State
Inter	Intermediate structures
TST	Transition State Theory

PES	Potential Energy Surfaces
SOC	Spin-Orbit Coupling
MECP	Minimum Energy Crossing Point
NOON	Natural Orbital Occupation Numbers
HOMO	Highest Occupied Molecule Orbital
LUMO	Lowest Unoccupied Molecule Orbital
EA	Electron Affinity
IMOMM	Integrated Molecular Orbital Molecular Mechanics
SIMOMM	Surface Integrated Molecular Orbital Molecular Mechanics
IRC	Internal Reaction Coordinate
QM	Quantum Mechanical
MM	Molecular Mechanical
LSCF	Local Self Consistent Field
GHO	Generalized Hybrid Orbital
ECP	Effective Core Potential

LIST OF TABLES

LIST OF FIGURES

CHAPTER I

Introduction to the Silicon Surface Chemistry

Silicon is one of the most important materials in the modern semiconductor industry. In the past 60 years, there has been great development in the manufacture technology of the silicon devices. Upon approaching the limitation of the Moore's law [1], the understanding of the silicon surface chemistry is especially important on further improving the silicon manufacture technology.

Silicon (100) surface is one of the most studied subjects in the silicon surface chemistry field due to its high chemical reactivity. Once cut through the (100) plan of the silicon crystal, each silicon atoms on the Si(100) surface is only bonded to another two under layer silicon atoms through two Si-Si σ bonds, and two valence electrons are left unsatisfied. Thus this first obtained surface has very high energy and is unstable. It quickly goes through a surface reconstruction process, in which every two surface silicon atoms pair with each other and form a two atom dimer. After this "dimerization" process, one obtains the Si(100)-2x1 reconstructed surface. Experiment measurement indicates the bond distance between the silicon dimer atoms equals 2.26 Å [2], which is shorter than the Si-Si single bond length of 2.35 Å and lies within the bond length range of 2.14-2.29 Å for disilene molecules [3]. So the bond between silicon dimer atoms is generally recognized

(a)

(b)

(c)
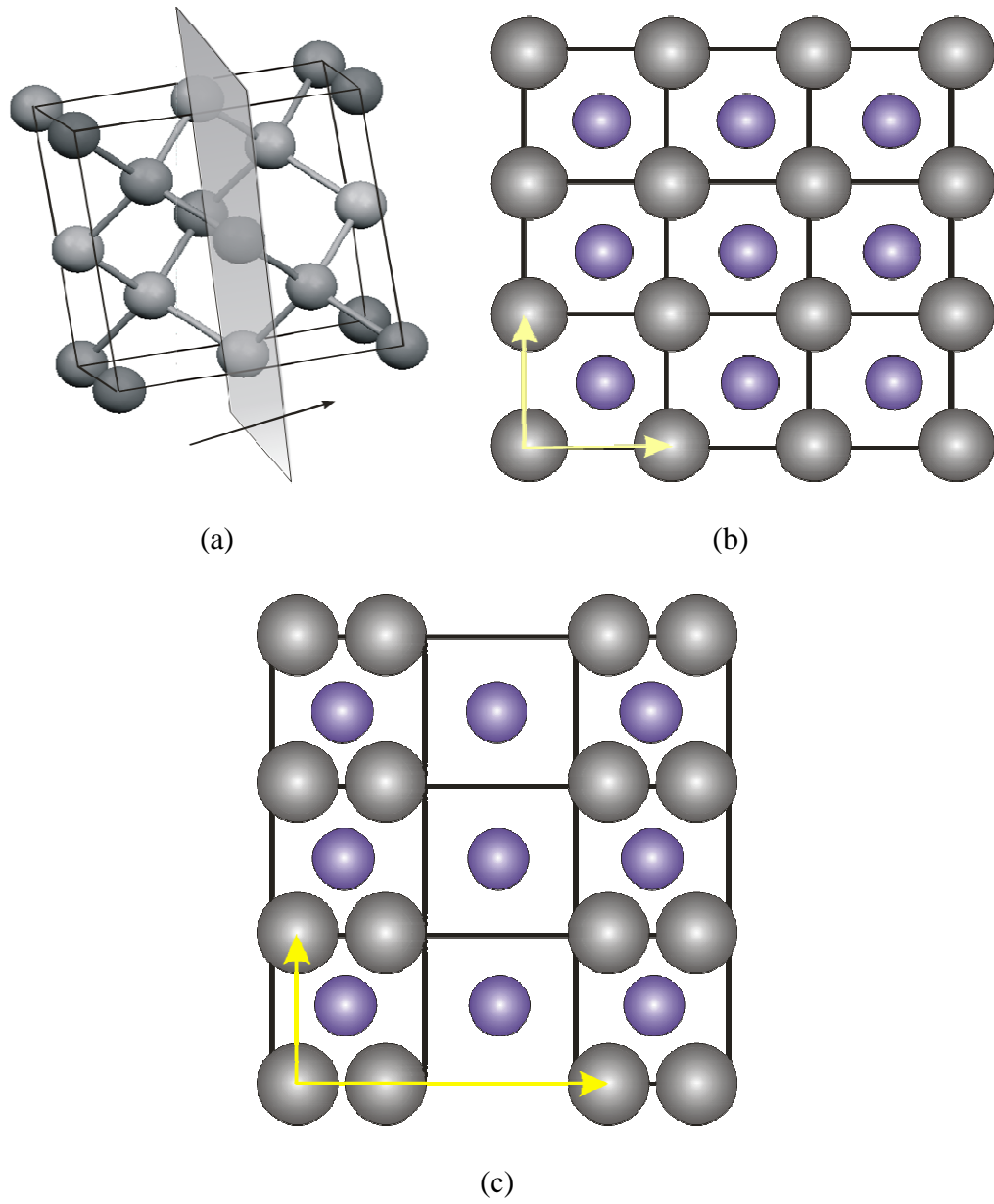
Figure I-1. Sketch of (a) the silicon crystal structure and the (100) plan, (b) Si(100) surface before the surface reconstruction and (c) Si(100)-2x1 reconstructed surface.
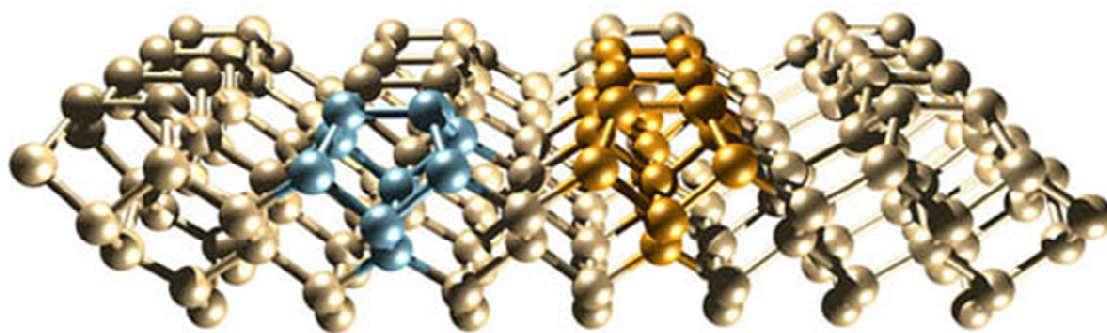
Figure I-2. Illustration of the Si(100)-2x1 reconstructed surface. Figure adapted from

http://chemeng.stanford.edu/html/musgrave.html

as Si-Si double bond. However, it has been pointed out that the silicon dimers have multi-configuration character[4-9], which means the bond between silicon dimer atoms is not pure Si-Si double bond. Instead, the p electrons in the silicon dimer atoms have both π bonding and diradical characters, and the bond between silicon dimer atoms is between a Si-Si single bond and double bond. There have been debate on whether the Si(100)-2x1 reconstructed surface is symmetrical or buckled too. Both experimental and theoretical studies have suggested controversial conclusions [4-22].

There are two common approaches to model the Si(100) surface in theoretical studies. The first one is the slab models, in which a super cell is chosen and repeated under periodic boundary conditions. Slab models reproduce large areas of surface structures and have very small edge effects. However, slab models can encounter sizable errors when low-coverage surface adsorption process takes place unless a relative large super cell is chosen, due to the interactions between the adsorbates and the neighbor cells [23]. Also, since slab models include large number of silicon atoms, only low cost computational methods, such as Hartree-Fock (HF) or density functional theorem (DFT) methods are applicable to the slab models. In addition, the current available periodic DFT methods (i.e. Perdew-Wang 1991 [24]) do not include a portion of the exact exchange which eliminates the accuracy of the slab models [23]. Another approach to model the Si(100) surface is the silicon dimer cluster models, in which a finite size of silicon atoms are chosen to construct a cluster module that represents the silicon dimer structures. Silicon dimer cluster models include relatively smaller amount of atoms. High level a,b-initio methods, such as Møller–Plesset perturbation theory (MP), coupled cluster method (CC),
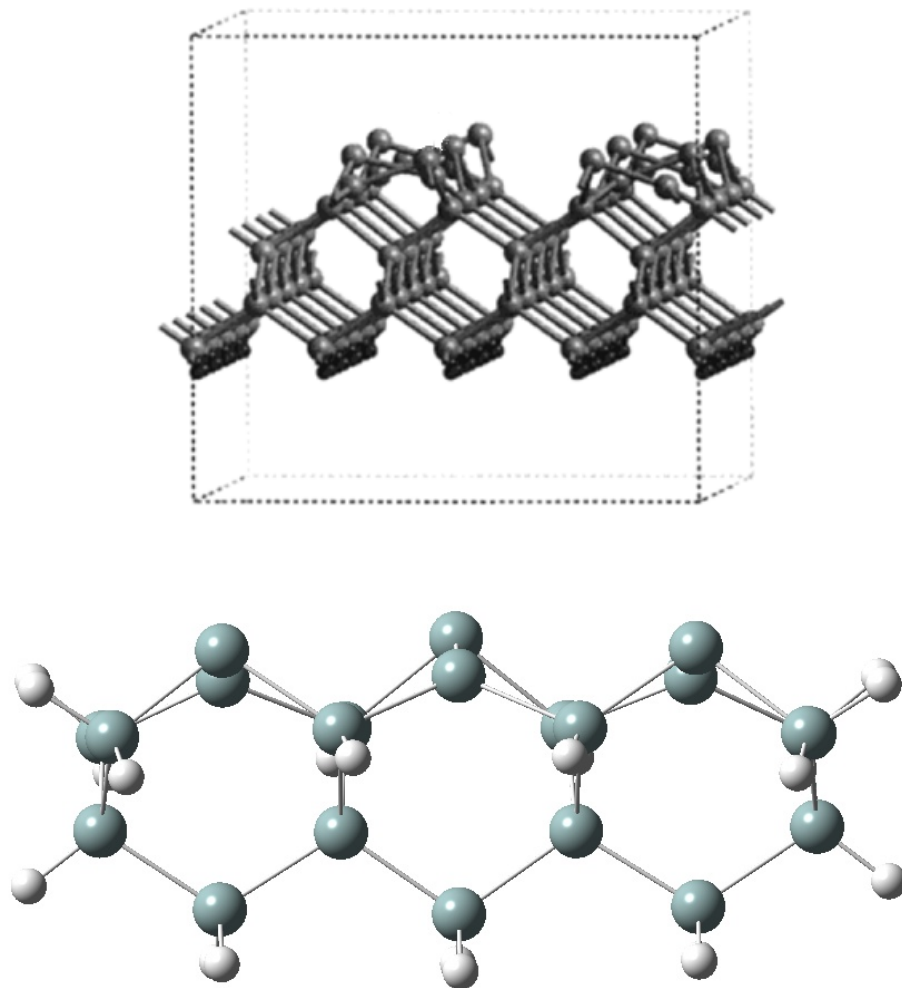
Figure I-3. (a) a super cell used in the silicon slab models and (b) a silicon triplet dimer silicon cluster model. Figure (a) adapted and modified from reference [23].

as well as hybrid functional DFT that includes a portion of the exact exchange are applicable the silicon dimer cluster models. The major drawback of the silicon dimer cluster models is that since only small areas of the Si(100) surface are represented, there is relatively larger edge effect for this model. Also, full geometry optimization of silicon dimer cluster models with aborbates on them may result with unphysical distorted dimer cluster configurations. Once the unphysical distortion happens, it usually requires one to constrain a few layers of the silicon atoms into the positions as in bulk structure, which may not be adequate if the surface adsorption requires a certain level of crystal relaxation.

In this dissertation, we focus on the theoretical investigation of the silicon surface chemistry. The adsorption of small organic molecules on the Si(100) surface, including the chlorine cyanide (ClCN), benzene (C_6H_6) and phenanthrene ($C_{14}H_{10}$), have been conducted by the means of first principle density functional theorem, a,b-initio theories, or both of them. We have only adapted the silicon dimer cluster models to perform the surface adsorption modeling as the high level a,b-initio theories are only applicable through this model. Ultraviolet photoelectron spectroscopy (UPS) and X-ray photoelectron spectroscopy (XPS) studies[25,26] have shown that upon annealing to room temperature, the cyanogen halides (XCN, where X = I, Br, Cl) can go through molecule dissociation process after adsorbing on the Si(100) surface. The earlier studied dissociation mechanism of ClCN on Si(100) surface under a single dimer cluster model indicates that intermediate structures should be seen during the dissociation process, which is in consistent with the experimental observations [25,26]. In Chapter II, we have

6

carried out more detailed theoretical calculations of the ClCN dissociation process using

larger silicon dimer cluster models. We have found that silicon multi dimer cluster

models can provide reaction pathways that are more feasible than the one from using the

silicon single dimer cluster model, and the multi dimer reaction pathways are able to

explain the lack of the observation of dissociation intermediate structures. The adsorption

and dissociation mechanism of the benzene molecule on the Si(100) surface have been

studied in the Chapter IV. There have been many experimental and theoretical studies of

the intact chemisorption of benzene molecule on the Si(100) surface in the past [27-44 45].

We have obtained adsorption configurations and adsorption energies of the intact

chemisorbed benzene molecule on the Si(100) surface that are consistent with several

previous studies. Scanning tunneling microscopy (STM) [35], XPS and temperature-

programmed desorption (TPD) experiments [33,36] have shown that halogenated benzene

can go through dissociation process upon adsorption. A recent theoretical study of the

benzene adsorption on Si(100) surface has suggested that the benzene can go through

dissociation process at a cost of moderate amount activation energy [27], which puzzles us

because no experimental observation of benzene dissociation on Si(100) surface has been

reported yet. Thus we have performed more careful examination of the dissociation

process of benzene molecule on the Si(100) surface. We have found that the spin crossing

process has to be involved during the benzene dissociation process and a much higher

activation barrier has been predicted from our calculations. The detailed studies of the

spin crossing process for a silicon single dimer cluster have been conducted back in

Chapter III. Our results shows that the spin crossing process barrier for the bare silicon

dimer cluster is moderate and thermodynamic equilibrium between the singlet ground

state and the triple excited state of the silicon dimer cluster can be established at room temperature. Non-negligible population of triplet silicon dimer cluster will present at the Si(100) surface at high temperature. In Chapter V, a short study of the phenanthrene molecule adsorption and dissociation on Si(100) surface has been conducted. It is found that the adsorption and dissociation of phenanthrene molecule on Si(100) surface takes a fashion that is analogous to that of the benzene molecule, except additional geometrical selection rules have been observed for phenanthrene adsorption. Finally, in Chapter VI, we have tested the application of a quantum capping potential (QCP) method on building the silicon dimer cluster. Using single dimer cluster, the QCP method has shown promising results for the hydrogen terminated cluster model. However, for the bare cluster model, it has failed on reproduction the electronic property of larger size silicon dimer cluster models.

CHAPTER II

Dissociation Pathways for ClCN on Si (100)-(2x1) Modeled by Multiple Si-Dimer

Clusters

A. INTRODUCTION

The adsorption of organic molecules to fine-tune the chemical and physical properties of

group IV semiconductor surfaces has applications in chemical sensors, biological

recognition, and molecular and optical electronics.[46-48] The ability to functionalize the

Si(100) surface is particularly important in order to create surfaces that are compatible, in

principle, with materials currently employed in device manufacturing. Towards this end,

a recent review addresses the experimental and theoretical understanding of chemical

manipulations of organic molecules on silicon surfaces.[49] From the perspective of

chemical reactivity of the Si(100) surface, Si-dimers are the important structural motif

that dominates the chemistry.[50] These Si-dimer atoms play a critical role in the

adsorption chemistry of nitrogen containing organic compounds.[51] Relevant to this work,

the adsorption and decomposition of N and O containing compounds on the Si(100)

surface[9] and the surface chemistry of nitriles on Si(100)-2x1 and Ge(100) surfaces[52] have

been reviewed.

In this chapter, we investigate both the adsorption and dissociation pathways across adjacent Si-dimers and across two Si-dimer rows for ClCN on the Si(100) surface using multiple Si-dimer clusters. The adsorption and subsequent thermal chemistry of the cyanogen halides (XCN, where X = I, Br, Cl) have been investigated using ultraviolet photoelectron spectroscopy (UPS) and X-ray photoelectron spectroscopy (XPS).[25,26] UPS measurements show that the CN triple bond of the XCN species remains intact upon adsorption. XPS analysis of the C 1s photoelectron peak following low XCN exposures at low temperatures (100 K) indicates that some molecular adsorption occurs. Upon annealing to room temperature, the XC bond of the molecularly adsorbed XCN species dissociates and the adsorbed species rearranges to form a CN group bound through the C atom and an adsorbed Cl atom. A single-dimer cluster has been previously utilized to model the adsorption and decomposition of XCN.[26,53] Although the lowest energy reaction product, an adsorbed atomic halide and a molecular CN group, is in agreement with experimental results,[25,26] the activation energies computed along the single-dimer pathways suggest that at least one intermediate structure should have been observed.

One possible explanation is that additional reaction pathways with multiple Si-dimers clusters can provide alternative decomposition pathways with lower activations energies than those found in the single-dimer studies.[26,53] High resolution scanning tunneling microscopy (STM) studies of organic adsorption have demonstrated the importance of multiple Si-dimer interactions with adsorbates. For example, analysis of STM images for acetylene shows evidence that this species can adsorb across two adjacent Si-dimers, in addition to the traditional adsorption geometry across a single dimer.[54] In addition, STM

images of 1,3-cyclohexadiene,[55,56] maleic anhydride,[57] and benzene[58] adsorbed on Si(100) show a distribution of different bonding sites involving multiple Si-dimers both in the same row and across rows.

M. C. Lin and coworkers have experimentally and computationally studied hydrogen cyanide (HCN) and cyanogen (C_2N_2) adsorption and decomposition on the Si(100) and Si(111) surfaces.[59-63] Bu and Lin have also studied a similar compound, s-triazine (($HCN)_3$), on the Si(100) surface.[64] For HCN, the transition state barrier for dissociation which results in atomic H and molecular CN adsorbed on adjacent Si-dimers within the same row is lower than that found for the cleavage across one Si-dimer bond.[59] Adsorption and dissociation pathways of C_2N_2 and N_2H_4 on double-dimer clusters are also found to have slightly lower activation barriers than the single-dimer based pathways.[63,65] In addition to reactions across adjacent Si-dimers, cross Si-dimer row mechanisms are also possible. One relevant example is the decomposition of chloromethane which decomposes into a final geometry with the CH_3 group and the Cl atom adsorbed on different Si-dimer rows.[66] Similar cross Si-dimer row dissociations are seen for chlorinated benzenes[34], glycine,[67] and propenyl alcohol.[68] To illustrate the potential complexity, computational studies of the decomposition of acrylonitrile have found intermediates spanning two adjacent Si-dimers in the same row and spanning across two Si-dimers rows.[69,70]

B. COMPUTATIONAL PROCEDURE

The Si(100) surface is represented using clusters containing 9 to 55 Si atoms with the edges capped by H atoms. Details of each cluster model are described in the appropriate

a) Single-Dimer Cluster   b) Double-Dimer Cluster
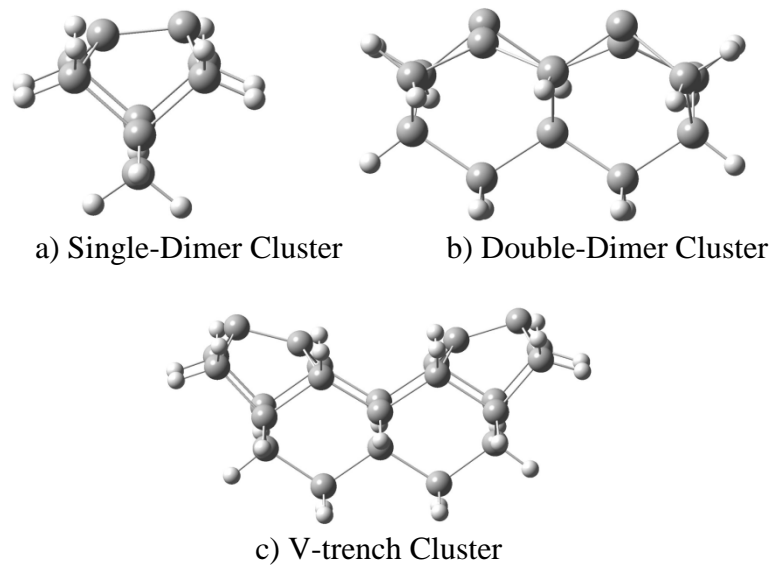
c) V-trench Cluster

Figure II-1. The (a) single-dimer (Si_9H_{12}), (b) double-dimer ($Si_{15}H_{16}$) and (c) V-trench ($Si_{23}H_{24}$) clusters used to model the Si(100) surface. The atoms are ◗ hydrogen, ● nitrogen, ◗ carbon, ● silicon and ● chlorine.

sections below. Energy calculations, geometry optimizations and frequency calculations are performed using the hybrid density functional method that includes Becke's 3-parameter nonlocal-exchange functional[71] with the correlation functional of Lee-Yang-Parr, B3LYP.[72] The 6-31G(d) all-electron split-valence basis set,[73] which includes the polarization *d*-function on non-hydrogen atoms, was employed for calculations. Both Gaussian 98 and 03[74] are utilized with identical results. The reported adsorption energy is defined as the difference between the total electronic energy of the adsorption model and the isolated molecule and cluster. All energies are reported without zero-point corrections. Except when noted, frequency calculations confirm that the stable geometries have no imaginary vibrational frequencies. All the transition states have only one imaginary normal mode, except when explicitly stated in the text. All connections between stable structures and their transition states are confirmed by internal reaction coordinates calculations. Partial optimization may have been used to assist the initial optimization of the stable structures. However, unless explicitly stated in the text, the reported energies are from total energy optimizations performed without any geometrical constraints.

C. RESULTS AND DISCUSSION

C.1. Reaction Pathways on a Single Si-Dimer

Kadossov *et al.* has previously investigated the adsorption and decomposition of ClCN using single-dimer models.[26,53] Figure 1a shows the bare single-dimer cluster, while Figure 2 shows the resulting five stable geometries formed by the reaction of ClCN with this cluster. The double-dimer versions (Figure 1b) of the single-dimer models are

13

a) ClCN1   b) ClCN2   c) ClCN3

d) SiNC1   e) SiCN1
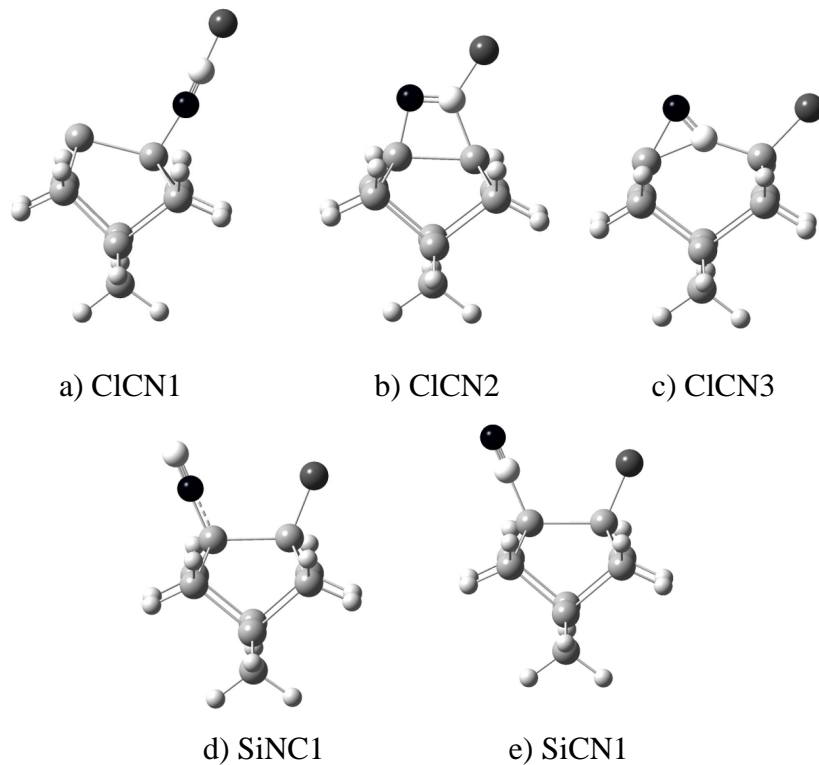
Figure II-2. ClCN adsorption models on the Si single-dimer cluster: (a) ClCN adsorbed on Si(100) surface in an end-on position. (b) ClCN adsorbed in a side-on position. (c) Dissociated species with Cl and CN adsorbed in a side-on position with both the Cl-C and the silicon dimer bonds broken. (d) Dissociated Cl and NC. (e) Dissociated Cl and CN. The atoms are ● hydrogen, ● nitrogen, ● carbon, ● silicon and ● chlorine.

created by adding one additional Si-dimer to one side of the single-dimer cluster. The addition of a Si-dimer to the other side of the single-dimer clusters results in a non-superimposable mirror image with an identical total energy. The triple-dimer variety is created by adding additional Si-dimers to both sides of a single-dimer cluster. Since the single-dimer based decomposition reaction takes place only on the center Si-dimer, these triple-dimer clusters are symmetrical.

Figure 3 shows the reaction pathways for the adsorption and dissociation of ClCN into adsorbed atomic Cl and molecular CN on the single-dimer cluster. The solid line is the lowest energy pathway and the activation energies in kJ/mol are given in parentheses next to each transition state label. The initial dative bonded structure (ClCN1) is bounded by a square box in Figure 3 and is formed from the gas phase absorption of ClCN onto the the electrophylic (buckled-down) Si-dimer atom. The species bounded by an oval are consistent with experimental observation of the final room-temperature decomposition product.[25,26]

Table 1 contains the adsorption energies computed for these species on the single-, double- and triple-dimer clusters. These stable structures are computed without geometrical constraints and contain no imaginary frequencies. With the exception of the dative bonded ClCN1 geometry, the adsorption energies between these stable structures are approximately independent of the cluster size. The single- and triple-dimer energies are within 5% on average after excluding ClCN1 and the two transition states, TS1 and TS2, originating from this geometry. The relatively large differences in adsorption energy for the dative bonded ClCN1 geometry and its associated transition states is

15
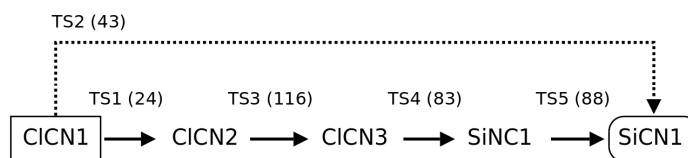
Figure II-3. The single-dimer adsorption and decomposition pathways for ClCN. The solid line is the lowest energy pathway and the activation energies in kJ/mol are given in parentheses next to each transition state label. The TS3 transition state only exists on the single-dimer cluster. The initial dative-bonded structure (ClCN1) is bounded by a square while the final structure consistent with the experimental data is bounded by an oval.

Model	1D	2D	3D
ClCN1	-44.4	-62.8	-72.5
ClCN2	-202.0	-198.2	-189.9
ClCN3	-289.1	-279.8	-266.0
SiNC1	-365.0	-365.4	-359.0
SiCN1	-397.7	-397.4	-390.3
TS1	-20.9	-33.2	-36.8
TS2	-1.2	-2.5	2.9
TS3	-86.2	-83.9	-76.3
TS4	-206.6	-212.2	-209.9
TS5	-276.9	-277.7	-268.9

Table II-1. Calculated B3LYP/6-31G(d) adsorption and transition state energies (kJ/mol) for the single-dimer based adsorption models on single-dimer (1D), double-dimer (2D) and triple-dimer (3D) clusters. These structures are illustrated for a single-dimer cluster in Figure 1. All structures are computed without geometrical constraints and contain no imaginary frequencies. All transitions states, with the exception of TS3 for the 2D and 3D models (see text), are computed without geometrical constraints and contain one imaginary frequency.

attributed to the greater degree of delocalization of the electrons in the weak dative bond in the larger clusters, similar to that observed in an ammonia adsorption study using clusters of different sizes.[75] The transition state energies are also listed in Table 1. Except when noted, the transitions states are optimized without geometrical constraints and contain one imaginary frequency. In addition, the connection between each pair of stable structures and the respective transition state is confirmed by internal reaction coordinate calculations.

There are two different reaction pathways (Figure 3) starting from absorbed ClCN (ClCN1). The single-dimer activation energy (23.5 kJ/mol) for the first pathway, over transition state TS1 (solid line in Figure 3), is 20 kJ/mol less than that for the second pathway (43.2 kJ/mol) over TS2 (dashed line in Figure 3). On the larger Si-dimer clusters, TS1 becomes increasing favorable with respect to TS2. In addition, the TS2 activation energy is close to the desorption energy of ClCN. For the triple-dimer cluster (see Table 2) this activation energy exceeds the desorption energy, implying that desorption is favored over a possible transition over the TS2 barrier. Thus, the dissociation of ClCN on the single-dimer clusters is expected to take place along the pathway associated with TS1 instead of one associated with TS2.

The TS1 pathway starts with a physisorbed ClCN (ClCN1) species in end-on geometry with a dative bond through the N atom to an electrophylic (buckled-down) Si-dimer atom. There is no barrier for the formation of this initial species from the gas phase. This structure can then react across the Si-dimer bond (TS1) to form a side-on intermediate (ClCN2). After which, the side-on intermediate can further react (TS3),

with relatively large activation barrier of 115.8 kJ/mol, to form a broken-dimer geometry (ClCN3) in which the CCl bond breaks and the C end of the CN group inserts into the Si-dimer bond. The insertion intermediate (ClCN3) rearranges (TS4) to form an adsorbed atomic halide and an adsorbed NC species (SiNC1). Once SiCN1 formed, the final step is the isomerization into the more stable CN geometry where the C is bound to the Si-dimer atom (SiCN1).

This insertion intermediate (ClCN3), discovered by internal reaction coordinates calculations started in the forward direction from TS3 and the reverse direction of TS4, is surprising. On larger clusters (see below) the TS3 transition state, which leads to the insertion intermediate (ClCN3), does not exist and no insertion intermediate is required. Since the aim of this paper is to examine the decomposition of ClCN into the experimentally observed room temperature products, absorbed atom Cl and molecular CN, higher energy pathways leading to the complete decomposition of the CN group into additional SiC and SiN insertion products are not considered. Insertion products can result in unrealistic deformation of the cluster and require the use of constraints in the geometry optimization step. Adsorption energy for unconstrained and constrained insertion products were examined by Rodriguez-Reyes *et al.* for ammonia decomposition in Si(100).[76,77] For insertion reactions that result in minimal deformation of the single-dimer cluster, the difference between the unconstrained and constrained optimizations on the adsorption energy are found to be minimal (< 1%) for the symmetrical N insertion into the Si-Dimer (B1 and B2 models[77]). For ClCN3, which involves the insertion of a C atom into the Si-Dimer bond, the energy difference is also less than 1%. This result is

consistent with the observation of no unrealistic deformations of the bottom layers of the Si cluster for ClCN3.

Experimentally, the dative bonded ClCN molecule is observed on the Si(100) surface at 80 K. [25,26] Upon moderate heating, ClCN completely dissociates and the products, Cl and CN adsorbed on Si(100) surface, are observed. XPS $1s$ binding energy of the C in the CN group indicate that the species is bound to the surface through the C atom.[25,26] Thus, both the ClCN1 and the SiCN1 single-dimer structures are observed experimentally. However, neither the ClCN2, ClCN3 nor the SiNC geometry is observed.[25,26] This result might be expected if the adsorbate (ClCN) utilizes its absorption energy to overcome the four transition state barriers. Starting from the gas phase absorption, at least 200 kJ/mol of energy is available to help the reaction across the 115.8 kJ/mol barrier of TS3. Since the dative bonded structures can be experimentally observed,[25,26] the energy used to overcome TS3 must come from the ClCN1 to ClCN2 reaction. In addition, some accommodation or energy loss to the substrate is expected. Thus, one might expect that at least one additional intermediate, for example the bridged ClCN2 species, would be experimentally observed if the dissociation of ClCN is constrained to follow only single-dimer based pathways.

Given the larger TS3 barrier, the critical step in the single-dimer based reaction pathway is the reaction of ClCN2 to form ClCN3. Computations using the larger double- and triple-dimer clusters cast some doubt on the existence of transition state TS3 on these larger clusters and, thus, on the real Si(100) surface. Optimization of TS3 on the double-dimer cluster required the Cl displacements to be constrained to a plane through the Si-

20

dimer on which the absorption occurs and the bridging CN group. Without this constraint, optimization on double-dimer clusters results in a new transition state geometry (TS6 in Section 2 below) that is incompatible with the single-dimer models. In this new transition state, the Cl atom tends to migrate towards the adjacent dimer. On the triple-dimer cluster, no additional geometry constraints are required due to the symmetry around the center Si-dimer. However, a second imaginary frequency with a displacement vector pointing along the dimer-row toward the adjacent Si-dimer atoms is observed. These results on the larger clusters indicate that Cl migration to an adjacent dimer pathway is more likely than the single-dimer pathway over TS3, which leads to the ClCN3 structure.

C.2. Reaction Pathways Across Two Adjacent Si-Dimers in the Same Row

The double-dimer cluster (Figure 1b) is utilized to examine reactions occurring across two adjacent Si-dimers in the same row. Figure 4 shows three additional stable geometries formed by the reaction of ClCN with a double-dimer cluster. ClCN4 is the dissociation product suggested by the optimization of TS3 on double- and triple-dimer clusters. SiNC2 and SiCN2 are two additional end-on products. For ClCN4, SiNC2 and SiCN2, additional structures can be generated by moving the Cl across the Si-dimer. These new species are denoted by the addition of a prime and are not shown in Figure 3. Of the three possible prime structures, only the SiCN2' model is required to describe the adsorption and decomposition of ClCN into adsorbed atomic Cl and molecular CN on thedouble-dimer clusters. The energies for these structures are listed in Table 2. All structures, with exception of SiCN2' (see below), are computed without geometrical

a) ClCN4   b) SiNC2   c) SiCN2
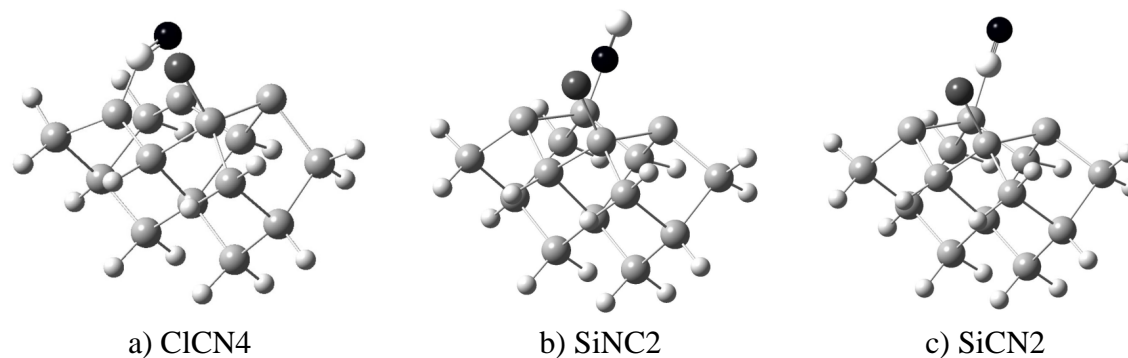
Figure II-4: ClCN adsorption models on the Si double-dimer cluster: (a) ClCN adsorbed in a side-on position. (b) Dissociated Cl and NC on adjacent Si-dimers. (c) Dissociated Cl and CN on the adjacent Si-dimer. The atoms are ⬤ hydrogen, ⬤ nitrogen, ⬤ carbon, ⬤ silicon and ⬤ chlorine.

constraints and contain no imaginary frequencies. The final geometries are carefully

compared to the bare double- or triple-dimer cluster to ensure that no unrealistic

distortions have occurred during the optimization. The transition state energies are also

listed in Table 2. All transitions states are optimized without geometrical constraints and

contain one imaginary frequency. The connection between each pair of stable structures

and the respective transition state are confirmed by internal reaction coordinates

calculations. Since many of the double-dimer structures have non-superimposable mirror

images with identical total energies, care must be taken to ensure that the transitions

states are computed between compatible symmetries.

Cluster size effects are explored using triple-dimer based double-dimer models

generated by adding an extra dimer to the right side (3D-R) or the left side (3D-L), with

respect to the origination of the clusters in Figure 4. Typically the 3D-R geometry has an

extra dimer added to the side containing the Cl atom while the 3D-L geometry has an

extra dimer added to the side containing the CN group. The adsorption energy

differences between the double-dimer and the two triple-dimer configurations (3D-R and

3D-L) are 4% or less with an average difference of less than 3%. For the transition

states, the adsorption energy differences between the double-dimer and the two triple-

dimer configurations are 5% or less with an average difference of less than 4%. The only

exceptions are TS6 and TS12, which differ by approximately 8%. Overall, the average

energy differences between all stable structures and transitions states are 3%, indicating

that cluster size effects on the resulting reaction pathways are minimal.

Figure 5 summarizes the reaction pathways for the adsorption and dissociation of ClCN

Model	2D	3D-R	3D-L
ClCN4	-284.3	-287.6	-275.0
SiNC2	-272.7	-284.5	-273.9
SiCN2	-304.9	-314.0	-304.8
SiCN2'	-334.6	-326.5	-330.4
TS6	-132.8	-143.0	-127.3
TS7	-269.8	-272.5	-262.5
TS8	-264.6	-258.3	-267.7
TS9	-268.0	-275.6	-281.0
TS10	-224.6	-229.4	-224.1
TS11	-236.5	-244.1	-249.9
TS12	-180.7	-195.5	-184.0

Table II-2. Calculated B3LYP/6-31G(d) adsorption and transition state energies (kJ/mol) for double-dimer based adsorption models on double-dimer (2D) and triple-dimer (3D-R and 3D-L) clusters. These structures are illustrated for a double-dimer cluster in Figure 3. All structures, with exception of SiCN2' (see text), are computed without geometrical constraints and contain no imaginary frequencies. All transitions states are optimized without geometrical constraints and contain one imaginary frequency.

into adsorbed atomic Cl and molecular CN pathways on the double-dimer cluster. The solid line is the lowest energy pathway and the activation energies in kJ/mol are given in parentheses next to each transition state label. The initial dative bonded structure (ClCN1) is bounded by a square box while the species bounded by an oval are consistent with experimental observation.[25,26] All pathways occurring across two adjacent Si-dimers start with ClCN adsorbing on the surface (ClCN1) through a dative bond and reacting across one Si-dimer to form a ClCN2 geometry. As suggested by the TS3 computations on the double- and triple-dimer clusters, the CCl bond can dissociate across the Si-dimer rows through TS6 to form a bond with adjacent Si-dimer forming ClCN4. On the double-dimers, this barrier is 65.4 kJ/mol or approximately 50 kJ/mol less than that found for the competing barrier over TS3 to form ClCN3. This value corresponds to a 40% reduction in the barrier energy. Assuming that the dative bonded structure fully accommodates with the surface, approximately 150 kJ/mol of energy is available to push the molecule over this 65.4 kJ/mol barrier and form ClCN4. Structures similar to ClCN2 should rapidly react, consistent with the experimental observation of no ClCN2 type intermediates.[25,26]

Once ClCN4 forms, the bridging CN group can stand up by breaking a SiC or a SiN bond. The adjacent Si-dimer pathway with the lowest activation barrier from ClCN4 involves the dissociation of the SiN bond to form a C bound CN species (SiCN2'). The activation barrier for this transition state (TS7) is only 14.5 kJ/mol. This barrier should be easily overcome to form a resulting final structure consistent with the experimental observations. For direct comparison with the single-dimer results, the lowest energy route to the SiCN1 geometry involves two Cl migrations. The Cl atom from the SiCN2'
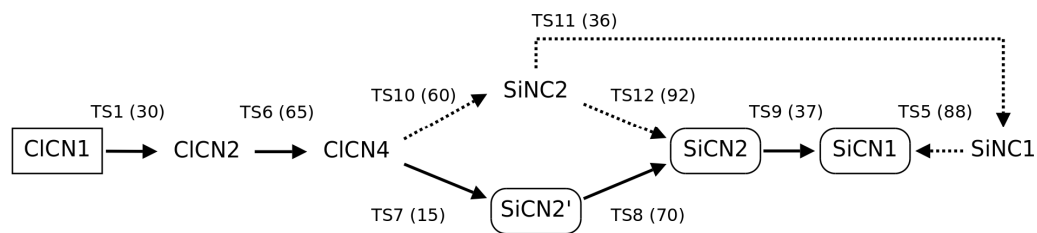
Figure II-5: The double-dimer adsorption and decomposition pathways for ClCN. The solid line is the lowest energy pathway and the activation energies in kJ/mol are given in parentheses next to each transition state label. The initial dative-bonded structure (ClCN1) is bounded by a square while the final structures consistent with the experimental data are bounded by an oval.

model first migrates across the Si-dimer through TS8 over a 70.0 kJ/mol barrier to form

SiCN2. Starting with the ClCN4 species shown in Figure 4a, the final SiCN2 will be the

mirror image of that shown in Figure 4c. To form SiCN1, another migration of the Cl

atom to the adjacent Si-dimer occurs via TS9 over a 36.9 kJ/mol barrier.

As mentioned above, the SiCN2' intermediate is unstable with respect to unconstrained

total energy optimizations. An unconstrained optimization leads to a highly deformed

configuration cluster on both the double- and triple-dimer clusters. The quoted energy

for SiCN2' is based on a total energy optimization with the Si atoms of the two bottom

layers frozen at clean double-dimer cluster positions. With this constraint, the resulting

final configuration contains an imaginary frequency corresponding to a cluster

deformation. One possible explanation is that steric repulsion of the CN and Cl species

placed on the same side of the cluster induces the bending of the dimer and results in the

appearance of an imaginary frequency in the constrained cluster. It is also possible that

stress-induced unfavorable interactions of the unsymmetrical substituted Si-dimer results

in lattice deformation. Regardless of the reason, the constrained cluster is expected to

correctly model an extended Si surface in which such deformations are extremely

unlikely. Thus, the SiCN2' type geometry is probable on the Si(100) surface and the

resulting reaction pathway is feasible.

There are two additional adjacent Si-dimer reaction pathways (dashed lines in Figure 5)

that start with the ClCN4 intermediate. Unlike the pathway discussed above involving

breaking a Si-N bond, these additional reaction pathways start with the dissociation of the

SiC bond to form an N bound CN species (SiNC2) through TS10 with a barrier of 59.7

kJ/mol. This barrier is larger than the 14.5 kJ/mol barrier to form SiCN2' and represents, assuming first order kinetics and similar pre-exponential factors, a process that is approximately 60 times less likely than that across TS7. After forming SiNC2, the pathway can continue with a Cl migration (dashed the line in Figure 5) to the adjacent Si-dimer bond through TS11 (36.2 kJ/mol barrier) to form SiNC1. SiNC1, as in the single-dimer pathway, can then isomerize over an 87.7 kJ/mol barrier (TS5) to form SiCN1. This isomerization barrier is similar to the 88.1 kJ/mol barrier found for the single-dimer cluster. Alternatively (see Figure 5), SiNC2 can first undergo an isomerization (TS12) over an 92.0 kJ/mol barrier to form the more stable C-bonded CN isomer represented by SiCN2. Next, the Cl atom can migrate to the adjacent Si-dimer bond through TS9 with a 36.9 kJ/mol barrier to form SiCN1. Both the SiCN1 and SiCN2 structures are consistent with experimental observations.[25,26]

We considered and discounted two additional possibilities for the dissociation of ClCN on double-dimer clusters. The first starts with the ClCN4 species and involves Cl migration across the Si-dimer bond to form ClCN4'. This process has a 214 kJ/mol barrier and, assuming first order kinetics and similar pre- exponential factors, is at least 10^6 times less likely than that across TS7. This significantly large barrier with respect to those over both TS10 and TS7 casts doubt on the feasibility of this pathway and it was not explored further. Another alternative possibility starts with ClCN absorbing on the surface (ClCN1) followed by a reaction across two adjacent Si-dimer to form the side-on intermediate that, unlike ClCN4 is bound across two Si atoms within a single Si-dimer (see Figure 4a). Reaction pathways involving adjacent Si-dimer have been computationally investigated on double-dimer clusters for the decomposition of C_2N_2.[63]

However, the CN group is significantly shorter than the distance from one N atom to either the other N atom or to the C atom bound to the other N in C_2N_2. In addition, when considering the possibility of a bridging CN between two adjacent Si-dimer in reference to the bridge structures determined after C_2H_2 and C_2H_4 absorption,[54,70,78-81] the shorter SiN and CN bond lengths need to be taken into account. On the clean double-dimer surfaces, the separation between two Si atoms on the adjacent Si-dimers is about 4.0 Å, almost two times the 2.3 Å distance between two Si atoms on the same Si-dimer. The average CN double bond is 1.3 Å,[82] while the SiC and SiN single bond lengths are 2.0 Å and 1.8 Å, respectively.[82] Assuming an ideally sp^2 hybridized C and N, the CN double bond length would have to exceed 2.0 Å. Optimization of this cross-dimer species results in severe distortion of the cluster as the optimization attempts to bring the two Si atoms on the different Si-dimers closer together to obtain a reasonable CN double-bond length. Further optimizations with the bottom Si atoms frozen at the positions found for the clean double-dimer results in a structure with unrealistic distortion in the first layer and a relatively small adsorption energy (-152.3 kJ/mol) when compared to the other geometries. Thus, this pathway was also deemed improbable and not explored further.

The SiCN2 to SiCN1 conversion (TS9) was discussed as occurring through Cl migration across two Si-dimers. An alternate mechanism involving the upright CN group diffusing across the two Si-dimers was considered. Transition states containing a bridging C or N over the Si-dimer could be found. However, internal reaction coordinates calculations indicate that these states lead to a bridging CN group, with C bonded to one Si on the Si-dimer and N bonded to the other one, on a highly distorted cluster for reasons discussed above. Thus, the large separation between Si atoms on the

adjacent Si-dimers precludes an upright CN group from migrating across two Si-dimer rows (SiCN2 to SiCN1). The conversion of SiCN2'to SiCN2 (TS8) was also discussed above as occurring through a Cl migration. For this transformation, an upright CN group diffusing across a Si-dimer should be considered. Although transition states containing a bridging C or N could be found, internal reaction coordinates calculations again indicate that these state also lead to a bridged CN intermediate. Since the average bond energies of the SiC (435 kJ/mol), SiN (439 kJ/mol) and SiCl (456 kJ/mol)[82] are within 20 kJ/mol of each other, the preference of the bridging pathway over the upright migration is probably related to the 300 kJ/mol[82] cost of breaking the CN triple-bond to form a CN double-bond. The transition state leading to the bridging intermediate compensates for this energy cost by initiating the formation of additional SiC or SiN bond. For the double-dimer SiCN2'to SiCN2 reaction pathways (see Figure 5), the diffusion of CN through a bridging CN intermediate corresponds to reforming the ClCN4 intermediate and proceeding to SiCN2' over TS7.

C.3. Reaction Pathways Across Si-Dimer Rows

The possibility of ClCN dissociation pathway across two Si-dimers in different rows was investigated with trench type clusters. The $Si_{23}H_{24}$ cluster, generated by attaching two single-dimers in an end-to-end fashion, has two possible isomers, the V-trench and the Λ-trench.[75] The V-trench cluster (Figure 1c) has both the buckled-down atoms of each Si-dimer facing the center of the cluster, resulting in a mirror plane through the center of the cluster. The other possible geometry is the Λ- trench cluster in which one of the buckled up Si atoms faces the edge of the cluster. The bare Λ-trench cluster is

slightly higher in energy than the V-trench and structures starting from the Λ-trench geometry tend to revert to a V-trench based geometry during optimization. For the $Si_{23}H_{24}$ cluster, this paper only utilizes the V-trench isomer, which have also been used by Widjaja et al.[75] to examine cluster size effects in ammonia adsorption.

Given the large distance (5.4 Å) between silicon atoms in different dimer rows, the only additional pathway involves Cl atom migration from one Si-dimer row to another. With this constraint, Figure 6 shows the five additional stable geometries formed by the reaction of ClCN with a V-trench cluster. The energies for these structures and possible transitions states are listed in Table 3. Frequency calculations were performed for the 1D-Row and 2D-Row structures. The stable structures contained no imaginary frequencies and the transitions states contained only one imaginary frequency. Again, each connection between a pair of stable structures and the respective transition state was confirmed by internal reaction coordinates calculations. Due to the flexibility of these clusters, the final geometries were carefully compared to the bare cluster to ensure that no unrealistic distortions have occurred during the optimization. No additional constraints were required for the geometries shown in Figure 6 and the respective transitions states.

The larger $Si_{39}H_{32}$ and $Si_{55}H_{40}$ clusters were utilized to investigate cluster size effects. The $Si_{39}H_{32}$ cluster models were created from the V-trench geometries by adding two additional Si-dimers onto the V-trench model (see Figure 6) to create a cluster consisting of two double-dimers attached in an end-on fashion. For $Si_{55}H_{40}$ cluster, two extra Si-dimers were added to both sides of the V-trench model to create a cluster consisting of two triple-dimers attached in an end-on fashion. As expected from single-, double- and

a) ClCN1   b) SiNC3   c) ClCN5

d) SiCN3   e) SiCN4
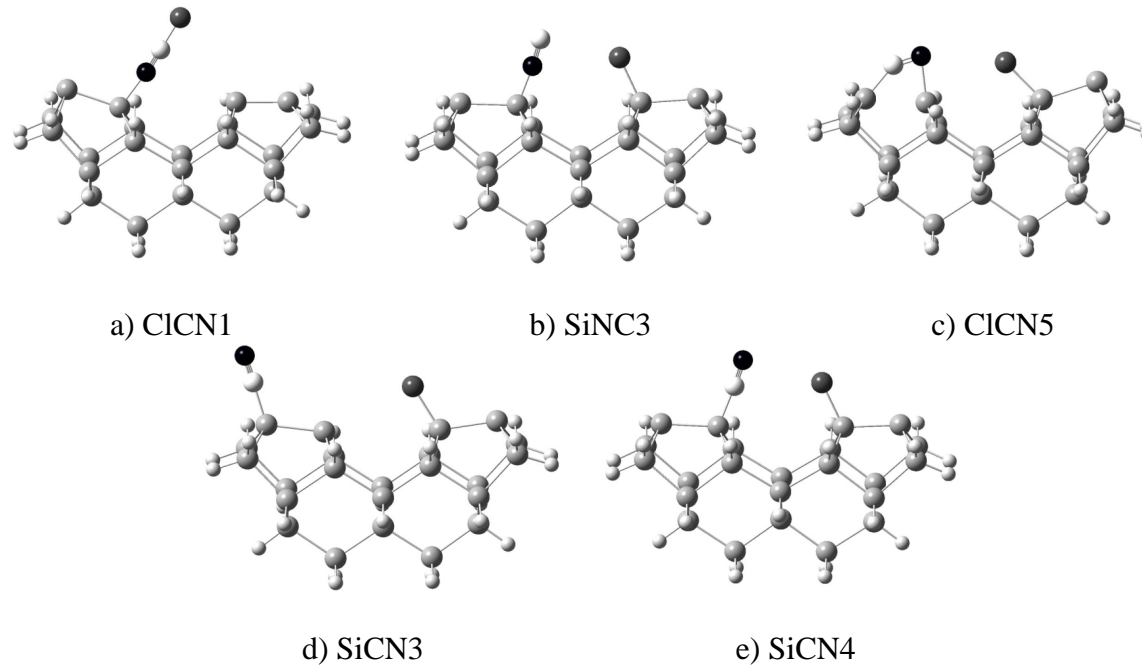
Figure II-6: ClCN adsorption models on the Si V-trench cluster: (a) ClCN adsorbed in an end-on position. (b) Dissociated Cl and NC on different Si-dimers. (c) Dissociated species with Cl and CN adsorbed in a side-on position. (d) Dissociated Cl and CN on different Si-dimers. (e) Dissociated Cl and CN on different Si-dimers. The atoms are ● hydrogen, ● nitrogen, ● carbon, ● silicon and ● chlorine.

Model	1D-Row	2D-Row	3D-Row
ClCN1	-51.6	-65.3	-74.2
SiNC3	-240.2	-251.2	-271.7
ClCN5	-215.2	-255.1	-274.8
SiCN3	-293.2	-295.7	-299.6
SiCN4	-272.0	-282.0	-302.2
TS13	-17.9	-26.2	-27.2
TS14	-168.3	-172.7	-168.7
TS15	-192.9	-234.3	-255.7
TS16	-150.8	-158.9	-183.4

Table II-3. Calculated B3LYP/6-31G(d) adsorption and transition state energies (kJ/mol) for V-trench (1D-Row) based adsorption models. The larger $Si_{39}H_{32}$ (2D-Row) and $Si_{55}H_{40}$ (3D-Row) contain two or three Si-dimers in each row, respectively. All stable structures and transitions states were optimized without geometrical constraints. Frequency calculations were performed for the 1D-Row and 2D-Row structures. The stable structures contained no imaginary frequencies and the transitions states contain only one imaginary frequency.

triple-dimer computations, the dative bonded species (ClCN1) and transition state

connected to this species (TS13) are strongly affected by the cluster size. Surprisingly,

the ClCN5 structure with a bridging CN group and its associated transitions state (TS15)

are strongly affected by the cluster size. Possibly, the larger clusters allow the relatively

isolated CN group, not found for the double- and triple-dimer clusters, to delocalize its

charge more effectively. An average cluster size effect of 11% is observed for the other

stable structures and transition states. This value is larger than the 5% average energy

difference (Section 1) observed between the single-dimer and the analogous triple-dimer

models and the 3% average difference (Section 2) observed between the double-dimer

and the analogous triple-dimer models. Nevertheless, the cluster size effects do not

significantly influence the resulting reaction pathways.

Figure 7 summarizes the reaction pathways for the adsorption and dissociation of ClCN

on the V-trench based models. The solid line is the lowest energy pathway and the

activation energies in kJ/mol are given in parentheses next to each transition state label.

The initial dative bonded structure (ClCN1) is bounded by a square box while the species

bounded by an oval are consistent with experimental observation.[25,26] This reaction

pathway starts with the V-trench equivalent of the ClCN1 species (Figure 6a). The CCl

bond then dissociates across the Si-dimer rows through TS13 to form a bond with an

adjacent Si-dimer to form SiNC3. The 33.7 kJ/mol barrier for this process is greater than

the 23.5 kJ/mol barrier over TS1 to form ClCN2 on the single-dimer clusters. Since TS1

and TS13 involve a dative bonded species, cluster size effects become important. For the

large $Si_{55}H_{40}$ cluster, the TS13 barrier increases to 47.0 kJ/mol. Using this value, TS13
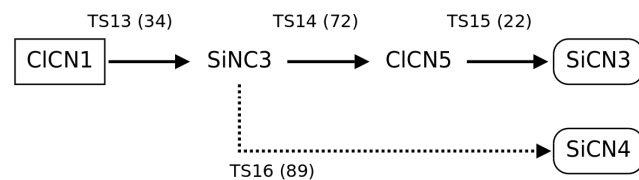
Figure II-7: The V-trench based adsorption and decomposition pathways for ClCN. The solid line is the lowest energy pathway and the activation energies in kJ/mol are given in parentheses next to each transition state label. The initial dative-bonded structure (ClCN1) is bounded by a square while the final structures consistent with the experimental data are bounded by an oval.

barrier is still approximately 10 kJ/mol larger than that for TS1 (35.7 kJ/mol), computed with triple-dimer clusters. Assuming first order kinetics and similar pre-exponential factors, this cross dimer-row process should proceed at a significantly slower rate that occurring over TS1 on the single-, double- and triple-dimer clusters.

Once SiNC3 forms, the C atom in the N-bonded CN species can react with the other Si atom on the Si-dimer (TS14) forming a bridging CN species, ClCN5. An alternate mechanism based on the migration of an upright CN group was excluded for reasons given in Section 2. Assuming that the dative bound ClCN is fully accommodated, there is approximately 220 kJ/mol of energy available to help traverse this 72.0 kJ/mol barrier (103.0 kJ/mol for the $Si_{55}H_{40}$ cluster). After which, the SiN bond can break through a relatively small 22.3 kJ/mol barrier (TS15) to form an upright CN species with a SiC bond, SiCN3. This transformation is similar to the conversion of ClCN4 into SiCN2' on the double-dimer clusters, which has a similarly small barrier of 14.5 kJ/mol. Alternatively, SiNC3 can isomerize (TS16) over an 89.4 kJ/mol barrier, similar to that found on the single- and double-dimer clusters, to form the more stable C-bond CN isomer represented by SiCN4. Both the SiCN3 and SiCN4 structures are consistent with experimental observations.[25,26]

D. CONCLUSIONS

The final structures from the single Si-dimer, the adjacent Si-dimers in the same row and the cross Si-dimers in different rows reaction pathways (SiCN1, SiCN2, SiCN2', SiCN3 and SiCN4) are in agreement with experimental results.[25,26] Kadossov *et al.* have previously investigated the adsorption and decomposition of ClCN, BrCN and ICN using

single-dimer models.[26,53] However, the large transition state barrier of TS3 for the dissociation of the CCl bond on the single-dimer clusters raised questions as to why none of the intermediates, for example the bridged ClCN2 species, were observed in the experiment. To complicate matters further, the TS3 transition state on larger multiple Si-dimer models could not be found with only one imaginary frequency or without constraints.

The cross Si-dimer and cross Si-dimer row pathways on larger clusters resolve this question by providing pathways with significantly lower activation energies with respect to the single-dimer based model. The key step in lowering the activation barriers with respect to the single-dimer model is the dissociation of the CCl bond across two Si-dimers, either in the same row or in different rows. For the pathways involving adjacent Si-dimer in the same row, the large activation barrier over TS3 is reduced by 40% by replacing it with a new cross-dimer CCl dissociation transition state (TS6). For the trench clusters, a cross-row CCl bond dissociation (TS13) occurs as the first step. This step has activation energy of approximately 10 kJ/mol larger than that found for the initial step for the adjacent Si-dimer pathways. Assuming that the datively bonded ClCN species is fully accommodated, significant kinetic energy is now available to traverse the adjacent Si-dimer and the cross-row pathways to form a structure consistent with the experimentally observed Si bound CN species.[25,26] Thus, multiple-dimer pathways explain the lack of intermediates observed experimentally during the dissociation of ClCN on the Si(100) surface.

CHAPTER III

Theoretical Investigation of the Si(100) Surface Excited State and the Spin-Forbidden

Crossing Probability

A. INTRODUCTION

Recently, a theoretical study of the excited states of Si(100) surface has been reported
[83]. This paper is of great interest to us because it relates the wide seen spin forbidden

reactions in organic/inorganic chemistry with the surface chemistry at solid surfaces.

Even though not many efforts have been put into the investigation of spin forbidden

reactions on solid surfaces, these reactions are not rare. The oxidation process of Si to

SiO_2, for example, could be treated as starting with triplet reactants (singlet Si surface

atoms combined with triplet O or O_2) go through spin crossing process, and yield singlet

product SiO_2. Or the Si surface can go through spin crossing process first, then couple

with triplet O or triplet O_2 in an antiferromagnetic fashion to form overall singlet spin

reactants. After that, the oxidation process can take place through the normal transition

state theory (TST) [84]. Through either approache, nonadiabatic spin crossing process has

to be involved. Several theoretical studies on the oxidation process of Si [85-87] have shown

the importance of incorporating spin crossing processes to understand the experimental

data correctly.

One way of incorporating nonadiabatic spin crossing process with the conventional TST is to treat the spin crossing barrier as an extra activation entropie required for the reaction [88]. Spin crossing process are characterized by an avoid-crossing seam between the potential energy surfaces (PES) of two different electron spin states [89,90]. Under Born-Oppenheimer approximation, when incomplete electronic Hamiltonian with some terms dropped (i.e. spin-orbital term) is used, the diabatic PES of two spin states can cross through a seam that is orthogonal to the reaction coordinate. However, Born-Oppenheimer approximation will be invalid near the spin crossing seam since even very small change of nuclear positions can completely change the electronic state of the system. When full electronic Hamiltonian is used, two non crossing adiabatic PES that are separated by the spin-orbit coupling (SOC) coefficient Hamiltonian can be obtained, and the 'crossing seam' is indeed avoid crossing (Figure1). Along the avoid-crossing seam, the global minimum is defined as the minimum energy crossing point (MECP), which is the most important vicinity for the spin crossing process to take place. Most of the time, when the SOC term is not very large, non-adiabatic spin crossing process will take place and the spin crossing probability will be smaller than unity because there is non-zero surface hopping probability from one adiabatic surface to another. Several theories are available to calculate the spin crossing probability, the classical Landau-Zener theory [91-93] has one of the easiest forms and can give satisfactory results [94]:

$$P_{sh}(E) = 1 - \exp\left(\frac{-4\pi^2 H_{SOC}^2}{h\Delta F} \sqrt{\frac{\mu}{2E}}\right)$$

In this equation h is the Planck's constant, H_{SOC} is the SOC coefficient, ΔF is the difference in slope of the two PES along the direction crossing coordinate at the MECP, μ is the reduced mass of the system as it moves along the crossing coordinate and E is the
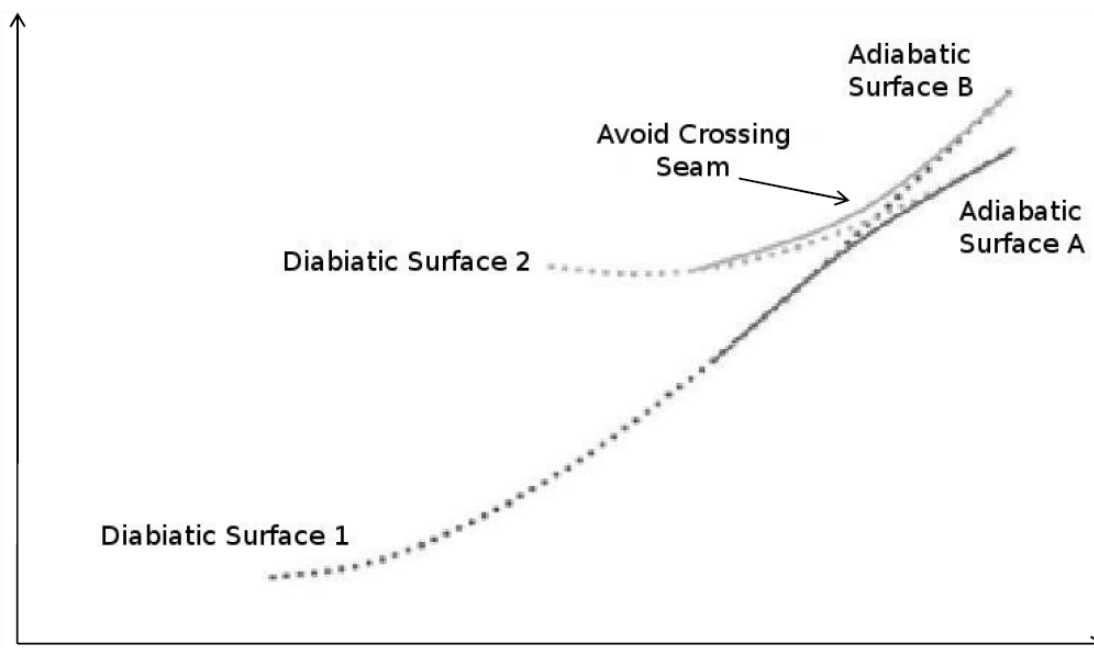
Figure III-1. Schematic diabatic and adiabatic potential energy surface and the non-crossing seam for a spin-forbidden reation.

kinetic energy available to pass through the MECP.

As the referenced paper [83] has initiated the study of spin forbidden reactions on solid surface, we find more care has to be taken to correctly reveal the pictures of these chemical processes. The result obtained from the referenced paper indicates there is essentially no spin crossing difficulty (~100% of spin crossing probability) from the ground singlet state of Si(100) surface 2×2 dimer model to its first excited state (triplet). This result is quite surprising when taking account the fact that there is no heavy atoms that can give strong SOC coefficient in the silicon dimer cluster model. Also, among previous studies of Si oxidation process, it is clearly shown O_2 plus Si(100) system have a very limited spin crossing probability [87], which suggests the spin crossing probability of bare Si(100) surface cannot be too large. So we have decided to perform a more careful and detailed study of the spin crossing effect on the bare Si(100) surface.

Before investigating the triplet excited state of the dimer clusters and the kinetic pathways to accomplish the excitation process, we must first understand its ground state (singlet) configuration. There have been debates on whether the ground state of Si(100) should be symmetrical or buckled as shown in Figure 2. Depending on the different theoretical levels used to treat the electron correlation, controversial results have been obtained. As the electron correlation can be separated into static correlation and dynamic correlations, theoretical methods that reveals static correlation (i.e. MCSCF) predicts symmetrical ground geometry [4-9], while methods recovers dynamical correlation (i.e. DFT) tend to prefer buckled configurations [8-14]. The ideal method that can incorporates

41
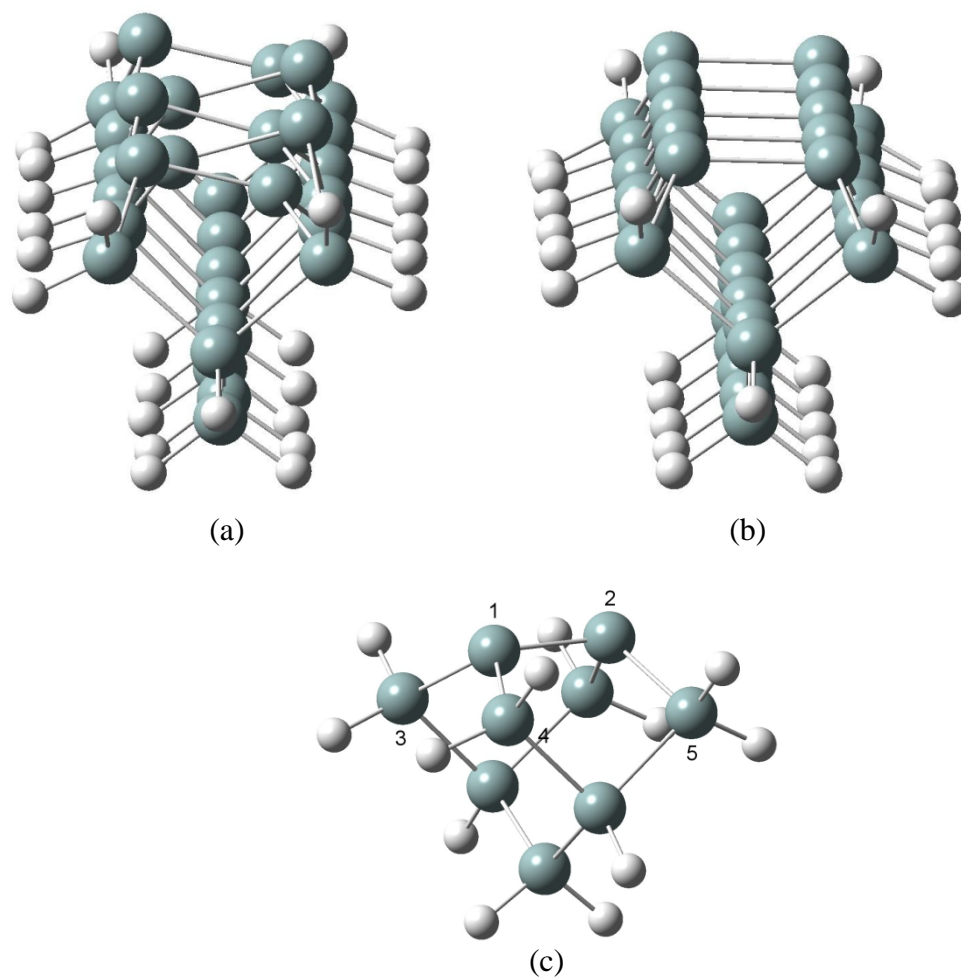
Figure III-2. Si$_{33}$H$_{28}$ 5-dimer cluster model in (a) buckled geometry and (b) flat geometry. (c) The buckling angle in this study is defined as the angle between the normal vector of the line connecting 1 and 2 and the normal vector of the surface of the plane containing 3, 4 and 5.

both static and dynamical correlations are multi-reference perturbation theory (MRMP)[8] or diffusion Monte Carlo (DMC) calculation[15]. Unfortunately, no direct complete geometry optimization at these high level theories has been done yet because of the unavailability of the analytical gradients from these methods. Experimental results have also showed controversial conclusions [16-22]. We will not attempt to resolve this dispute, but various theoretical methods will be used in this study to investigate whether the kinetic process of spin crossing is selective to the theoretical level.

B. THEORETICAL METHODS

The geometry optimization and frequency analysis of the singlet ground state and triplet excited state of Si_9H_{12} single dimer cluster are preformed with Gaussian 03 software package [74]. Starting from Hartree-Fock theory, higher level ab-initio methods were used after, to incorporate the electron correlations. First, the singly and doubly excited configuration interaction (CISD) calculation is performed. Then the coupled cluster calculation with singly and doubly excitations (CCSD) are used after to overcome the size inconsistency issue of CISD method. These two methods are expected to recover the dynamical electron correlations both. We also performed B3LYP functional [71,95] calculations to test the result from the low cost density functional theorem (DFT). Finally, complete active space SCF (CASSCF) calculations are carried out in order to incorporate static electron correlations. All stationary geometries are confirmed to be global minimums by performing frequency analysis. MECP between the singlet ground state and the triplet excited state are obtained from the code provide by Harvey [96] based

upon the algorithm proposed by Bearpart et al. [97]. Several different theoretical methods, including HF, CISD, CCSD, B3LYP, CASSCF are employed to do the MECP search. All calculations are accomplished by using 6-31G(d) Gaussian-type basis set [73]. Frequency analysis of every stationary configuration has been performed, except for the triplet state at CCSD level due to the limit of computer power. All stationary configurations contain no imaginary normal mode. Additional calculations of ground state, excited state and MECP search with larger basis sets are carried out by applying 6-311G and 6-311+G(2df) basis set to the two silicon dimer atoms in the CCSD and B3LYP calculations individually, to investigate the basis set size dependence

Spin orbital coupling (SOC) coefficients are computed by GAMESS (US) [98] using the same 6-31G(d) Gaussian-type basis set as in Gaussian 03, at various MECP geometries obtained from different theoretical methods. In addition, SOC coefficient with 6-311+G(2df) basis set at the two silicon dimer atoms are calculated at the MECP geometry found by CCSD/6-31G(d) method to test the sensitivity of SOC coefficient with basis set size.

C. RESULTS AND DISCUSSION

C.1. Choice of Active Space for CASSCF

It is very important to choose a proper active space for the complete active space SCF calculations (CASSCF). Pulay has suggested that if the natural orbital occupation number

Method	NOON				
CAS(2,2)	1.74(0.26)	—	—	—	—
CAS(4,4)	1.80(0.20)	1.98(0.02)	—	—	—
CAS(6,6)	1.80(0.20)	1.97(0.02)	2.00(0.01)	—	—
CAS(8,8)	1.80(0.20)	1.97(0.03)	1.98(0.02)	1.99(0.01)	—
CAS(10,10)	1.80(0.20)	1.97(0.03)	1.98(0.02)	1.98(0.02)	1.98(0.02)

Table III-1. Calculated natural orbital occupation numbers (NOON) for the Si_9H_{12} single

dimer cluster model. The numbers listed in the parentheses are the NOON for the

corresponding anti-bonding orbitals.

of an anti-boding orbital exceeds 0.1, this anti-boding orbital and the corresponding bonding orbitals should be included in the active space [99-101]. So we performed a series of CASSCF calculation of the NOON for the Si_9H_{12} single dimer cluster model. The results are listed in Table 1. It is found that among all the virtual orbitals, only the LUMO has NOON larger than 0.1, this is consistent with some researchers chooses CAS(2,2), which includes two electrons and two orbitals (HOMO and LUMO) as the active space [5,6,8]. But we have noticed that when increase the active space to four electrons and four orbitals from CAS(2,2), the NOON for the HOMO and LUMO have non negligible changes, while further increasing the active space till CAS(10,10) has essentially caused no change to the NOON of the HOMO and LUMO. This is consitent with some other researchers describing the active space as the surface dimer σ, σ*, π, π* orbitals [83]. Since the computational cost of CAS(4,4) is not much larger than that of the CAS(2,2), we have decided to carry out our complete active space calculation at the CAS(4,4) level in this chapter.

C.2. Ground and Excited State Geometry

Several methods have been used to reveal an insight about the effect of different electron correlation methods on the geometry of optimized Si dimer cluster. Hartree-Fock method with no electron correlation predicts a relatively shorter Si dimer bond length (2.19 Å) and a stronger character of Si-Si double bond at the ground state of the Si dimer cluster. After electron correlation is added, the Si dimer bond length gets larger (2.21 Å - 2.27 Å) and the π bond between the two Si dimer atoms becomes less obvious, more

diradical pattern that corresponds to have an unpaired electron on each Si dimer atom is

revealed. Comparing to the experimental value of 2.26 Å [2], it can be seen that electron

correlation is very important for the systems that contain dangling electrons. Another fact

that can further strength the requirement for electron correlation is that Hartree-Fock

(both UHF and ROHF) methods without size correction have mistakenly predicted the

triplet state of Si dimer cluster has lower energy than the singlet state. This is possibly

because when at the singlet state, the Si dimer bond length is shorter and the Si dimer

cluster has stronger electron correlation dependence on lowering the total energy

comparing to the triplet state. Thus, electron correlation can decrease the energy for

singlet state more than the triplet state, and result in a relatively more stable singlet state

correctly. As the most expensive method here, CCSD is the most reliable ab-initio

method in this paper. CCSD/6-31G(d) revealed a better Si dimer bond length and

correctly predicted the singlet state of the Si dimer cluster as the ground energy state.

Also, density functional method also works very well on the Si dimer cluster model as it

shows very close results to the CCSD method. However, we also can see controversial

results on the buckling angle of the Si dimer cluster between the DFT method and ab-

initio methods. Even though both CCSD method and DFT method recovers the

dynamical electron correlation of the Si dimer cluster, CCSD method predicts a flat

symmetric surface just as the other ab-initio methods that are used in this paper, while

DFT method shows a picture of buckled surface and this buckling angle increase as

bigger basis set is used. In retrospect of the previous work [4-15], not only the difference of

whether to focus on the dynamical electron correlation (DFT) or the static electron

correlation (MCSCF) could give different buckling angles, two methods (DFT and

CCSD)

Method	Dimer Bond Length (Å)	Buckling Angle	ΔE (T-S) (eV)	ΔE (C-T) (eV)	SOC (cm^{-1})
UHF/6-31G(d)	2.19 / 2.16 / 2.40	0.0	-0.687	0.696	1.07
ROHF/6-31G(d)	2.19 / 2.18 / 2.41	0.0	-0.570	0.570	0.74
CISD/6-31G(d) [a]	2.19 / 2.36 / 2.39	0.0	0.255	0.011	25.05
CCSD/6-31G(d)	2.21 / 2.38 / 2.39	0.0	0.276	0.007	25.06
CCSD/Mix1 [b]	2.21 / 2.38 / 2.39	0.0	0.278	0.007	-
B3LYP/6-31G(d)	2.22 / 2.40 / 2.42	4.0	0.304	0.004	25.32
B3LYP/Mix2 [c]	2.22 / 2.39 / 2.41	5.6	0.335	0.002	-
CAS(4,4)/6-31G(d)	2.27 / 2.50 / 2.41	0.0	0.471	0.090	25.87

Table III-2. Calculated dimer bond length for the singlet ground state / MECP / triplet excited state, dimer buckling angle, energy gap from triplet state to singlet state, energy gap from MECP to triplet state and the SOC at the MECP that are obtained at each methods. All stationary structures are computed without geometrical constraints and contain no imaginary frequencies. [a] CISD with Davidson correction. [b] Mixed basis set: 6-311G basis set for the two Si dimer atoms and 6-31G(d) for the rest. [c] Mixed basis set: 6-311+G(2df) basis set for the two Si dimer atoms and 6-31G(d) for the rest.

that both focus on the dynamical electron correlation could also result in different pictures. So besides the difference between dynamical and static electron correlation, one may have to take account the different ways how DFT methods and ab-initio methods handle the dynamical electron correlation to find out the reason why different buckling angles are predicted.

C.3. Comparison with Experimental Data

We can justify our calculation by comparing the computational results with the experimental data. Several experimental studies of the excitation energy of Si(100) surface have been carried out before [102-106]. Techniques like photoemission/inverse photoemission and STM measurements that inject or extract electrons have indicated an indirect band gap of 0.9 eV for the Si(100) surface [102-104], while optical measurements suggested this value is 0.44 eV-0.64 eV [105,106]. The smaller energy gap from the optical measurements is attributed to the extra stabilization effect that comes from the electron-hole attraction during the physical process of optical excitation. Our calculated energy difference between the optimized singlet ground state and the optimized triplet first excited state corresponds to the adiabatic excitation energy between the two states with no electron injection or extraction. Thus our computational result should be comparable with the optical experimental measurements. Hess and Doren did such a comparison in their paper [83]. However, the optical excitation process follows the Frank-Condon principle, which does not allow geometry relaxation. As a result, vertical excitation from the optimized singlet ground state to the first triplet excited state that retains the singlet

50

ground state geometry should be the closer to the optical experimental measurements, instead of the adiabatic excitation energy. We have calculated this vertical excitation energy equals to 0.63 eV at CCSD/6-31g(d) level. We also did the calculation at B3LYP/6-31g(d) level with applying 6-311+G(2df) basis set to the two dimer silicon atoms in order to compare to the results give by Hess and Doren [83]. A value of 0.73 eV is obtained at this level, which is a little smaller than the value of 0.79 eV as reported by Hess and Doren [83]. When comparing to the optical experimental results of 0.44 eV-0.64 eV, our calculated values are generally higher. This result is surprising because optical excitation actually measures the excitation energy between the singlet ground state to the first excited singlet state as limited by the selection rule. This energy gap should be higher than that between the singlet ground state to the first excited triplet state according to the Hund's rule. However, it is indicated that the optical excitation is indeed from the bulk valence band maximum instead of the π surface state at the Γ point [105], which is 0.3 eV lower than the formal one. Taking account of this fact, the optical experimental measurement actually indicated a π-π^* excitation energy of 0.74 eV-0.79 eV, which is now a consistent upper limit to our calculated values of 0.63 eV or 0.73 eV.

C.4. MECP Optimization

Minimum energy crossing point search were carried out with several different methods. As mentioned above, we combined the code provide by Harvey and the Gaussian 03 program to compute all the different MECP structures. All methods predict the MECP geometry is fairly close to the electronic state that has higher energy. For

51

example, the lack of electron correlation in Hartree-Fock method predicts the MECP is very similar to the Hartree-Fock singlet state, while CCSD level indicates the MECP is located right by the CCSD triplet state, in terms of both geometry and electronic energy. Again we can see the B3LYP method works very well when compared with the results obtained from the expensive CCSD level. This confirms the validity of using B3LYP/CCSD(T) hybrid method on MECP optimization, which was proposed by Harvey when studying the singlet and triplet states of phenyl cation [96]. Among all the different MECP configurations we have computed, the one predicted from CCSD level is the most reliable one on the basis of recovering the dynamic correlations. A problem has come to us on whether to focus on the CCSD or the CASSCF level, as there is a difference between them on which part of electron correlation is recovered. We have decided to focus on the CCSD level here in this paper, even though it is shown the multi-reference configuration is important on Si dimer models [5]. The reason is that the calculated MECP geometry from CCSD or B3LYP level is very close to that of the triplet excited state, while the CASSCF level gives a silicon dimer bond length of 2.50 Å, which is larger than both the singlet and the triplet states. It has been concluded that most of the MECP geometry should be located very close to the excited state [67,68,88,107]. It seems that either the CASSCF method has overestimated the diradical character of the dimers, or the dynamic correlations that have been neglected by the CASSCF method is very important on determining the MECP. On the other hand, the CCSD level is shown to be more suitable. Since the basis set size dependence is very weak on the MECP optimization, we will simply adapt the geometry predicted by CCSD/6-31G(d) method for the following study of spin crossing.

C.5. Spin-Orbit Coupling Coefficient

The Breit-Pauli spin-orbit Hamiltonian including both one and two electron terms is used to compute the spin-orbit coupling (SOC) coefficient. The procedure starts from performing a full second order CI calculation at the MECP geometry. Then the optimized MO coefficients are read into the spin-orbit coupling coefficient calculation program. Active space is chosen to be same as CAS(4,4) (4 active orbitals and 4 active electrons). As in Table 2, SOC coefficients at different geometry are essentially different from each other, especially between the methods including the electron correlations and the methods that don't include electron correlations. More specifically, the Hartree-Fock (both UHF and ROHF) methods with no electron correlations recovered, have shown very small SOC coefficients of approximately 1 cm^{-1}, while the electron correlations methods have given almost 25 times larger SOC coefficients (~ 25 cm^{-1}). This can be explained from the fact that larger Si dimer atom bond length comes with stronger diradical pattern on the Si dimer atoms, and will result with strong spin-orbit coupling effect. For the Hartree-Fock methods, the predicted MECP has even smaller Si dimer atom bond length than the singlet state, which corresponds to almost pure double bond between the dimer silicon atoms and near zero diradical character. Thus, there is very weak spin-orbit coupling effect in the Hartree-Fock optimized MECP configurations. On the other hand, the electron correlation methods predict that the MECP configurations are close to the triplet state configurations, which correspond to larger bond length and stronger diradical character. As a result, a much larger spin-orbit coupling effect will be found at the MECP configurations that are optimized by correlation methods. We also notice that the SOC coefficient difference is small among all the correlation methods, this indicates that as the

53

dimer silicon atom bong length is close or larger than the ones at the triplet state, the

diradical character will be almost completely recovered, and the obtained SOC

coefficients will not be much different. Upon all the obtained SOC coefficient, we are

most interested in the one obtained at the MECP configuration that is optimized at

CCSD/6-31G(d) level, and the SOC coefficient is found to be 25.06 cm^{-1} at this

configuration. Applying 6-311+G(2df) basis set to the two silicon dimer atoms at the

same MECP geometry gives a SOC coefficient equals 26.07 cm^{-1}, which is very close to

that from using the 6-31G(d) basis set. This indicates there is no obvious basis set size

dependence on computing SOC coefficient.

C.6. Spin Crossing Probability

   As the MECP and the SOC coefficient at MECP has been found, we can apply the

Landau-Zener formula to compute the spin crossing probably (P_{sh}) from singlet ground

state to triplet excitation state of the Si dimer cluster model. Since P_{sh} is a function of the

kinetic energy of the system available to pass through the MECP ($P_{sh}(E)$), we need to

take into account the strength of the motion that corresponds to the spin crossing process.

This motion takes place mostly between the two Si dimer atoms, as the biggest geometry

change from the singlet state to the triplet state is the elongation of the Si dimer atoms

bond length. Thus the reduced mass of the system (μ) as it moves along the crossing

coordinate can approximately be set as the same as the reduced mass between the two Si

dimer atoms, which is equals to 14.04 g/mol. This approximation is used in the Hess and

Doren's paper [83]. However, the two dimer atoms are tightly bonded to the under layer Si

atoms, the motion between the two dimer atoms is correlated to the under layer atoms. One alternative way is to examine the vibration modes of the cluster model and use the reduced mass indicated by the vibration mode that corresponds to the same motion of the dimer bong elongation. We have found a reduced mass equals to 11.51 g/mol at CCSD/6-31G(d) level using this approach. The slope difference of the two PES along the direction of the crossing coordinate at the MECP (ΔF) is taken as the norm of the 63 dimensional vector that corresponds to the gradient difference between the two potential energy surface at the MECP calculated at CCSD/6-31G(d) level, which has determined to be 2.53 eV/ Å.

As we have just discussed above, the major geometry difference from the ground singlet state to the excited triplet state is the elongation of the surface dimer bond. This physical process is similar to a harmonic oscillator with the two Si dimer atoms on each side. On the clean silicon surface when no chemical reaction that provides additional energy to the surface environment is taking place, the kinetic energy available along this motion equals to the vibrational energy of the vibration mode that corresponds to the same motion. We have found this energy equals to 2.958 kJ/mol at 298.15 K and 6.837 kJ/mol at 800 K. Comparing to the value of 3.156 kJ/mol from Maxwell-Boltzmann distribution approximation as used in Hess and Doren's paper [83] at 298.15 K, our result is a little bit smaller. Plug in SOC coefficient equals to 25.06 cm^{-1} and ΔF equals to 2.53 eV/Å, we have obtained the spin crossing probably (P_{sh}) equals to 0.005 at 298.15 K and 0.003 at 800 K. This is a much smaller value than unity, and falls into the typical range of

a few thousandth for a spin crossing probably, when not too big SOC coefficient is

observed [88].

C.7. Lifetime and Population of the Triplet Excited State

To obtain the total free energy of a molecule, frequency analysis is required. However, we are unable to perform the CCSD/6-31g(d) frequency calculation for the triple state of the Si_9H_{12} single dimer cluster due to limited computer power. Since the results from the B3LYP method have been found to be very close to the ones from the CCSD method in this work, we performed frequency calculations at the B3LYP/6-31g(d) level instead, and expected to get a good estimation of the CCSD/6-31g(d) result. We found that at 298.15 K, the free energy correction to the singlet state and triplet state of the Si_9H_{12} single dimer cluster equal 1.82 eV and 1.80 eV, respectively, at the B3LYP/6-31g(d) level. This gives a free energy correction of -0.02 eV, to the energy gap between the triplet state and the singlet state. When we look at the free energy correction to the singlet state at 298.15 K calculated at CCSD/6-31g(d), the value equals 1.90 eV, which is very close to that of the B3LYP level. Thus we decide to use the free energy corrections calculated at the B3LYP/6-31g(d) level to estimate the energy gap between the triplet state and the singlet state. Using approximation, we have calculated the Triplet-Singlet free energy difference equal 0.257 eV at 298.15 K and 0.241 eV at 800 K, respectively. This corresponds to 0.0045% of the surface dimers adopting the triplet exited state at 298.18 K and 3.0% at 800 K, if thermodynamic equilibrium can be reached. The thermal rate constant for a spin

crossing reaction can be approximately calculated by combing the transition state theory (TST) with the spin crossing probability [88]:

$$k(T) \approx \langle P_{sh} \rangle \times \frac{k_B T}{h} \exp\left(\frac{-\Delta G}{RT}\right)$$

At 298.15 K, P_{sh} equals to 0.005 is equivalent to add 44.1 J·mol^{-1}·K^{-1} of activation entropy to the spin crossing reaction. The total energy barrier is found to be 40.4 kJ/mol for the spin crossing from singlet to triplet state, and the calculated k(T) equals to 5.1×10^5 s^{-1}. This is a very larger rate constant, which indicates that the spin crossing reaction is very quick. So we can conclude that the chemical equilibrium will be reached at normal conditions. Upon this point, we can see that there is a small amount of the Si-dimers staying at its triplet excited states at room temperature. As temperature increases, the population of the excited triplet state can increase dramatically and reach a considerable amount that could play a very important role in many chemical reactions. The oxidation process of Si(100) surface, for example, has been shown that a too small reaction rate is calculated when only taking account the spin crossing effect when the triplet O_2 coming right close to the singlet Si(100) surface [87]. Our calculation of the non-negligible population of the triplet Si(100) surface can give an increased reaction rate and detailed calculation of this factor should be very beneficial for the understanding of the silicon oxidation process.

D. CONCLUSIONS

We have shown that the electron correlation is very important on revealing the correct geometry and energy of the Si(100) dimer cluster models. Even between the DFT and the

CCSD method, which are both expected to recover the dynamical correlation of the system, controversial results on whether a buckled or flat surface is the minimum ground state can be obtained. It is also found out that the MCSCF method as suggested by other researchers on treating the Si(100) dimer cluster models is not adequate at MECP searching calculation. Even though the MECP geometry from different methods are not quite the same, the spin-orbit coupling (SOC) coefficient, which is the most important fact that determines the spin-crossing probability, is not very sensitive to the geometry difference as far as the correlation methods are used in the MECP search. Thus, our calculated room temperature spin-crossing probability of 0.005 is expected to be qualitatively correct. Large rate constants obtained from combing the transition state theory (TST) and Landau-Zener crossing probability suggest thermal equilibrium between singlet ground state and the first triplet excited state of Si(100) surface can be reached. The population of the triplet excited state is very small at room or lower temperature, but it can increase dramatically with increasing temperature. The non-negligible amount of triplet excited state of Si(100) surface dimers at high temperature may play an important role on explaining many silicon surface chemical reactions, such as the silicon oxidation process and other chemisorbed reactions.

CHAPTER IV

Dissociative Adsorption of Benzene Molecule on the Si(100) surface

A. INTRODUCTION

In the past two decades, the adsorption and the reaction of unsaturated aromatic

organic molecules on the Si(100) surface have received intense attention from many

research groups [27-44,108-115 45]. Among all the aromatic compounds, benzene has one of the

simplest form and is of particularly interest to lots of researchers. Although many results

of the adsorption of benzene on Si(100) surface in terms of both experimental and

theoretical techniques have been reported [27-44 45], the picture of the benzene adsorption

and chemical behavior on the Si(100) surface is yet still not clear. The debate on the most

stable adsorption configuration of benzene onto Si(100) surface has lasted for over a

decade. In theory, there are six possible adsorption configurations of benzene on Si(100)

surface that are commonly recognized: the standard butterfly (SB) or [4+2] butterfly,

tilted (T) or [2+2] tilted, pedestal (P), twisted bridge (TwB) and the diagonal-bridge

butterfly (DBB) configurations [32].The center of the debate lies between the preference of

the di-σ configurations (SB, T) and the tetra-σ configurations (TB,TwB).

An early 90th study using high resolution electron energy loss spectroscopy

Standard Butterfly (SB)   Pedestal (P)   Tight Bridge (TB)

Tilted (T)   Twisted Bridge (TwB)   Diagonal-Bridge Butterfly (DBB)
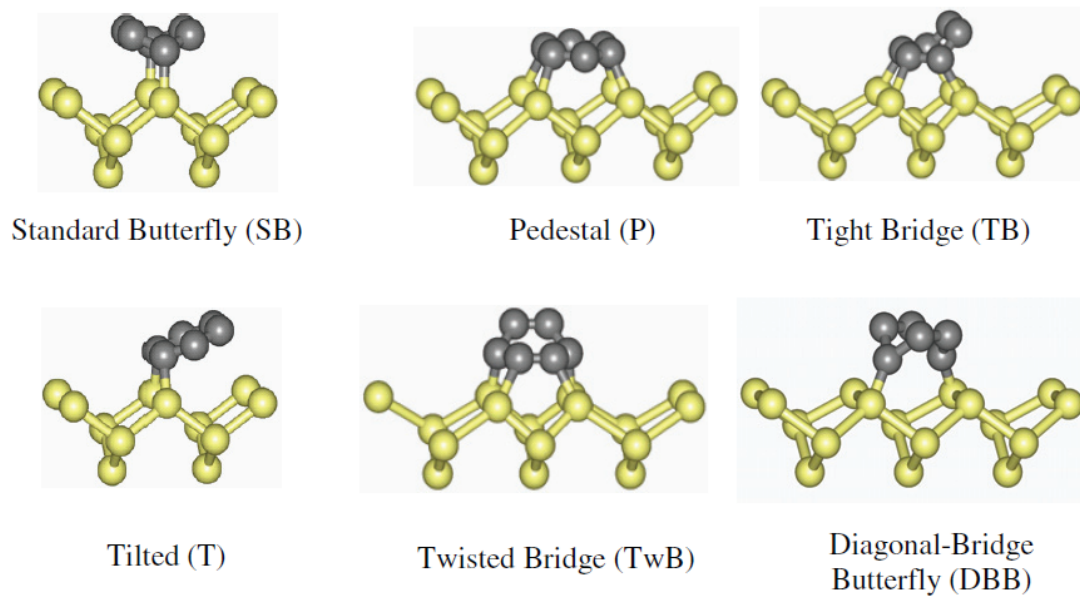
Figure IV-1. Sketch of the six most commonly recognized configurations of benzene adsorbs on Si(100) surface. Figure adapted from reference [32].

(HREELES), thermal desorption spectroscopy and Auger electron spectroscopy (AES) has concluded that the benzene molecule chemisorbs on Si(100) surface through the [4+2] butterfly and [2+2] tilted, two different di-σ fashions at both 90K and 300K [37]. Similar conclusion has been addressed by Brovsky et al. through STM experiments. They have pointed out that the [2+2] tilted product is the most stable configuration, while the [4+2] butterfly product is a metastable structure. The energy difference between these two states is estimated to be 13.5 KJ/ mol [38]. Gokhale et al. performed a combined study of angle-resolved photoemission spectra and density functional theory (DFT) method and have concluded the [4+2] butterfly configuration is the final adsorption product [43].

However, the room temperature STM studies by Lopinski et al. [41,42,116] have revealed the presence of three different adsorption configurations, including one di-σ product ([4+2] butterfly) and two tetra-σ products (TB and TwB). Their density functional singlet point energy calculation at Hartree-Fock optimized geometry (DFT/HF) studies suggest that the the tetra-σ (TB) configuration is more stable than di-σ [4+2] butterfly configuration by 3.9 kJ/mol, and later configuration can convert into formal one through a 91.7 kJ/mol activation barrier. Similar conclusions are also suggested by Silvestrelli et al. [45] through Car-Parrinello molecular dynamic simulations in the framework of density functional theory. They have indicated that the tetra-σ configurations (TB, TwB) are more stable than the butterfly structures (i.e. SB, DBB) and they estimated an activation barrier of 50.2 kJ/mol for the transition from the [4+2] butterfly (SB) to the TB adsorption state. Also, a recent study from Nisbet et al. using photoelectron diffraction technique has observed both di-σ [4+2] butterfly and tetra-σ (TB) tilted configurations,

the composition of the [4+2] butterfly configuration is determined to be 58±29% and the Gibbs free energy difference between these two different states ($\Delta G(TB) - \Delta G(SB)$) is estimated to be between -2.2 and 4.7 kJ/mol [32]. The vibrational IR spectroscopy, thermal desorption and near-edge X-ray absorption fine structure (NEXAFS) experiments from Kong et al. indicates the chemisorbed product of Benzene on Si(100) surface at room temperature is mainly di-σ ([4+2] butterfly) while trace amount of tetra-σ configuration (TwB) is also observed. It is found that the abundance of TwB configuration increases as the time scale gets longer. This observation could be interpreted as the [4+2] butterfly configuration is a metastable structure that is kinetically easy to access, and the formation of the stable tetra-σ product from [4+2] butterfly configuration is limited by the activation energy barrier, which could be considered to be consistent with the Lopinski and Silverstrelli's results to a certain extent.

The high-resolution core-level photoelectron spectroscopy and ultraviolet photoelectron spectroscopy study of Kim et al. has observed that the ratio between the di-σ and tetra-σ absorption configurations of benzene on Si(100) surface varies as the surface coverage changes [40]. More specifically, the [4+2] butterfly configuration becomes more favorable than the tetra-σ configuration (TB) at high surface coverage. The DFT calculations from Lee et al. [30] have indicated the tetra-σ configuration (TB) is 6.8kJ/mol lower in energy than the [4+2] butterfly configuration and the activation energy barrier for the transition from the [4+2] butterfly configuration to the TB configuration is 83.9kJ/mol, which is close to the results from Lopinski. However, they found that the energy of the tetra-σ configuration (TB) is even lower than the [4+2] butterfly

configuration at higher surface coverage. Thus they proposed the increment of [4+2] butterfly configuration comes from the steric effect at high surface coverage.

On the other hand, the polarization-resolved near-edge x-ray-adsorption fin-structure (NEXAFS) experiment from Witkowski et al. [39] shows that the di-σ [4+2] butterfly configuration is the only existing adsorption state and no di-σ configurations has been observed. Same result has also been addressed by Shimomura et al. [29] using the photoelectron diffraction (PED) technique. Jung and Gordon [28] performed a study using the hybrid multi-reference Moller-Plesset second-order perturbation theory and complete active space self consistent field method (MRMP2//CASSCF). They concluded that the di-σ [4+2] butterfly is the most stable adsorption product with a total energy 9.6 kJ/mol lower than that of the tetra-σ TB configuration. The barrier for the transition from the [4+2] butterfly configuration to the tetra-σ TB configuration, if were to happen, is estimated to be 154.8 kJ/mol.

Besides the debate on the preference of the di-σ or the tetra-σ adsorption configurations, there is also a lot of discussion between the two different di-σ adsorption configurations of benzene and other unsaturated organic molecule adsorbing on Si(100) surface. The [4+2] butterfly configuration is analogous to a [4+2] Diels-Alder cycloaddition product, which requires very small or no activation energy to form. However, the tilted di-σ configuration is an analogy to a [2+2] cycloaddition product, which in principle is symmetry forbidden according to the Wooward-Hoffmann rules.
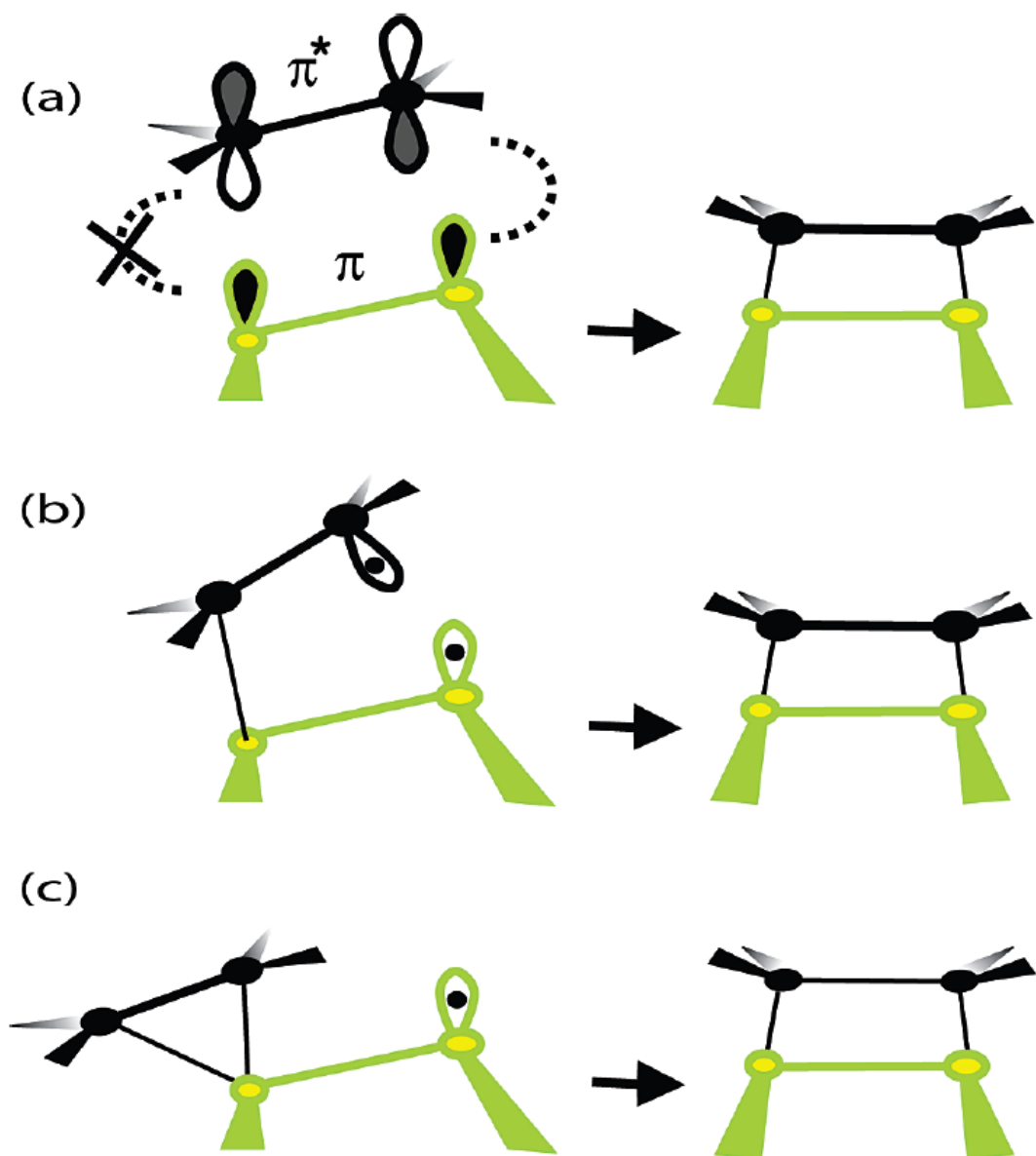
Figure IV-2. Sketch of (a) concerted symmetry forbidden, (b) biradical and (c) π complex precursor reaction mechanisms for the [2+2] ethylene adsorption on Si(100) surface. Figure adapted from reference [117].

This means the formation of the tilted di-σ adsorption product of benzene or any other alkenes is expected to be very difficult, which is not consistent with several experimental studies that have showed non-negligible amount of tilted (T) configuration [37,38]. Thus, two alternative reaction routes, namely the biradical [118] and π complex precursor [119] mechanisms, have been proposed for the absorption of unsaturated organic molecules on Si(100) surface, when the adsorption is through the [2+2] fashion. However, a recent DFT study of the frontier orbital of the Si(100) surface from Ryan et al. has shown that the concerted [2+2] symmetry forbidden addition could take place through a route that is symmetry allowed [117]. So the [2+2] adsorption mechanism of benzene on the Si(100) surface is also a mystery.

Besides the tremendous amount of studies on the adsorption process and products of benzene chemisorbs on Si(100) surface, the post-adsorption chemistry of the benzene on Si(100) surface, on the other hand, has received much less attention. This is because unlike the small unsaturated organic molecules (i.e. C_2H_4, C_2H_2), benzene molecule is believed to chemisorbs nondissociatively and reversibly on the Si(100) surface most of the time. Several studies of the halogen derivatives of benzene can go through dissociation process after adsorption [120 35 36 33], whereas benzene molecule is still considered as inert after adsorption in general. At the early 90th, one semi-empirical study that predicts the dissociated benzene structures are not as stable as the intact chemisorbed configurations has been reported [121]. After that, no more efforts have been put into the benzene dissociative adsorption study for a long time.

Recently, a DFT study of the benzene dissociative reactions on the Si(100) surface has been reported by Nunzi et al. [27]. They have ruled out the dissociative reactions for the two tetra-σ configurations due to the high energy barrier and have only considered the dissociative reactions for four different di-σ configurations, including the tilted and [4+2] standard butterfly configurations that are located within a single dimer surface, and another two di-σ adsorption products that lies either between two dimers in the same row or two dimers across two different rows. They concluded that the tilted configuration (T) and the cross dimer row configuration are the only two qualified candidates to go through the cleavage processes, and yield with dissociative products that are lower in energy than the original intact chemisorbed structures. However, none of the configurations that lie between two dimers in the same row or two different rows has ever been observed experimentally. Thus these two models are of less significance comparing to the tilted (T) and [4+2] butterfly configurations. Also, the activation energy barrier of the dissociation process for tilted configuration (T) is estimated to be 92.5 kJ/mol, which is comparable to the predicted energy barrier for the transition from the [4+2] butterfly configuration to the tight bridge tetra-σ (TB) configuration [41,42,116]. As the later transformation is believed to be accessible under mild conditions, we should also expect to see the dissociation product for the tilted configuration (T) in experiments, which in contrast, has never been observed yet. In addition, the transition state predicted by Nunzi et al. that leads to the dissociative product requires the concurrent cleavage of two hydrogen atoms. Considering that multi-atom transfer in one step rarely occur in chemistry reactions, we have several doubts about this result.

We have decided to perform a careful examination of the dissociative reactions of benzene on Si(100) surface. Taking account the history of the experimental results [29,31,32,37,39,41-43,116] and the suggestions from Nunzi's paper [27], the candidates we consider in this work include only the di-σ tilted (T) and the [4+2] butterfly configurations.

B. COMPUTATIONAL DETAILS

We use the $Si_{15}H_{16}$ double dimer cluster models to reproduce the Si(100) surface for most of our calculations. Single simer cluster model Si_9H_{12} is also used for those adsorption configurations that could be represented by this model, in order to compare with the results from the double dimer models. Triplet dimer cluster model $Si_{21}H_{20}$ is used when the adsorption configuration requires at least three dimers. Unless explicitly stated in the test, the geometry of all the cluster models and the adsorption/dissociation configurations are fully optimized with no constrains applied. Energy calculations, geometry optimization and frequency calculations are performed using the hybrid density functional method that includes Becke's 3-parameter nonlocal-exchange functional[71] with the correlation functional of Lee-Yang-Parr, B3LYP.[72] The 6-31G(d) all-electron split-valence basis set,[73] which includes the polarization *d*-function on non-hydrogen atoms, was employed for calculations. The Gaussian 03[74] software package is utilized to perform the geometry optimization and frequency calculations. The reported adsorption energy is defined as the difference between the total electronic energy of the adsorption model and the isolated molecule and cluster. All energies are reported without zero-point corrections. Unless explicitly stated in the test, frequency calculations confirm that all the

stable geometries have no imaginary vibrational frequencies and all the transition states have only one imaginary normal mode. All connections between stable structures and their transition states are confirmed by internal reaction coordinates calculations.

Since there has been an argument that multi-reference description is need accordingly to describe the adsorption of benzene the Si(100) surface [28], we have performed several calculations at the multi-configuration self consistent field (MCSCF) level for the purpose of comparison. More specifically, complete active space self consistent field involving 10 active electrons and 10 active orbitals (CASSCF(10,10)), which includes the four active electrons and four dangling bonds in the two silicon dimers and the six active electrons and six delocalized π orbitals from benzene molecule, has been used to perform single point energy calculations at the B3LYP/6-31G(d) optimized geometry.

We have noticed, during our calculation, the spin crossing processes are involved. Thus, we have performed a search for minimum energy crossing point (MECP), and have calculated the Spin orbital coupling (SOC) coefficients to find out the spin crossing probability. Required MECP geometries are obtained from the code provide by Harvey [96] based upon the algorithm proposed by Bearpart et al. [97] at B3LYP level. Spin orbital coupling (SOC) coefficients are computed by GAMESS (US) [98] using the same 6-31G(d) Gaussian-type basis set as in Gaussian 03 at the obtained MECP geometries.

C. RESULTS AND DISCUSSION

C.1. Initial Adsorption Products and Their Energies

As mentioned above, we have limited our studies within the di-σ adsorption configurations that are located within the same silicon dimer surface. Besides the conventional [2+2] tilted (T) and [4+2] standard butterfly configurations ,we also considered another [2+2] adsorption state, which has the two hydrogen atoms from the two bottom carbon atoms that attached with the silicon dimer atoms located on the two different sides of the benzene molecule (see Figure 3c). To distinguish the two different [2+2] products, we name the conventional tilted (T) configuration as the 1,2-cis configuration and the one with two hydrogen atoms on the two different sides as the 1,2-trans product. The new 1,2-trans configuration has never been studied by theoretical researchers before, however, the existence of this configuration may still be possible since the intact chemisorbed 1,2-cis and 1,2-trans configurations are indistinguishable to most of the experimental methods discussed in the introduction.

The adsorption energies of the intact1,2-cis, 1,2-trans and [4+2] standard butterfly configurations are listed in Table 1. We have used the Si double dimer cluster models for the conventional [2+2] 1,2-cis (or tilted) and [4+2] standard butterfly configurations. For the [2+2] 1,2-trans configuration, we choose to model it with the Si triple dimer cluster since the potential dissociation process through this configuration needs a minimum of one dimer on each side. The adsorption energies of all the three configurations under Si

a) 1,2-cis   b) [4+2] butterfly   c) 1,2-trans
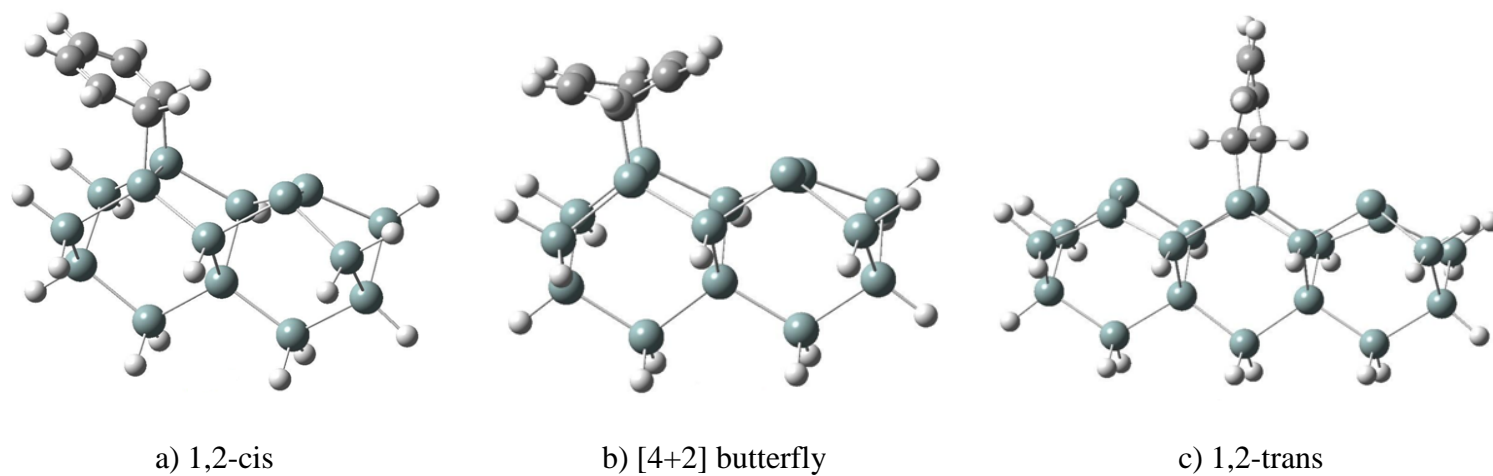
Figure IV-3. Benzene adsorption models on the: a) $Si_{15}H_{16}$ silicon double-dimer cluster through [2+2] 1,2-cis fashion, b) $Si_{15}H_{16}$ silicon double-dimer cluster through [4+2] butterfly fashion and c) $Si_{21}H_{20}$ silicon triple-dimer cluster through [2+2] 1,2-trans fashion.

the adsorption energy difference between the Si single dimer cluster models and the corresponding larger cluster models is very small for the 1,2-cis and [4+2] butterfly configurations (< 6%). However, 1,2-trans configuration has a very strong cluster size effect, the calculated adsorption energy from a single dimer cluster model is about 50% larger (more negative adsorption energy) than that of the triple dimer cluster model.

We have consistently predicted the [4+2] butterfly adsorption configuration to be the global minimum among the three candidates. On the other hand, the 1,2-trans configuration is predicted to have positive adsorption energy which excludes the possibility of its formation, thus we have discontinued the exploration of this configuration. The calculated adsorption energy for the 1,2-cis configuration and [4+2] butterfly configurations are -20.6 kJ/mol and -88.0 kJ/mol, respectively, which are consistent with the -20.5kJ/mol and -85.8 kJ/mol values calculated by Nunzi et al. without zero point energy corrections, at the same theoretical level and with the same basis set as well as same silicon dimer cluster model [27]. However, Jung and Gordon [28] have performed a MRMP2 calculation at the geometry optimized by the CASCF(10,10) lever with the Dunning-Hay double zeta valence (DZV) basis plus d polarization functions DZV(d) basis set using the surface integrated molecular orbital mechanics (SIMOMM) model, and have predicted higher adsorption energies (more negative value) of -26.4 kJ/mol and -121.3 kJ/mol for the 1,2-cis configuration and [4+2] butterfly configurations, respectively.

Gordon [28] has argued that the single reference methods like DFT cannot describe the

Model	1,2-cis	1,2-trans	[4+2] butterfly
Multi Dimer	-20.6	22.8	-88.0
Single Dimer	-19.6	12.0	-90.0

Table IV-1. Calculated B3LYP/6-31G(d) adsorption energies (kJ/mol) for the three different models of the intact chemisorbed benzene molecules on the Si(100) surface. The single dimer refers to the Si_9H_{12} single dimer cluster model. The multi dimer cluster used for the 1,2-cis and [4+2] butterfly configurations is the $Si_{15}H_{16}$ double dimer cluster model and the multi dimer cluster used for the 1,2-trans configurations is the $Si_{21}H_{20}$ triple dimer cluster model. Geometries are fully optimized and frequency analysis shows no imaginary normal mode for all the configurations.

silicon dimer models correctly because there are strong multi-configurational characters among the silicon dimer cluster models on several papers. The reasoning is that there are less than full (smaller than two) natural orbital occupation numbers in the active bonding orbitals among the silicon dimer cluster models and the natural orbital occupation numbers on the corresponding anti-bonding orbitals are relatively large. The proper description of the multi-configurational character of a chemistry system has been proved to be important to the correct calculation of the system property [122]. As Jung and Gordon [28] have pointed out that there are also strong multi-configurational characters within the configurations of intact chemisorbed benzene molecules on the silicon dimer clusters, such as the 1,2-cis configuration (tilted) and [4+2] butterfly configurations, it seems the use of multi-reference methods is essential.

However, we have concluded on Chapter III that the single reference CCSD and B3LYP methods are actually more reliable than the multi-reference CASSCF method in the study of searching for the minimum energy crossing point (MECP) of the silicon dimer cluster. Taking account that the multi-reference character of the silicon dimer cluster comes from the two surface silicon dimer atoms (four for double dimer cluster models and so on), it seems doubtful that the multi-configurational character from these surface silicon dimer atoms can strongly affect the energy profile of the Si cluster models. As for the benzene chemisorbed silicon dimer clusters, it is necessary to clarify whether the multi-configurational character comes from the interaction between the benzene molecule and the Si dimer atoms, or simply from the spectating neighbor silicon dimer, before a conclusion of if the multi-reference method is a must can be made. Thus we

have calculated the natural orbital occupation numbers (NOON) for the 1,2-cis

configuration (tilted) and [4+2] butterfly configurations, which have been shown to carry

strong multi-configurational character from Jung and Gordon's paper[28]. The CAS(10,10)

method has been used for the calculation of the 1,2-cis configuration (tilted) and [4+2]

butterfly configurations on the silicon double dimer clusters in order to be consistent with

Jung and Gordon's approach. However, we used the 6-31G(d) basis set instead of the

HW(d) effective core potential and 6-31G(d) mix basis set or the DZV basis set [28]. We

have also performed the same calculations on the Si single dimer cluster model for

comparison. For the Si single dimer cluster, we used the CAS(8,8) method,

corresponding to 8 active electrons and 8 active orbitals, including the two active

electrons and two dangling bonds in the silicon dimers plus the six active electrons and

six delocalized π orbitals from the benzene molecule. The calculated NOON for the two

adsorption configurations on the two different Si dimer cluster models is listed in the

Table 2. Taking account we have used different Si(100) model (dimer cluster model

versus SIMOMM) and different basis sets, our result is reasonably consistant with the

values from Jung and Gordon's paper[28], and also suggests a strong multi-configruational

character of the benzene on Si double dimer cluster adsorption models. However, the

NOON for the Si single dimer cluster model shows near full occupation number in the

bonding orbitals and all the anti-bonding orbitals have natural occupation numbers no

more than 0.09. According to the standard suggested by Pulay[99-101], which states that

NOON equals or larger than 0.1 for a virtual orbital is the bottom limit for a multi-

configurational description, we can conclude that the benzene on Si single dimer cluster

adsorption models do not possess a critical requirement for multi- configurational

Model		NOON				
Double Dimer	1,2-cis	1.79(0.21)	1.91(0.09)	1.97(0.03)	1.97(0.03)	1.98(0.02)
	[4+2] butterfly	1.84(0.15)	1.96(0.03)	1.98(0.02)	2.00(0.01)	2.00(0.00)
Single Dimer	1,2-cis	1.91(0.09)	1.97(0.03)	1.98(0.02)	2.00(0.01)	—
	[4+2] butterfly	1.91(0.08)	1.92(0.08)	1.98(0.02)	2.00(0.00)	—
Previous Work	1,2-cis	1.69(0.31)	1.88(0.12)	1.93(0.07)	1.97(0.03)	1.98(0.02)
	[4+2] butterfly	1.69(0.31)	1.91(0.09)	1.92(0.08)	1.98(0.02)	1.98(0.02)

Table IV-2. Calculated natural orbital occupation numbers (NOON) for the 1,2-cis configuration (tilted) and [4+2] butterfly configurations of the intact chemisorbed benzene molecules on the Si(100) surface. The numbers listed in the parentheses are the NOON for the corresponding anti-bonding orbitals. The NOON for the Si double dimer cluster model and the Si single dimer cluster model include five and four active bonding orbitals and the correspond ing anti-bonding orbitals, respectively. The data from the previous work is adapted from reference[28].

description. Taking account that the major difference between the Si double dimer cluster and single dimer cluster models is the existence of an extra neighbor Si dimer, we can conclude that the multi-configurational characters we have observed in the double dimer cluster adsorption models mostly come from the two dangling bonds at the neighbor Si dimer, instead of the benzene-Si dimer moiety. We have pointed out that the multi-configurational characters from the dangling bonds on the bare silicon dimer cluster are not necessarily better described by the multi-reference theories in Chapter III. Thus, the single reference DFT methodology should be reliable of obtaining qualitative results.

C.2. Dissociation Products and Their Energies

We have considered three different dissociation products for the 1,2-cis (tilted) and [4+2] butterfly adsorption configurations, consisting two products from the 1,2-cis adsorption configuration and one from the [4+2] butterfly adsorption configurations. The pictures and the adsorption energies for these dissociation products are listed in Figure 4 and Table 3, individually. The first product from the 1,2-cis adsorption state involves the breaking of both C-H single bond from the two adsorbing carbon atoms of the benzene molecule, then the two hydrogen atoms migrate through the gap between the two dimer in the same row and form new Si-H bonds with the dimer silicon atoms on the next neighbor. Since the both C-Si bonds keep intact after the dissociation, we name this final complex as 1,2-cis dissociative double adsorption product or 1,2-cis-double. The other product from the 1,2-cis adsorption state consists of breaking one of the C-Si single bond and abstracting the hydrogen atom from the other adsorbing carbon atom. The abstracted

76

hydrogen atom then transfers to the silicon dimer atom to which the first carbon atom was connected. In this dissociative product, there is only one C-Si bond remains connecting the benzene molecule with the silicon dimer cluster, we name this final complex as 1,2-cis dissociative single adsorption product or 1,2-cis- single.

For the dissociation product from [4+2] butterfly adsorption structure, the result configuration is similar to that of the 1,2-cis-double product, both C-H single bond from the two adsorbing carbon atoms of the benzene molecule break apart and the two hydrogen atoms migrate through the gap between the two dimer in the same row and form new Si-H bonds with the dimer silicon atoms on the next neighbor. Both of the C-Si bonds keep intact after the dissociation as well. The result indicates that the [4+2] butterfly dissociative adsorption product has +47.7 kJ/mol adsorption energy, which is consistent with the +50.2 kJ/mol value obtained from the previous study[27], and has suggested the unavailability of this dissociative product. This result may appear surprising at the first glance because the abstraction of the two hydrogen atoms on the two adsorbing carbon atoms resume the sp^2 hybridization of the two carbon atoms and the aromatic of the benzene molecule is expected to be resumed as well, which should bring down the system energy significantly. However, the C-Si adsorption bond is almost vertical to the benzene molecule, the bond angle among the adsorbing silicon atom, adsorbing carbon atom and the para-carbon relative to the adsorbing carbon atom is found to be 88.6° instead of 180° in an ideal benzene ring. This large angle inconsistency has caused a strong distortion force on the benzene molecule and makes it nonplanar, which breaks the symmetry requirement for the aromaticity. On the other hand, the
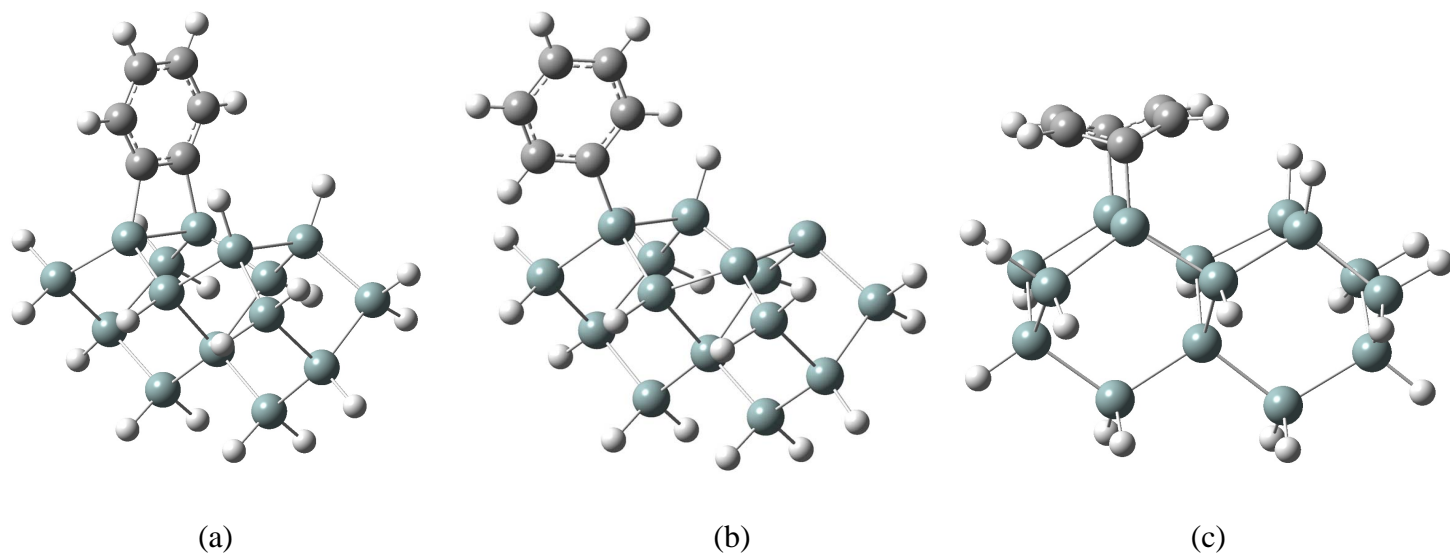
Figure IV-4. Benzene dissociation products on the $Si_{15}H_{16}$ silicon double-dimer cluster: (a) 1,2-cis dissociative double adsorption product (1,2-cis-double) , (b) 1,2-cis dissociative single adsorption product (1,2-cis-single) and (c) [4+2] butterfly dissociative double adsorption product.

Model	1,2-cis-double	1,2-cis-single	[4+2] butterfly-double
Double Dimer	-272.8	-187.1	47.7

Table IV-3. Calculated B3LYP/6-31G(d) adsorption energies (kJ/mol) for the three different models of the dissociative chemisorbed benzene molecules on the Si(100) surface using $Si_{15}H_{16}$ double dimer cluster. Geometries are fully optimized and frequency analysis shows no imaginary normal mode for all the configurations.

original intact chemisorbed [4+2] butterfly adsorption configuration requires an ideal 90°
for the same angle and the calculated number is 83.2°, which is not far from the desired
value, and much small distortion force on the six carbon ring is expected. Thus, because
of the failure of resuming aromaticity and the strong distortion force on the benzene
molecule, the dissociative product from the [4+2] butterfly adsorption configuration is
less stable than the intact structure.

   The two dissociation products from the intact 1,2-cis chemisorbed configuration have
252.2 kJ/mol (1,2-cis-double) and 166.5 kJ/mol (1,2-cis-single) more adsorption energy
than the original precursor. The gain of the adsorption energy can be explained by the
resume of the aromaticity for the benzene molecule in both products. The C-Si bonds in
these two dissociation products lie in the same plane of the benzene molecule, thus the
resume of sp^2 hybridization of the adsorbing carbon atoms can also restore the
aromaticity of the benzene molecule. In summary, we can conclude that the di-σ [4+2]
butterfly chemisorbed configuration should stay intact with no dissociation process takes
place, while the dissociation process for the benzene 1,2-cis chemisorbed configuration is
possible and the 1,2-cis-double dissociation product is expected to be thermodynamically
favorable.

C.3. Transition State for the Initial Adsorption

   We first consider the initial adsorption mechanism of the intact chemisorbed 1,2-cis
(tilted) and [4+2] butterfly configurations. The formation of the 1,2-cis adsorption

configuration is analogous to a [2+2] cycloaddition reaction. At the introduction of this chapter, we have given a short review of the [2+2] cycloaddition reaction mechanism of unsaturated organic molecule adsorbing on the Si(100) surface. It is generally believed that the concerted [2+2] cycloaddition reaction is difficult to take place, because this reaction is symmetry forbidden. We have found the transition state (1,2-cis-TS0) that connects the free reactants and the adsorbed product has a configuration with benzene molecule leans to one side of the Si(100) surface first. The carbon atom of the benzene molecule on the same side gets close to the cluster and forms a dative bond with one silicon dimer atom. At the same time, the neighbor carbon atom relative to the first carbon atom lies above the Si dimer at a longer distance. This configuration is very analogous to the one seen in the "diradical" mechanism, which has been predicted to be the correct mechanism that accounts for the adsorption of ethylene on Si(100) surface [123]. On the other hand, the formation of [4+2] butterfly configuration follows a fashion that is consistent with the symmetry allowed [4+2] cycloaddition, so the concerted [4+2] cycloaddition of benzene on Si(100) surface is expected to take place with no or very small barrier. However, we have found that the transition state ([4+2] butterfly-TS0) leads to the formation of chemisorbed [4+2] butterfly structure has a configuration that is similar to the one leads to the 1,2-cis (tilted) adsorption. Instead of engaging both adsorption carbon atoms concurrently at the same time, as has been predicted by Jung and Gordon [28], it starts the adsorption from one side of the benzene molecule first, and then the ring closes through the other adsorbing carbon atom after. This indicates that a "diradical" mechanism may actually have taken place in the benzene adsorption process for the formation of [4+2] butterfly configuration as well.

Then we looked through the adsorption energies of these two transition states, the energy barrier for the formation of 1,2-cis-TS0 is found to be 41.6 kJ/mol, while the one for [4+2] butterfly-TS0 is only 1.2 kJ/mol. This result is consistent with the argument that energy barrier for a symmetry forbidden [2+2] cycloaddition reaction is much larger than symmetry allowed [4+2] cycloaddition reaction. We have found a strong cluster size effect on the adsorption energies of these two transition states, the activation energy decreases by 26% and 83% for the 1,2-cis-TS0 and [4+2] butterfly-TS0 configurations, respectively, when the silicon dimer cluster size increase from single dimer cluster to double dimer cluster. This strong cluster size reveals the identity of the formed C-Si adsorption bond is indeed dative and is supportive to the "diradical" adsorption mechanism for both reactions. Because the unpaired electrons on the long distance side between the benzene molecule and the dimer surface can be dispersed and stabilized by extended surface dimer sites. Our calculated activation energy for the 1,2-cis-TS0 is consistent with the value of 48.1 kJ/mol at the B3LYP/MIX level found by Jung and Gordon [28] , but is lower than the value of 92.0 kJ/mol at CAS(10,10)/DZV level and slightly higher than the 37.2 kJ/mol at MRMP2/DZV level at the same B3LYP/MIX optimized geometry. As for the [4+2] butterfly-TS0 configuration, Jung and Gordon only performed the geometry optimization at CAS(10,10)/MIX level and has obtained an energy barrier of 74.1 kJ/mol, which is abnormally high for a [4+2] cycloaddition reaction. Thus they have performed MRMP2 single point energies for several geometries along the pathways indicated by the IRC calculation for the transition state. They have found that the MRMP2 single point energies are actually lower than the free reactants and no reaction barrier is observed, so they pointed out the dynamic correlation is very
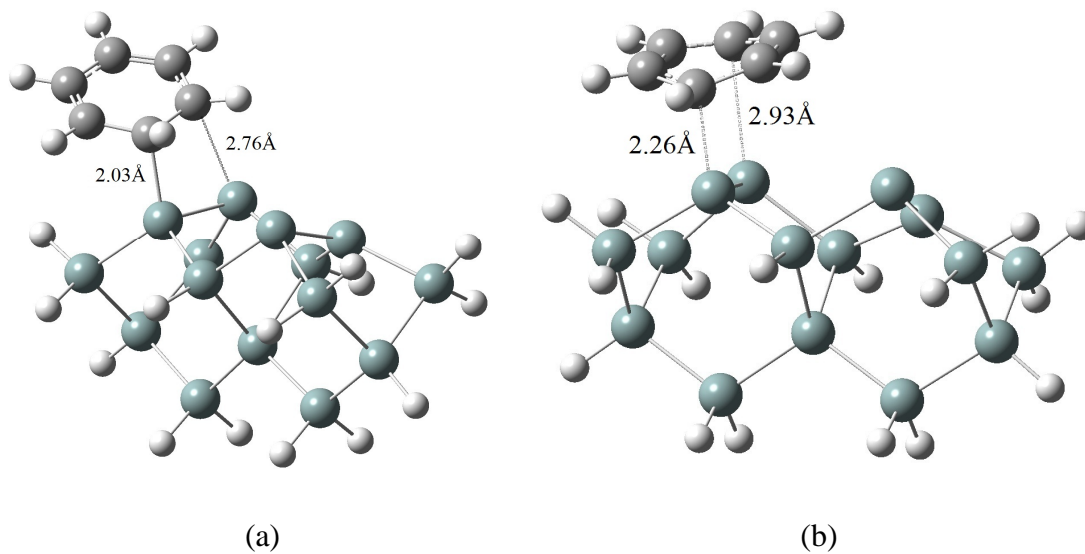
Figure IV-5. Transition states that lead to the formation of intact chemisorbed benzene molecule on the $Si_{15}H_{16}$ silicon double-dimer cluster: (a) transition state that leads to 1,2-cis configuration (1,2-cis-TS0) and (b) transition state that leads to [4+2] butterfly configuraiton ([4+2] butterfly -TS0).

Model	1,2-cis-TS0	[4+2] butterfly-TS0
Double Dimer	41.6	1.2
Single Dimer	56.5	7.0

Table IV-4. Calculated B3LYP/6-31G(d) adsorption energies (kJ/mol) for the transition states (TS0) that lead to the formation of the 1,2-cis and [4+2] butterfly adsorption configurations. Both of the Si_9H_{12} single dimer cluster model and the $Si_{15}H_{16}$ double dimer cluster model are used. Geometries are fully optimized and frequency analysis shows only one imaginary normal mode for all the configurations. Internal reaction coordinate (IRC) calculations have been performed to confirm the found stationary points do connect between the reactants (free reactants) and products (chemisorbed configuration).

important for the correct description of these transition structures. We have discussed in section C.1 that the multi-configurational characters of the benzene adsorption models on Si(100) mostly come from the dangling bond of the spectator silicon dimers and they don't play very important roles in the correct calculations of the system energies. So the static correlations included in the multi-configurational character are not critical to the calculations. The CASSCF method, which only recovers these static correlations but no remaining dynamical correlations, would not be proper in performing the calculations of benzene adsorption on silicon dimer cluster models. Actually at Jung and Gordon's calculations, the single point energy difference between MRMP2 method and B3LYP method at the same optimized 1,2cis-TS0 geometry is not far from each other from, when the same MIX basis set is used for the MRMP2 method, the energy barrier increases to 51.5 kJ/mol, which is very close to the value of 48.1 kJ/mol from B3LYP method [28]. This further proves that dynamical correlations are much more important than the static correlations in the benzene adsorption on silicon dimer cluster models, because the B3LYP and MRMP2 method are both considered to be able to recover the dynamical correlations, except the later one can also recover the static correlations in the selected active space. Thus, the B3LYP method we use in this chapter should be more reliable than the CASCF method.

C.4. Reaction Mechanism for the Dissociations Process

As we have discussed that the hydrogen dissociation process is not thermodynamically accessible for the [4+2] butterfly configurations, we will only have to consider the

dissociation process for the 1,2-cis adsorption configuration. After the formation of the intact chemisorbed species, we need to abstract two hydrogen atoms to get the more stable 1,2-cis dissociative double adsorption product (1,2-cis-double). Nunzi et al. has addressed this reaction as a one step cleavage process [27]. He reported a transition that directly connects between the intact 1,2-cis chemisorbed structure and the dissociative double adsorption product, and the energy barrier for this transition state is found to be 92.0 kJ/mol relative to the intact chemisorbed structure (74.9kJ/mol above free reactants). This conclusion is very surprising because the migration of two atoms at one step in chemistry reactions is very rare. We performed the transition state search at the same B3LYP/6-31G(d) level and found a transition state structure (1,2-cis-TS1) that is very similar to the one reported by Nunzi et al. The C-H bond lengths between the two leaving hydrogen atoms and the original carbon atoms they were connected to are found to be 1.50 Å and 1.16 Å respectively, which are very similar to the value of 1.48 Å and 1.17 Å reported by Nunzi et al. [27]. Also, the Si-H bond lengths between the two leaving hydrogen atoms and the silicon atom destinations are found to be 1.77 Å and 2.28 Å respectively, which are also very close to the reported values of 1.78 Å and 2.23 Å. Our calculated energy barrier for this transition state structure (1,2-cis-TS1) equals to 91.5 kJ/mol, and is consistent with the reported value of 92.0 kJ/mol as well.

However, the internal reaction coordinate (IRC) calculation has shown that 1,2-cis-TS1 doesn't lead to the doubled dissociated product. Instead, it terminates at an intermediate structure that consists with only one hydrogen atom abstracted (1,2-cis-inter0). When we try to perform geometry optimization on this potential intermediate structure, the benzene

molecule fails to stay adsorbed through two C-Si bonds and ends up with a dissociative

single adsorption structure. The reason is that there exists a strong force vector that is

breaking a C-Si bond and leading to the formation of a single adsorption configuration

(Figure 7).Whereas very interestingly, we have found that the desired intermediate

structure can be successfully obtained when the system multiplicity is changed to a triplet

state. We performed a single point energy calculation for the singlet spin state at the

optimized triplet intermediate structure, the adsorption energy is found to be -7.0 kJ/mol,

which is 25 kJ/mol less than that of the triple state. It may appear to be gratuitous to

change the multiplicity of the system, but spin forbidden/crossing reactions are not rare

in organic chemistry reactions. In fact, Naumkin and Polanyi et al. [120] have noticed that

the use of triplet spin state is necessary for several structures that are involved in the

dissociation process for chlorinated benzene on Si(100) surface. Forcing a singlet

multiplicity for the adsorption system can cause unphysical strained structures and result

with much higher system energy. However, they didn't specify when the spin crossing

process is required, and their discussion on the dissociation mechanism for chlorinated

benzene on Si(100) surface is based on the transition states that are approximated by

performing several single point energy calculations along a geometry change direction

that is responsible for the majority configuration change between the reactants and

products, through semiempirical (AM1) method. More importantly, they didn't

investigate the kinetic difficulty for the spin flipping process.

The adsorption energies for all the required stationary configurations that are needed

to comply the entire dissociation process to form the 1,2-cis dissociative double

87
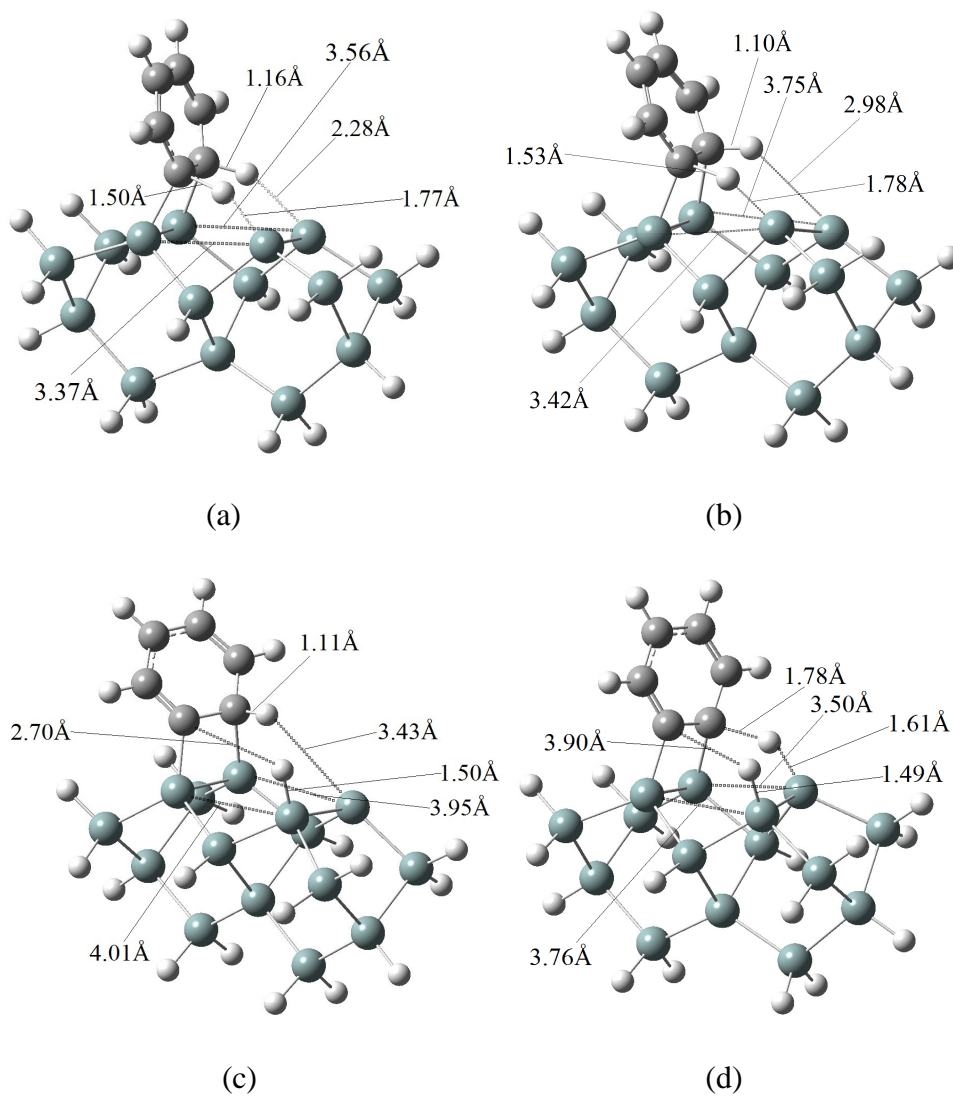
Figure IV-6. Transition states and intermediate that connect the intact chemisorbed 1,2-cis configuration and the dissociative double adsorption product (1,2-cis-double): a) singlet 1,2-cis-TS1, b) triplet 1,2-cis-TS1, c) triplet 1,2-cis-Inter0 and d) triplet 1,2-cis-TS2.
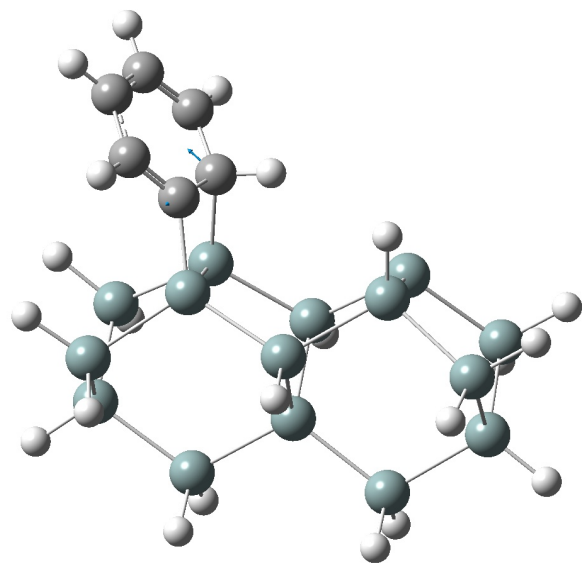
Figure IV-7. The force vector of the singlet spin state at the optimized triplet 1,2-cis-Inter0 configuration.

Model	1,2-cis-TS0	1,2-cis	1,2-cis-TS1	1,2-cis-Inter0	1,2-cis-TS2	1,2-cis-double
Singlet	41.6[a]	-20.6[b]	91.5	—	-42.2	-272.8[c]
Triplet	—	7.3(-51.0)	127.2(69.0)	-32.0(-90.2)	153.2(95.0)	-122.9(-181.2)

Table IV-5. Calculated B3LYP/6-31G(d) adsorption energies (kJ/mol) for the transition states and intermediate that connect between the free reactants and the dissociative double adsorption product (1,2-cis-double). Energies in the parentheses are the adsorption energies relative to the triplet Si double cluster dimer plus free singlet benzene molecule. Geometries are fully optimized and frequency analysis shows no imaginary normal mode for all the local or global minimum structures and only one imaginary normal mode for all the transition state configurations. Internal reaction coordinate (IRC) calculations have been performed to confirm the transition state configurations do connect between the reactants and products through that step.

(a). see table 4; (b). see table 1; (c). see table 3

adsorption product are listed in Table 5. Adsorption energies for both the singlet and triplet states, if available, are calculated for each structure. We can see that the transition state (1,2-cis-TS0) that leads to the intact chemisorbed 1,2-cis configuration is not available through a triplet spin state. So if the silicon dimer was at a triplet spin state when the benzene molecule approaches in the beginning, the adsorption would not occur. From the intact chemisorbed 1,2-cis configuration, the system has to pass through an activation barrier of 112.1 kJ/mol (1,2-cis-TS1) to proceed the hydrogen cleavage process. However, this activation barrier is larger than the barrier of 62.2 kJ/mol for the desorption barrier that goes back to free reactants. In addition, a spin crossing process has to be incorporated if the cleavage process were to happen, which adds more difficulty to the activation procedure. As a result, the singlet intact chemisorbed 1,2-cis configuration will prefer to desorb back to free reactants rather than proceed with the hydrogen cleavage process, when enough energy is available. In another alternative route, the intact chemisorbed 1,2-cis configuration can go through the spin crossing process first to reach the triplet state, then the triplet state passes through an activation barrier of 119.9 kJ/mol (triplet 1,2-cis-TS1) and leads to the triplet intermediate configuration (triplet 1,2-cis-Inter0). One may be concerned about that the triplet state of intact chemisorbed 1,2-cis configuration has a positive adsorption energy relative to the ground state of the free reactants, which may indicate this chemisorbed structure is not available. However, if we consider the energy difference from the triplet configuration with the total energy of the free triplet silicon dimer cluster and singlet benzene molecule, the adsorption energy changes to be -50.9 kJ/mol. Thus, triplet chemisorbed configuration is stable on the surface. Also, since the transition state (TS0) between the triplet free reactants and the

intact chemisorbed 1,2-cis configuration is not available, the desorption that goes back to free reactants is not expected to take place through a simple one step process. So there is no other reactions that compete directly with the hydrogen cleavage reaction for the triplet state of intact chemisorbed 1,2-cis configuration, which makes the hydrogen cleavage reaction feasible.

After the triplet chemisorbed 1,2-cis configuration passes through the 119.9 kJ/mol energy barrier (triplet 1,2-cis-TS1), one of the hydrogen atoms transfers to the neighbor silicon dimer and reaches the intermediate state (triplet 1,2-cis-Inter0) that has an adsorption energy of -32.0 kJ/mol relative to the free singlet reactants. The abstraction of the second hydrogen atom from the benzene molecule requires the intermediate configuration to pass through an energy barrier of 185.2 kJ/mol (triplet 1,2-cis-TS2). After the second hydrogen atom also migrates to the neighbor silicon dimer, the triplet state of the dissociative 1,2-cis double adsorption configuration, which has an adsorption energy that is 149.9 kJ/mol less than the singlet ground state is obtained. At final, another spin crossing process is required to reach the singlet dissociative 1,2-cis double adsorption product, which is the global minimum for this reaction route.

On the other hand, after the formation of the intermediate state (triplet 1,2-cis-Inter0), the system can pass through a much lower barrier of 4.2 kJ/mol (triplet 1,2-cis-TS3), and break the C-Si bond from the carbon atom that is connected with both the silicon dimer atom and a hydrogen atom. The resultant structure after the C-Si bond breaking has a benzene molecule bonded to one silicon dimer atom through a single Si-C bond, and a

hydrogen atom bonded to another silicon atom at the other Si dimer. The benzene molecule and the hydrogen atom are located on the same side of the silicon dimer cluster in this structure (triplet 1,2-cis-Inter1). It is found the full optimized singlet state configuration of this intermediate structure has a severe distorted silicon dimer cluster framework, even though its adsorption energy (-169.6 kJ/mol) is slightly larger than the triplet state configuration by 6.4 kJ/mol. Partial optimization by fixing the two bottom layers of silicon atoms successfully gives a reasonable configuration, and the frequency analysis of this partial optimized structure contains a weak imaginary normal mode that corresponds to the distortion of the fixed bottom layer silicon atoms. It is found that the resultant adsorption energy for the partial optimized structure is only -119.1 kJ/mol, which is 44.1 kJ/mol smaller than the triplet state. Taking account the results from both full and partial optimized singlet 1,2-cis-Inter1 configuration, we conclude that the singlet state of this configuration is the ground state. This is probably due to the fact the two dimer silicon atoms from the two different dimers both have unshared electrons, and they are located on the same side of the cluster model. When the system multiplicity is set as singlet, the two dimer silicon atoms will try to approach each other and share the unpaired electrons they carry. This results with strong distortion to the dimer cluster framework, which makes the system less stable. Whereas in the triplet state, the two unshared electrons have the same spin, and will not try to pair with each other due to the Pauli's exclusion principle. The hydrogen atom that bonded to the dimer silicon atom can then transfer to the other dimer silicon atom within the same dimer and form another intermediate structure (triplet 1,2-cis-Inter2) that has an adsorption energy of -163.4 kJ/mol. The energy barrier (triplet 1,2-cis-TS4) for this process is found to be 168.9

(a) (b) (c)

(d) (e)
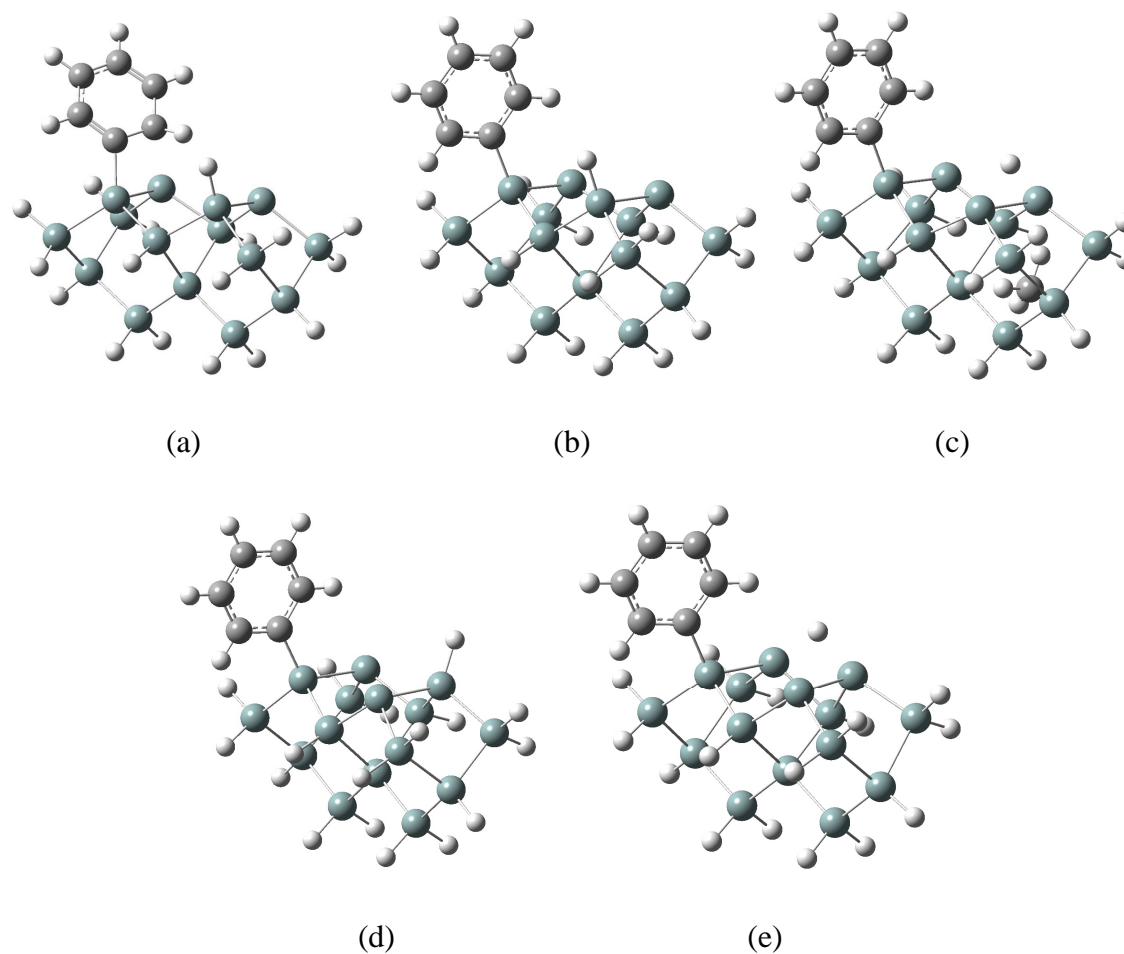
Figure IV-8. Transition states and intermediate that connect between the triplet 1,2-cis-Inter0 configuration and the dissociative single adsorption product (1,2-cis-single): a) triplet 1,2-cis-TS3, b) triplet 1,2-cis-Inter1, c) triplet 1,2-cis-TS4, d) triplet 1,2-cis-Inter2 and e) triplet 1,2-cis-TS5. Note, all structures are optimized at triplet multiplicity.

Model	1,2-cis-TS3	1,2-cis-Inter1	1,2-cis-TS4	1,2-cis-Inter2	1,2-cis-TS5	1,2-cis-single
Singlet	—	-119.1[b]	4.6	-93.0	57.9[d]	-187.1[a]
Triplet	-27.8(-86.0)	-163.2(-221.4)	5.7(-52.5)	-163.4(-221.6)	72.9(14.7)[c]	-158.1(-216.3)

Table IV-6. Calculated B3LYP/6-31G(d) adsorption energies (kJ/mol) for the transition states and intermediate that connect between the triplet 1,2-cis-Inter0 configuration and the dissociative single adsorption product (1,2-cis-single). Energies in the parentheses are the adsorption energies relative to the energy of the triplet Si double cluster dimer plus the energy of the free singlet benzene molecule. Geometries are fully optimized, except for the noted structures, and frequency analysis shows no imaginary normal mode for all the local or global minimum structures, except for that of the singlet 1,2-cis-Inter1 configuration. Only one imaginary normal mode is observed for all the transition state configurations. Internal reaction coordinate (IRC) calculations have been performed to confirm the transition state configurations do connect between the reactants and products through that step.

(a). see table 3; (b), (c), (d) configurations are partial optimized through fixing the bottom two layers of the silicon atoms.

kJ/mol. It is found the triplet state of this new intermediate structure is more stable than the singlet state too. So the system multiplicity will stay in triplet state, and the hydrogen atom that bonded to the dimer silicon atom can pass through an activation barrier (triplet 1,2-cis-TS5) of 236.3 kJ/mol, migrates across the gap between the two silicon dimers, and form a new Si-H bond with the free silicon dimer atom at the first silicon dimer. One thing we have to mention is that the full optimized 1,2-cis-TS5 configurations in both singlet and triplet state have severe distorted silicon dimer cluster framework, the energies optimized here are obtained from partial optimization by fixing the two bottom layers of silicon atoms. The frequency analysis shows that there is only one strong imaginary normal mode that corresponds to the migration of the hydrogen atom, for both multiplicities. Upon this point, we have obtained the triplet state of the dissociative 1,2-cis single adsorption product (triplet 1,2-cis-single). The calculation shows this product is more stable at singlet multiplicity. Thus, a spin crossing process from the triplet state to the singlet state is expected to reach the global minimum for this reaction route.

C.5. Kinetic Controlled versus Thermodynamic Controlled Dissociation Products

The energy calculation shows the dissociative 1,2-cis double adsorption product (1,2-cis-double) is more favorable than the single adsorption product (1,2-cis-single) thermodynamically. However, the actually population of these two different products could be different from the thermodynamic prediction, if the reaction rate is very limited and the equilibrium state cannot be reached under normal time scale. Especially spin crossing process is involved for the formation of both products here, which might cause
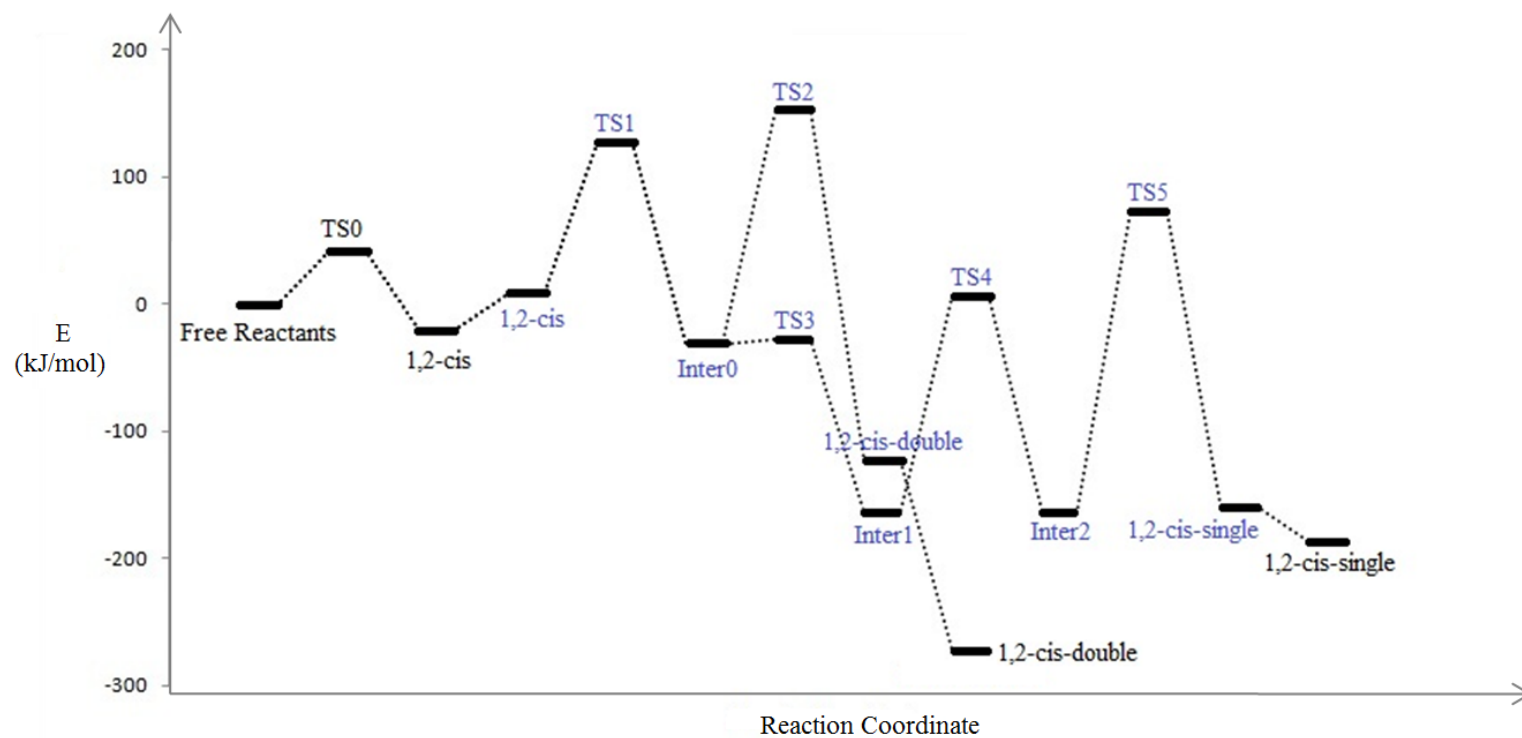
Figure IV-9. Adsorption energy profile for the single and double dissociation steps for the benzene molecule. Text with black color refers to singlet spin state configuration and text with blue color refers to the triplet spin state configuration.

the reaction rates limited to very small values if the spin crossing probability is low. Generally, the reaction rate should be limited by the step that encounters the largest activation energy for both reactions.

The difference between the double dissociation route and the single dissociation route begins after the formation of the triplet 1,2-cis-Inter0 configuration. From this intermediate structure, if we first disregard the spin crossing difficulty and only consider the energy difference between each transition states and the previous stationary point, we find that the largest energy barrier for the double dissociation route equals to 185.1 kJ/mol, which is at the step when the second hydrogen atom abstracts from the benzene molecule (1,2-cis-TS2). The largest energy barrier for the single dissociation route is 236.3 kJ/mol, which is at the step when the hydrogen atom migrates across the two dimers (triplet 1,2-cis-TS5). It first appears that the double dissociation route is also kinetically more favorable than the single dissociation route. However, the two larger activation barriers at the single dissociation route (168.9 kJ/mol for the formation of triplet 1,2-cis-TS4 and 236.3 kJ/mol for the formation of triplet 1,2-cis-TS5) are both at the hydrogen migration steps. If we only focus on the hydrogen cleavage process of the benzene molecule, the largest activation barrier for the single dissociation route is only 4.2 kJ/mol at the step of the formation of triplet 1,2-cis-TS3, and the largest activation barrier for the double dissociation route still remains to be 185.1 kJ/mol at the step of the formation of triplet 1,2-cis-TS2. Thus, we consider that the single dissociation route will not proceed all the way through to the final 1,2-cis-single dissociation product, due to the extreme kinetic difficulty at the hydrogen migration process. Instead, it will halt at the 1,2-cis-Inter1 configuration, and now the largest kinetic barrier for the incomplete single

dissociation route is only 4.2 kJ/mol. When the formation difficulty of the triplet 1,2-cis-Inter0 configuration is taken account, the largest energy barrier for the incomplete single dissociation route changes to be 119.9 kJ/mol, which lies right at the step of the formation of the triplet 1,2-cis-Inter0 configuration (triplet 1,2-cis-TS1), whereas the largest energy barrier for the double dissociation route remains the same. At this point, the single dissociation route is kinetically preferred than the double adsorption product, though an incomplete fashion.

Finally, we add in the effect of the spin crossing difficulty to the entire reaction kinetic. There are two steps that require the spin crossing to take place for the two routes. The first time is at the excitation from the singlet intact1,2-cis chemisorbed configuration to the triplet state, which is required for both dissociation routes. Our calculation shows the MECP for this configuration lies 28.2 kJ/mol above the singlet ground state. The spin-orbit coupling (SOC) coefficient is found to be 15.17 cm^{-1} and the slope difference between the singlet potential energy surface (PES) and the triplet state is 2.38 eV/Å, taking the Landau-Zener formula [91-93]:

$$P_{sh}(E) = 1 - \exp\left(\frac{-4\pi^2 H_{SOC}^2}{h\Delta F}\sqrt{\frac{\mu}{2E}}\right)$$

we have calculated a spin crossing probability of 1.7×10^{-3}. Combing transition state theory (TST) with the spin crossing probability [88]:

$$k(T) \approx \langle P_{sh}\rangle \times \frac{k_B T}{h}\exp\left(\frac{-\Delta G}{RT}\right)$$

the spin crossing difficulty is analogous to add 53.0 J·mol^{-1}·K^{-1} activation entropy to the reaction. This is also equivalent to add 15.8 kJ/mol activation energy to the reaction at

298.15 K, which gives a total activation barrier of 44.0 kJ/mol to this step. When the temperature increases to 1730 K or 2960 K, the total activation barrier of this step will be larger than the maximum spin allowed activation energy for the incomplete single dissociation route (119.9 kJ/mol) or the double dissociation route (185.1 kJ/mol), respectively. This indicates that when the temperature is too high (>1730), the dissociation for both routes will be limited by the spin crossing process at the intact chemisorbed 1,2-cis (tilted) configuration, and the kinetic difficulty will be the same for both single and double dissociation routes. However, this high temperature is not expected to be reached at normal experiment conditions. The other step that requires the spin crossing procedure is at the final step of the double dissociation route, when the triplet 1,2-cis-double product crosses back to the ground singlet configurations. For the triplet 1,2-cis-double configuration, the MECP is located at 5.5 kJ/mol above the triplet excited state, and the equivalent activation entropy increment from the spin crossing process is found to be 87.3 J·mol^{-1}·K^{-1}. At 298.15 K, the overall activation barrier for this spin crossing process is 31.5 kJ/mol. We can see the energy barrier for the formation of singlet ground state product is relatively smaller. This process won't become the rate limiting step for the double dissociation route till the temperature reaches 2057 K. One may think that the product of the single dissociation route also needs to go through a spin crossing process, this is true if the global minimum product (1,2-cis-single) of the single dissociation route can be reached since the singlet state of this product is 29.0 kJ/mol lower than the triplet state. However, we have concluded that the single dissociation route will not proceed all way through to the global minimum product due to the kinetic difficulty in the hydrogen migration process. Instead, a metastable product (1,2-cis-Inter1)

will be reached, and this ground state of this metastable product is actually a triplet state. Thus, the incomplete single dissociation route will give a triplet metastable product and no spin crossing process is needed.

In summary, the incomplete single dissociation route has lower activation energy barrier than the double dissociation route. At low temperature condition, the activation energy of the rate limiting step for the incomplete single dissociation route is 65.2 kJ/mol smaller than that of the double dissociation route. Assume the first order kinetics, the single dissociation reaction is approximately 2.6×10^{11} times faster than the double dissociation reaction, thus we expect the metastable triplet 1,2-cis-Inter1 configuration from the incomplete single dissociation route will be the major product. When the environment temperature increases over 1730 K, the reaction rate for both single and double dissociation route will be limited by the spin crossing process of the intact chemisorbed 1,2-cis configuration, and the more stable dissociative double adsorption product will become the major product instead. However, this high temperature is not usually seen in normal surface adsorption experiment, so the metastable triplet 1,2-cis-Inter1 configuration is expected to the major product under normal conditions.

D. CONCLUSIONS

We have used the DFT method to investigate the adsorption and dissociation process of benzene molecule on the Si(100) surface. For the di-σ intact chemisorbed products, it is found that the [4+2] butterfly configuration is more stable than the 1,2-cis (tilted)

configuration, which is consistent with previous works [27,28,38]. A new di-σ chemisorbed

product 1,2-trans is also studied, but the positive adsorption energy of this configuration

eliminates its existence. We also found that the multi-configurational character of the

benzene adsorption configurations mainly comes from the spectator silicon dimers, and is

not very important to the adsorption energy calculations and the dynamical correlation is

very important for the calculations of the studied benzene adsorption configurations.

Thus, the multi configurational method (CASSCF) that only recovers the static

correlations is not appropriate and the DFT method has shown better results. Once the

chemisorbed [4+2] butterfly configuration is formed, it will stay intact and no

dissociation process is expected. However, the 1,2-cis (tilted) configuration can go

through hydrogen cleavage process and form more stable dissociative adsorption

products. It is found that spin crossing process has to be involved during the hydrogen

cleavage reaction. Between the two possible products from the dissociation reaction of

the 1,2-cis configuration, the dissociative double adsorption product (1,2-cis-double) is

more stable than the dissociative single adsorption product (1,2-cis-single),

thermodynamically. But the kinetics for the single dissociation route is much faster than

the double dissociation route at low temperature. Thus the single dissociation route is

expected to be the major reaction pathway. On the other hand, it is found that the single

dissociation route will not likely go to completion due to the extreme difficulty of

hydrogen migration process. As a result, the metastable triplet 1,2-cis-Inter1 product will

be formed and is the major product of the benzene dissociation reaction. When the

environment temperature is raised over 1730 K, the reaction will become

thermodynamically controlled and the dissociative double adsorption product will turn to

be the major product instead. However, this high temperature is is not usually seen in normal surface adsorption experiment, so the metastable triplet 1,2-cis-Inter1 configuration is expected to the major product under normal conditions. In general, much higher activation barriers than the previous research are predicted for the hydrogen cleavage from benzene molecule, which explains the lack of experimental observation of the dissociative adsorption configurations of benzene molecule on the Si(100) surface.

CHAPTER V

Adsorption Models of the Phenanthrene Molecule on the Si(100) Surface

A. INTRODUCTION

After the investigation of the surface adsorption and dissociation models of the

benzene molecule, we have moved on to look through those larger aromatic molecules

adsorbing on the same Si(100) surface. Several researches of polycyclic benenoid

aromatic hydrocarbon molecules, pentacene [108-110,113-115], for example, have been reported

before. Phenanthrene ($C_{14}H_{10}$) is a wide used chemical in color dying and pharmaceutical

industries. It is as important as the many other compounds in the benzenoid aromatic

family. To our best knowledge, there hasn't been any theoretical studies of the adsorption

or dissociation of phenanthrene molecule on the Si(100) surface yet. Thus, we decide to

explore the surface chemistry of phenanthrene molecule with the silicon dimer cluster

models.

The adsorption configurations of the phenanthrene molecule on the Si(100) surface are

expected to be close to those of benzene molecules. In Chapter IV, we have seen that

there are di-σ and tetra-σ, two important intact chemisorbed configuration families of

benzene on Si(100) surface. For the larger phenanthrene molecule, configurations that

contain more than four C-Si σ bonds (tetra-σ) are possible. Researchers have seen intact

chemisorbed configurations with as many as eight C-Si σ bonds (Octa-σ) across four

silicon dimers for the pentacene molecule on the Si(100) surface [109,115]. So the

investigation of all the possible adsorption configurations of phenanthrene molecule on

the Si(100) surface should require relative large silicon dimer cluster models that are able

to handle the multi C-Si σ bonding structures. However, due to limit of computer

resource, we are not able to perform calculations on silicon cluster models that have more

than three dimers upon the time when this work is done. Also, in the Chapter IV, we have

seen that the dissociation process for benzene molecule is only accessible to the di-σ

chemisorbed configurations. So we focus our study on the di-σ chemisorbed

phenanthrene molecule and its dissociative derivatives that are located within a single

silicon dimer only.

B. COMPUTATIONAL DETAILS

The Si_9H_{12} single dimer cluster models is used to reproduce the Si(100) surface for

most of our calculations. V-trench ($Si_{23}H_{24}$) and triple ($Si_{21}H_{20}$) dimer cluster models are

also used to calculate the adsorption energies for several configurations, in order to

compare with the results from the single dimer cluster models. The geometry of all the

cluster models and the adsorption and dissociation configurations are fully optimized

with no constrains applied. Energy calculations, geometry optimization and frequency

calculations are performed using the hybrid density functional method that includes

Becke's 3-parameter nonlocal-exchange functional[71] with the correlation functional of

Lee-Yang-Parr, B3LYP.[72] The 6-31G(d) all-electron split-valence basis set,[73] which

includes the polarization *d*-function on non-hydrogen atoms, was employed for

calculations. The Gaussian 03[74] software package is utilized to perform the geometry

optimization and frequency calculations. The reported adsorption energy is defined as the

difference between the total electronic energy of the adsorption model and the isolated

molecule and cluster. All energies are reported without zero-point corrections. Frequency

calculations have confirmed that all the stable geometries have no imaginary normal

mode.

C. RESULTS AND DISCUSSION

C.1. di-σ Intact Chemisorbed Configurations

The phenanthrene molecular (Figure 1) is analogous to three benzene molecules fused

together in a non-linear fashion. The di-σ intact chemisorbed configuration requires two

carbon atoms to bond with the Si dimer atoms, there are in principle thirty nine different

possible combinations for the di-σ intact chemisorbed product. We have studied all the

thirty nine possibilities and found that several of them will interchange to the other

adsorption configurations during the geometry optimization procedure. After rule out

those duplicate configurations, we have found there are eighteen different adsorption

models can be successfully optimized with using the Si_9H_{12} single dimer cluster model.

The adsorption energies of the eighteen obtained adsorption models are listed in Table 1,

ranked by adsorption energy from high to low. Table 1 shows that there are eleven

configurations have positive adsorption energies, among the eighteen obtained adsorption
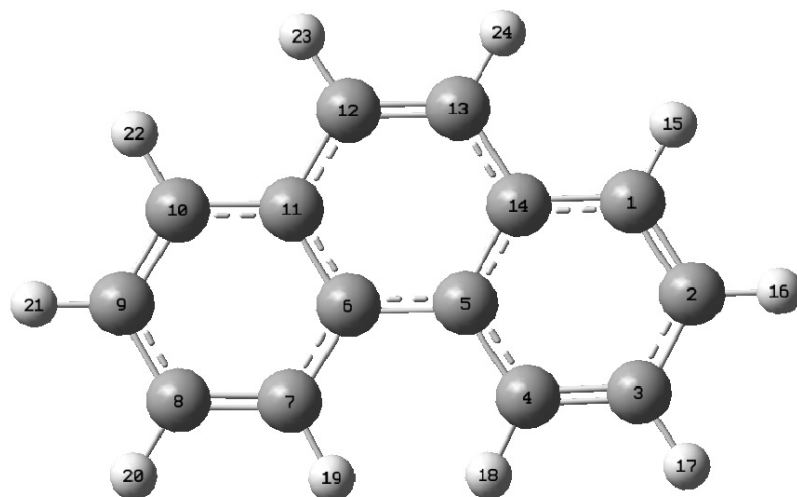
Figure V-1. Phenanthrene molecule and the orders assigned to the position of each carbon atoms. In this chapter, all the numbers that are used to specify the adsorption configuration orders correspond to the positions of the carbon atoms shown here.

Models	1,4	12,13	3,4	1,2	2,5	5,12	3,14
ΔE	-120.9	-75.2	-51.6	-47.4	-37.6	-37.0	-28.5

Continue:

Models	2,3	1,12	3,12	4,5	1,14	4,13	5,14	11,14	13,14	2,12	5,6
ΔE	11.7	15.7	18.5	36.7	43	79.2	81.9	84.9	121.1	154.7	172.5

Table V-1. Calculated B3LYP/6-31G(d) adsorption energies (kJ/mol) for the eighteen different models of the di-σ intact chemisorbed phenanthrene molecules on the Si(100) surface. The Si_9H_{12} single dimer cluster model is used to perform the calculation. Geometries are fully optimized and frequency analysis shows no imaginary normal mode for all the configurations.

models. As a result, these configurations are expected to be non-existing, and only the seven remaining di-σ intact chemisorbed configurations are thermodynamically favorable in theory. The pictures of these seven models are shown in Figure 2. We will focus on these seven thermodynamically favorable chemisorbed configurations in the following discussions.

Very similar to the chemisorbed configurations of benzene molecule on the Si(100) surface, the di-σ adsorption structures for the chemisorbed configuration of phenanthrene molecule on the Si(100) surface can be separated into two types. The 1,4-di-σ, 2,5-di-σ, 5.12-di-σ and 3,14-di-σ chemisorbed phenanthrene configurations are analogous to the [4+2] butterfly chemisorbed configuration for benzene molecule on the Si(100) surface. While the 12,13-di-σ, 3,4-di-σ and 1,2-di-σ chemisorbed phenanthrene configurations are analogous to the [2+2] 1,2-cis (tilted) chemisorbed configuration for benzene molecule on the Si(100) surface.

Comparing to the adsorption energy of the [4+2] butterfly chemisorbed benzene molecule for on the same Si_9H_{12} single dimer cluster (-90.0 kJ/mol), the four analogous configurations from phenanthrene have adsorption energies that scatter either higher or lower than that of benzene molecule. The most stable 1,4-di-σ configuration, has approximately 30 kJ/mol more adsorption energy (-120.9 kJ/mol), while the 2,5-di-σ (-37.6 kJ/mol), 5.12-di-σ (-37.0 kJ/mol) and 3,14-di-σ (-28.5 kJ/mol) configurations have approximately 50-60 kJ/mol less adsorption energies than the [4+2] butterfly chemisorbed benzene molecule. The higher adsorption energy of the 1,4-di-σ
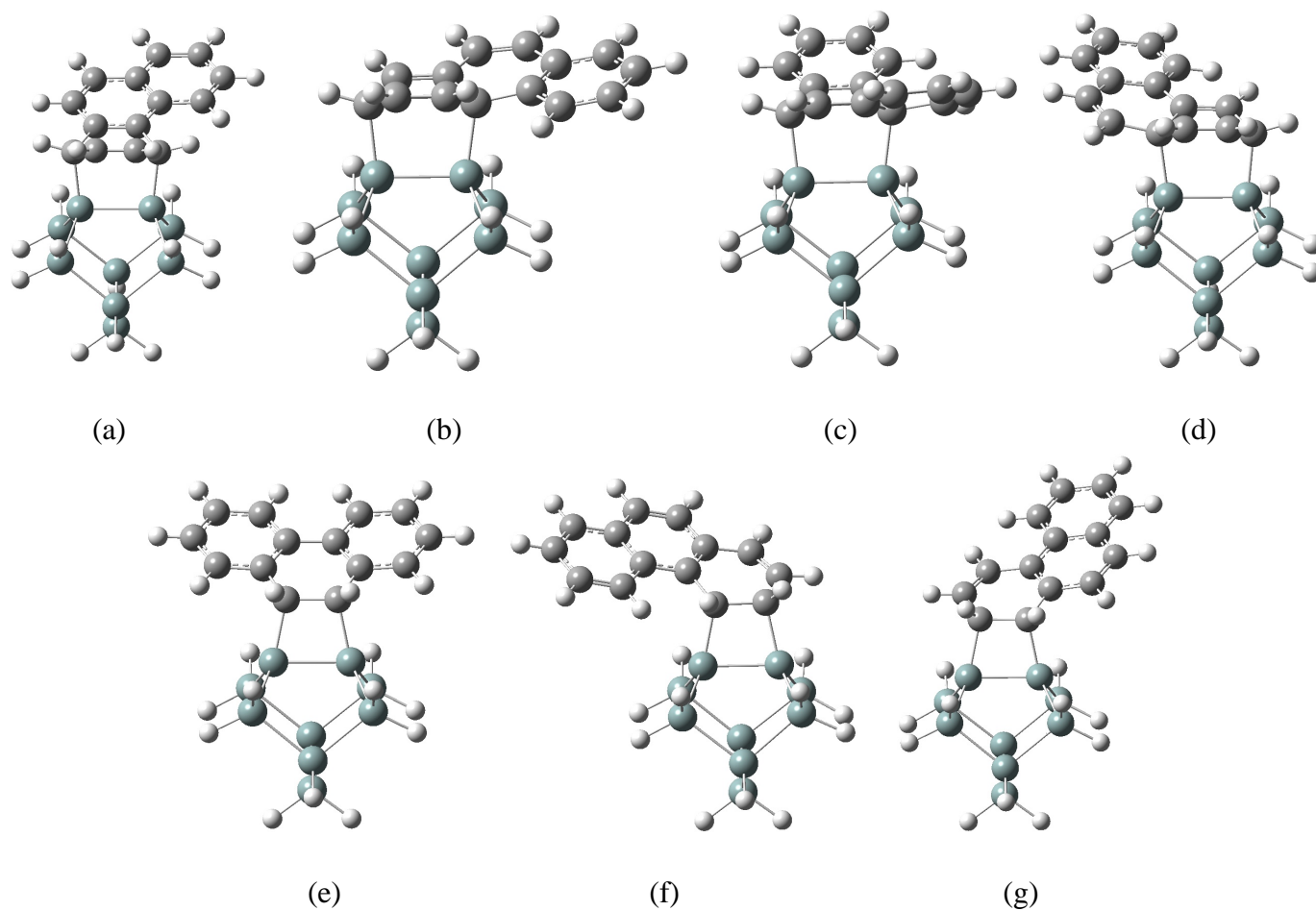
Figure V-2. Pictures of the seven configurations of di-σ intact chemisorbed phenanthrene molecules on the Si(100) surface that have negative adsorption energies: (a) 1,4-di-σ, (b) 2,5-di-σ, (c) 5,12-di-σ, (d) 3,14-di-σ, (e) 12,13-di-σ, (f) 3,4-di-σ and (g) 1,2-di-σ.

configuration comparing to the [4+2] butterfly chemisorbed benzene configuration is most likely because of the three unsaturated hexagonal rings can provide more stable resonance structures comparing to a single unsaturated hexagonal ring. The adsorption energy difference among the four chemisorbed phenanthrene configurations can be explained by the fact that, in the 1,4-di-σ configuration, the two sp^3 hybridized carbon atoms that bond to the dimer silicon atoms are connected to two other carbon atoms that are both located within the same hexagonal ring. Thus the distortion force on the phenanthrene molecule plane caused by the rehybridized carbon atoms is limited within a single hexagonal ring, while the remaining two rings are almost not affected and keep near perfect planar geometry. However, for the 2,5-di-σ, 5,12-di-σ or 3,14-di-σ configurations, one of the two sp^3 hybridized carbon atoms that bond to the dimer silicon atoms is shared by two hexagonal rings. As a result, the distortion force to the phenanthrene molecule plane caused by the rehybridized carbon atoms is spread out to two hexagonal rings, and causes a much less stable configuration. We can see that the type of the carbon atoms to which the dimer silicon atoms are connected, is very important in determining the system energy. In the 5,14-di-σ configuration, both of the sp^3 rehybridized carbon atoms are shared by two hexagonal rings, the distortion force from the two carbon atoms is so strong that the adsorption energy decreases by approximately 200 kJ/mol comparing to the 1,4-di-σ configuration, and this configuration ends up with a positive adsorption energy.

For the three [2+2] cycloaddition analogy adsorption configurations, we have found higher adsorption energies for all of them, comparing to the [2+2] 1,2-cis (tilted)

chemisorbed benzene molecule. The extra stability in the phenanthrene adsorption models most likely comes from the resonance effect from the two extra unsaturated hexagonal rings also. Similar to the [4+2] cycloaddition analogies, we have also noticed the selectivity on the carbon atoms to which the dimer silicon atoms are connected. The 12,13-di-σ, 3,4-di-σ and 1,2-di-σthree stable adsorption structures all have the sp^3 rehybridized carbon atoms located within the same hexagonal ring. Whereas configurations like 4,5-di-σ, 1,14-di-σ and etc. have at least one of the rehybridized carbon atoms shared by two rings, and result with much smaller adsorption energy. Very interestingly, the 2,3-di-σ adsorption configuration, with both sp^3 rehybridized carbon atoms located within the same hexagonal ring, has an unfavorable positive adsorption energy. We can address this result by examining the configuration of the phenanthrene molecule. As we can see in the Figure 1, the hexagonal ring on the right side of the phenanthrene molecule is connected to the other two rings through the carbon 5 and 14. The bond between the carbon 1 and 2, as well as the bond between the carbon 3 and 4 are located at the meta-position relative to the bond between carbon 5 and 14, whereas the bond between the carbon 2 and 3 are at the para-posotion. When the adsorption takes place through the 1,2-di-σ or 3,4-di-σ fashion, the resulted structure will have similar resonance configurations. However, if the adsorption takes place through the 2,3-di-σ fashion, a different type of resonance configuration is formed, and this resonance configuration is not as stable as the formal one. Thus the 2,3-di-σ configuration has a relatively smaller adsorption energy than the 1,2-di-σ and 3,4-di-σ configurations.

C.2. Dissociative Single Adsorption Configurations

We have seen in Chapter IV that the dissociative single adsorption configuration of

benzene molecule is easier to access under normal experimental conditions (see Section

C.5 of Chapter IV), thus we are interested in knowing the energy profile of the

dissociative single adsorption configuration of phenanthrene molecule. There are in

principle 5 different configurations of the dissociative single adsorption configuration for

the phenanthrene molecule, corresponding to the five different hydrogen atoms in the

phenanthrene molecule (see Figure 3). One thing we have to mention is that for every

adsorption configuration, there exist two different conformational isomers. They are

equivalent of each other by rotation along the C-Si bond by 180° (see Figure 4). We have

found that the adsorption energies for the conformational isomers that have the

phenanthrene molecule closer to the hydrogen atom on the silicon dimer have slightly

higher adsorption energy ($< 2\%$) than the other ones. This is probably due to the

repulsion force between the phenanthrene molecule and the hydrogen atom on the silicon

dimer is stronger when they are closer to each other. We disregarded the results from the

higher energy isomers and have only listed the adsorption energy for the lower energy

ones of each adsorption configuration. Comparing to the adsorption energy of the bezene

molecule on the same Si_9H_{12} single dimer cluster model (-187.1 kJ/mol), the adsorption

energy of the five phenanthrene adsorption isomers are either almost the same, or lower.

Generally, adsorption configurations that have the phenanthrene molecule further away

for the hydrogen atom at the silicon dimer have higher adsorption energies. The 2-mono-

σ configuration has the phenanthrene molecule lined furthest away from the hydrogen

atom at the silicon dimer, its geometry is almost the same as the one of benzene, and its

Models	2	3	13	1	4
Single Dimer	-187.1	-186.7	-179.2	-177.1	-145.2
V-trench Dimer	-188.2	-187.7	-178.0	-165.4	-141.4
Triplet Dimer	-180.8	-180.3	-172.9	-170.5	-137.5

Table V-2. Calculated B3LYP/6-31G(d) adsorption energies (kJ/mol) for the five different mono-σ dissociative single adsorption configurations of the phenanthrene molecule on the Si(100) surface. The Si_9H_{12} single dimer cluster model, $Si_{23}H_{24}$ V-trench and $Si_{21}H_{20}$ triplet dimer cluster models are used to perform the calculation. Geometries are fully optimized and frequency analysis shows no imaginary normal mode for all the configurations.
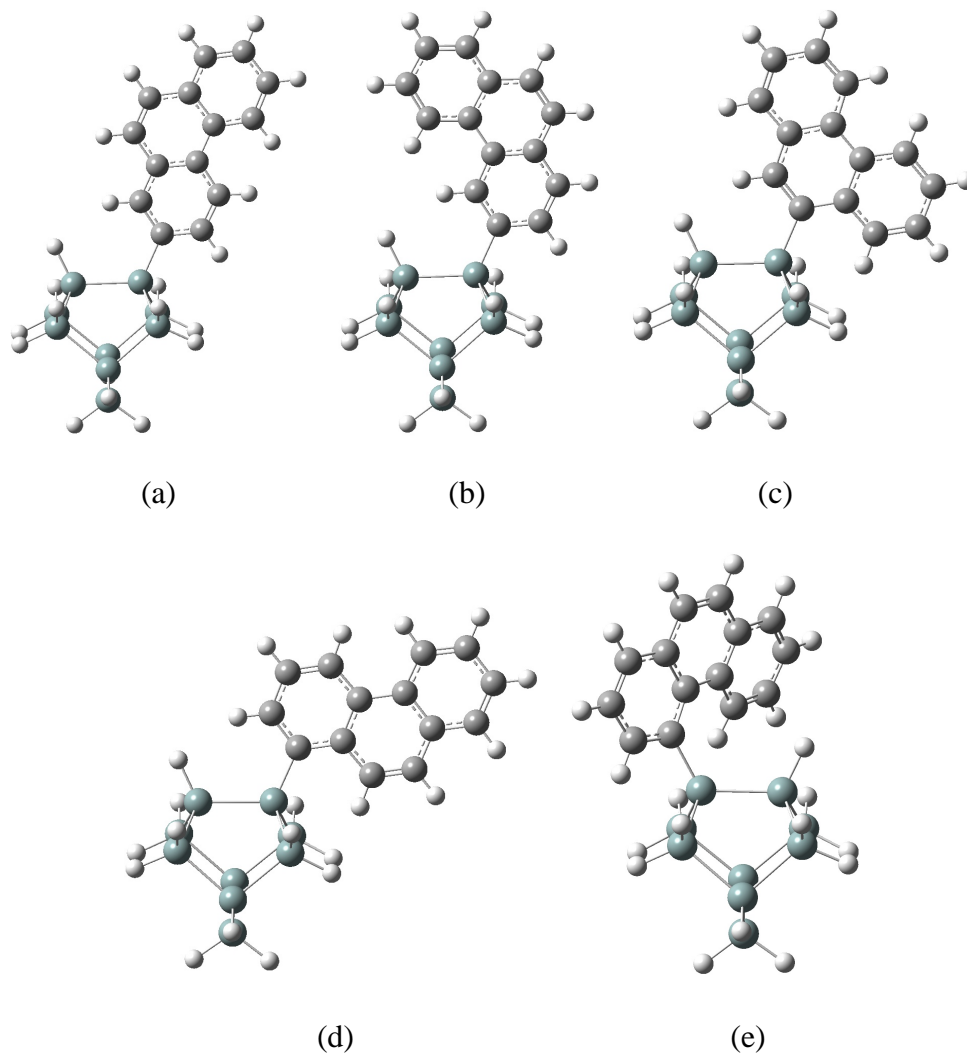
Figure V-3. Pictures of the five different mono-σ dissociative single adsorption configurations of the phenanthrene molecule on the Si(100) surface: (a) 2-mono-σ, (b) 3-mono-σ, (c) 13-mono-σ, (d) 1-mono-σ and (e) 4-mono-σ.
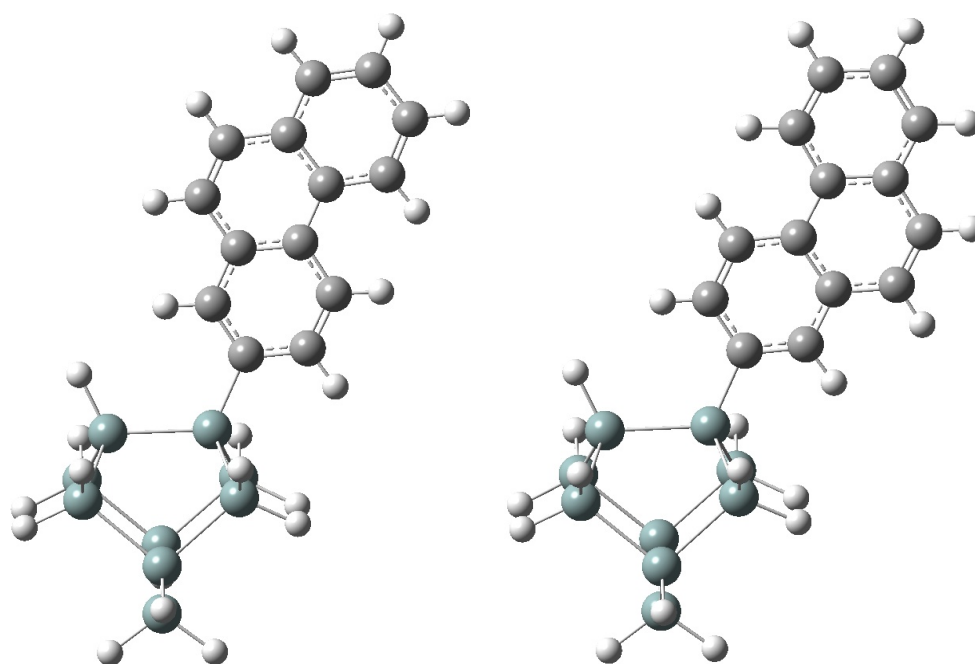
Figure V-4. Pictures of the two conformational isomers of the 2-mono-σ adsorption configuration.

adsorption energy is almost identical to the one of benzene too. Whereas the 4-mono-σ

configuration has the phenanthrene molecule closest to the hydrogen atom at the silicon

dimer, the repulsion force between them is so strong that it even caused noticeable

distortion to the planar geometry of the phenanthrene molecule. Thus the 4-mono-σ

configuration is much less stable than the 2-mono-σ configuration, and has about 30%

less adsorption energy than the later one.

   We have also explored the cluster size effect of the adsorption energy for the

dissociative single adsorption configuration of phenanthrene molecule. V-trench ($Si_{23}H_{24}$)

and triple ($Si_{21}H_{20}$) dimer cluster models are used to recover the surface interaction

between silicon dimers that are in different rows or in the same row, respectively. Unlike

the strong cluster size effect we have seen in Chapter II for some ClCN adsorption or

dissociation configurations (see Section C.1. of Chapter II), the adsorption energy of the

dissociated phenanthrene molecule cannot gain enhancement when larger cluster models

are used. This is due to the fact that the dissociated phenanthrene adsorption models have

normal C-Si covalent bond between the phenanthrene molecule and the dimer silicon

atoms. Unlike the dative bond we have seen in some ClCN adsorption and dissociation

structures, the normal C-Si covalent bond here for the phenanthrene molecule does not

have much electron density that needs to be dispersed by extended cluster surface dimers.

Thus, the larger cluster models cannot provide extra stabilization effect to the dissociative

single adsorption configuration of phenanthrene molecule. In fact, the repulsion force

from the neighbor dimers may actually increase the energy of the adsorption

configuration, which can cause smaller adsorption energies for the larger cluster models.

This explains that in a few occasions, when larger cluster models are used, the adsorption energy for the dissociative single adsorption configuration of phenanthrene molecule decrease by a small amount.

D. Conclusions

We have investigated the adsorption energy of the di-σ intact chemisorbed and mono-σ dissociative single adsorption configurations of the phenanthrene molecule adsorbing on the Si(100) surface. By using the silicon dimer cluster models, the DFT calculations have shown that the possible di-σ intact chemisorbed phenanthrene can be separated into [4+2] cycloaddtion and [2+2] cycloaddtion two different families, which is very similar to that of the benzene adsorption configurations on the same Si(100) surface. It is found that the adsorption energy is selective to the type of the carbon atoms to which the dimer silicon atoms are connected. The adsorption energy is at maximum when the two rehyridized carbons are located within the same hexagonal ring. When one or more of these rehyridized carbon atoms are shared by the other rings, the adsorption energy is much smaller due to the enhanced distortion effect from the rehyridized carbon atoms. The 1,4-di-σ and the 12,13-di-σ configurations are the most stable [4+2] cycloaddtion and [2+2] cycloaddtion products, respectively. Their adsorption energies are found to be larger than then benzene analogies, possibly duo to the resonance stabilization effect from the two extra unsaturated hexagonal rings. We have also noticed that the phenanthrene [2+2] cycloaddtion adsorption has a selection rule that's analogues to a meta-directed benzene molecule, 1,2-di-σ and 3,4-di-σ configurations are energetically favorable, while the 2,3-

di-σ configuration has positive adsorption energy. This selection rule is possibly due to the stability difference among the different resultant resonance structures.

For the mono-σ dissociative single adsorption configurations, we found that the phenanthrene adsorption models are less stable than that of benzene molecule, due to the larger repulsion force between the phenanthrene molecule and the hydrogen atom that locates on the silicon dimer surface. The cluser size dependence is found to be very small for the phenanthrene mono-σ dissociative single adsorption configurations, which is consistence with that the C-Si bonds for these configurations are normal covalent bonds instead of dative bonds.

CHAPTER VI

Quantum Capping Potential for Silicon Cluster Models

A. INTRODUCTION

In the previous chapters, we have shown the usage of hydrogen capped silicon cluster models to model chemistry reactions on Si(100) surface. Even though the hydrogen capped silicon cluster models are widely used, there are limitations on this method still. One biggest drawback is that the hydrogen capping atoms are artificial and will introduce unreal change the electronic environment of the surface cluster models. As a result, large cluster models are often needed to minimize the unphysical effect from the added hydrogen link atoms, which will cost a lot of computer time. In order to overcome the drawbacks of using hydrogen capping clusters, researchers have investigated several other approaches, such as surface slab models [23]. However, due to the expensive cost of computer time, the usage of slab models is very limited. Typically, only the low cost Hartree-Fock and density functional methods are applicable in slab model computation. Thus, the cluster models are still the center of interest for many research groups. In this chapter, we will discuss the alternative approaches to build cluster models that could result in better performance than the hydrogen capping method.

We start our discussion with a brief review of the development of cluster model. Despite the outstanding accuracy and wide usage of modern quantum chemistry theory in theoretical computations, its application is limited to small system models only due to the expensive cost of computer time. However, many areas of chemistry research nowadays require the treatment of large scale systems. For instance, the biochemistry reaction involving large protein molecules or the modeling of surface chemistry reactions often requires thousands of atoms. Pure quantum mechanical treatment of these systems is extremely difficult even at the modern super computers. Thus, researchers have developed a hybrid treatment of the large scale chemistry system by splitting it into a small quantum mechanical (QM) modeled region which is active during the interested chemistry reaction, and a lager molecular mechanical (MM) modeled region which remains almost unchanged during the chemistry reaction. The MM modeled region can be treated with very cheap computer time cost and yields an average electrical potential field that applies to the QM region. The biggest challenge of applying this method lies at the treatment of the boundary covalent bond between the QM and MM regions. The unsaturated electrons on the QM region can cause unphysical bonding. Two strategies have been used to solve this problem. The first method, namely the 'link atom' approach [124] [125] [126], uses single valence capping atoms like hydrogen atoms to terminate the unpaired electrons. The second formalism applies local self consistent field (LSCF) [127] [128] [129] [130] to the boundary atom. Link atom approach is easy to use with quantum chemistry software packages. Procedures like integrated molecular orbital molecular mechanics (IMOMM) method [131] or surface IMOMM (SIMOMM) [132] have been successfully developed and widely used by many researchers. However, it is discovered that the link

121

atom can change the electrical environment of the studied object, as we mentioned at the beginning of this introduction. On the other hand, the LSCF formalism does not require the artificial addition of link atoms and has shown good results in minimizing the energy of protein reaction pathways [127] [128] [129] [130]. To solve the issue that LSCF requires reparametrize when applied to new systems, another analogous approach, namely the generalized hybrid orbital (GHO) method, has been developed too [133]. Unlike the capping atom approach, the LSCF method requires extra programming and is harder to handle for researchers; care must be taken in order to obtain suitable LSCF parameters. When the charge of the frontier atom is large, big errors in energy calculations will occur [134]. Also, LSCF method is very sensitive to the size of the QM region, it is shown when small size of QM region is used, link atom approach is actually more preferred than the LSCF method[134].

Recently, several research groups have investigated the application of using pseudoatoms instead of hydrogen as the link atoms [135,136]. With effective core potential (ECP) parameters optimized to reproduce the truncated covalent bond, these pseduoatoms have shown great improvement over hydrogen atoms on recovering the chemistry environment of the studied object [135,136]. A study of applying silicon quantum capping potentials (QCP) has attracted our attention as this approach has shown promising results on recovering the chemistry properties of ideal extended surface using small cluster models to minimize the computer time cost [137]. We decided to test this approach, verify the suitability of this method, and apply this method to our silicon dimer cluster system.
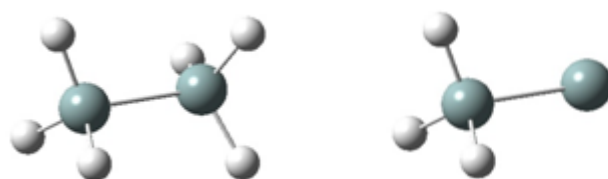
Figure VI-1. The molecule shape of disilane and the corresponding QCP model.

The development of silicon QCP starts with the H_3Si-SiH_3 disilane molecule. With keeping one SiH_3 moiety unchanged, a silicon atom with psudopotenials and valence basis sets of Ingel-Mann, Stoll and Preuss [138] were used to replace the other SiH_3 moiety (Figure 1). Then one shielding and three Pauli potentials were used to cap the empty valence at the 'pseudo silicon atom'. The exponents and coefficients of the applied potentials were optimized to reproduce the Si-Si bond length, H-Si-H bond angle and the Mulliken charge of the original disilane molecule. With applying 6-31G(d) basis set on the normal silicon and hydrogen atoms and using Gaussians to expand the potential of the form:

$$U(r) = r^{-2} \sum_i C_i r^{n_i} e^{-\xi_i r^2} \quad (1)$$

DiLabio and et al. have obtained the optimized Gaussian exponents and coefficients for a one electron QCP of the silicon atom (Table1). It has been shown QCPs are transferable and independent of the ECP type that is used to represent the core electrons [139], thus these optimized parameters can be applied to other silicon models including the silicon surface dimer models. Our exploration of the QCP method on the Si dimer models adapts the parameters from DiLabio's paper [137].

B. COMPUTATIONAL DETAILS

We limit our QCP calculation to small cluster models as the cluster property of small models are expected to improve the most from this approach. Bare single dimer cluster model Si_9H_{12} and the model with the surface dimer silicon atoms terminated by two hydrogen atoms (Si_9H_{14}) were constructed as the basis, QCP derivatives of these two

n_i	C_i	ξ_i
1	0.539	-2.97
2	0.448	188.0
2	0.437	-376.0
2	0.126	188.0

Table VI-1. Optimized Gaussian exponents and coefficients for a one electron QCP of

the silicon atom, table adapted from reference [137].

models are then built after them (Figure2).

Bigger cluster models including double dimer cluster ($Si_{15}H_{16}$) and triplet dimer cluster ($Si_{21}H_{20}$) models with both bare surface and hydrogen terminated surface were also constructed in order to compare with the results obtained from corresponding QCP calculations. To test the actual performance of the QCP cluster model on the surface chemistry reaction, we performed calculations of the single adsorption models of phenanthrene and the ClCN adsorption/dissociation models on the Si_9H_{12} cluster as well as the corresponding QCP derivatives. The B3LYP method [71,72] from Gaussian 03 software package [74] is used to perform all the calculations. Standard 6-31G(d) basis set [73] is applied to all the normal atoms. For the pseudo-silicon atoms that are used to perform quantum capping, the same basis set and identical parameters as those from DiLabio's paper [137] are used. All calculations include the full geometry optimization with no constrains. The validity of the resulted structures is verified by frequency calculation, every stationary structure is confirmed to contain no imaginary normal mode and every transition state structure is confirmed to have only one imaginary normal mode.

C. RESULTS AND DISCUSSION

We have listed our results for the electron affinity and HOMO-LUMO energy gap of both the bare and hydrogen terminated silicon cluster models in Table 2. When the surface dimer silicon atoms are terminated by hydrogen atoms, QCP method has shown very promising results on reproducing the electrical property of the large cluster models, while

using only a small single cluster model. When we increase the cluster size from single

dimer to triple dimers, the electron affinity of the hydrogen capped cluster model

increases from -0.433 eV to 0.830 eV (~291.7%) and the HOMO-LUMO gap increases

by 1.483 eV (~24.5%) during the same time. For the QCP models, the electron affinity is

quite close to that of the large cluster models for a single dimer cluster, and the electron

affinity only increase by 0.075 eV (~4.4%) when the cluster size grows from single dimer

to triple dimers. Also, the HOMO-LUMO gap shows no appreciable variation (<8.1%)

with the cluster size change. This observation is consistent with the result from DiLabio's

work [137] and our calculated EA and H-L gap for the single dimer cluster and double

dimer cluster are very close to those of DiLabio's.

The promising results of the QCP method on the hydrogen terminated cluster models

have shown a good potential of this approach in the surface chemistry research. However,

when we check the results from the bare cluster models, we have found much less robust

conclusions. The electron affinity of QCP increased by approximately 0.692 eV when

increase the cluster size from single dimer to triplet dimers, this increment is not much

less that the 0.772 eV increase observed in the hydrogen capped models, and is much

bigger than the 0.075 eV increase found in the hydrogen terminated QCP models. Also,

the HOMO-LUMO gap decrement was even larger for the QCP method (0.304 eV) than

in the normal hydrogen terminated clusters (0.228 eV). This result calls into question

whether the QCP methods can actually improve the performance of small silicon cluster

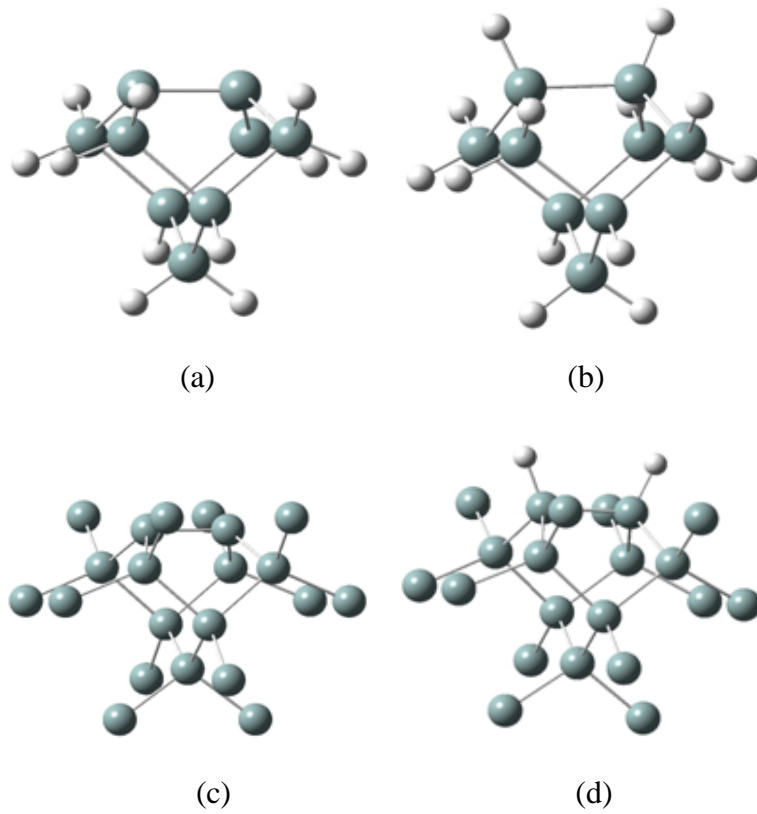models used for studying surface chemistry reactions.

Figure VI-2. Pictures of (a) Hydrogen-capped bare single cluster (b) Hydrogen-capped hydrogen terminated single cluster (c) QCP-capped bare single cluster (d) QCP-capped hydrogen terminated single cluster.

The result of applying QCP method to the single adsorption of phenanthrene on the

silicon single dimer cluster has confirmed our doubt (Table 3). The adsorption energies of

all the ten different adsorption configurations corresponding to the adsorption of

phenanthrene through the five different carbon atom positions are recomputed by QCP

approach, except for the adsorption configurations through the 1st carbon atom from the

phenanthrene molecule (see Section in Chapter V) due to the convergence problem. The

adsorption energy on the QCP models are 13-26% less than that of the hydrogen capped

models. Even though in Chapter V (see Section C.2 in Chapter V), we have found the

cluster size effect is not very significant on the phenanthrene single adsorption models,

and the adsorption energy may actually increase by a certain small amount ($< 6\%$)

possibly due to the dimer-dimer repulsion effect, the significantly reduced adsorption

energy for the QCP models casts doubt on the application of this methodology to Si

cluster systems.

To further verify the effect of applying QCP approach to the surface chemistry

reactions, we performed the calculation of the ClCN adsorption/dissociation energies

using QCP models. We have found that the similar adsorption energy reduces also after

applying the QCP method. As we have seen in Chapter II, the adsorption energies of

ClCN1 and TS1 structures have significant cluster size dependence, and will increase to a

higher value (more negative number) when larger cluster model is used due to the better

electron density delocalization effect on larger cluster models. Unfortunately, the

adsorption energy decreased by approximately 30% to 60%, when replacing hydrogen

capped cluster models with QCP ones. This observation has further confirmed our doubt

Model		EA(ev)	EA-Si^{QCP}(ev)	H-L gap(ev)	H-L gap-Si^{QCP}(ev)
Hydrogen Terminated	Single	-0.433	1.719	6.042	3.018
	Doubel	0.363	1.702	5.110	3.262
	Triple	0.830	1.794	4.559	3.177
Bare Surface	Single	1.731	1.804	2.294	2.145
	Doubel	2.285	2.365	2.125	1.879
	Triple	2.503	2.496	2.066	1.841

Table VI-2. Electron affinity (EA) and HOMO-LUMO gap (H-L gap) for the bare and hydrogen terminated, single cluster model, double cluster model and triple cluster model, with normal hydrogen atom capping and QCP capping methods.

about the applicability of QCP method to our surface chemistry studies.

In order to find out the reason for the failure of QCP method at the bare silicon cluster models, we have plotted the shape HOMO and the LUMO of the hydrogen capped and QCP capped bare silicon single dimer clusters (Figure 3). It is shown that the HOMO and LUMO for the QCP models are more compact than that of the hydrogen capped models. This could decrease the electron delocalization capability of the cluster and decrease the stability of the chemistry adsorption configurations. The plots of the HOMO of the ClCN adsorption configurations indicate that the electron density is more delocalized into the bottom silicon layers for the QCP models (Figure 4). However, the electron density of the covalent bond between the adsorbate and the substrate decreases and the stability of the adsorption configurations is weakened. Thus, the QCP models do not give better adsorption energies.

D. CONCLUSIONS

The QCP approach has been proposed as a cost efficient method on restoring the chemistry property of large bulk of silicon surface through using small clusters. It has shown promising results on the hydrogen terminated silicon cluster models. However, our calculation shows its application to the bare silicon cluster models, which are more commonly used in surface chemistry study, is problematic. The calculated electron affinity and HOMO-LUMO energy gap shows QCP approach has no significant improvement on recovering the properties of the bigger cluster models comparing to the

Order	H-Capping (kJ/mol)	Si^{QCP}-Capping (kJ/mol)	Adsorption Energy Differential
2	-187.1	-160.0	14.5%
3	-186.7	-161.0	13.7%
13	-179.2	-150.1	16.2%
4	-145.2	-107.6	25.9%
1	-177.1	N/A	N/A

Table VI-3. Calculated adsorption energy of the single dissociative adsorption of phenanthrene on the single silicon cluster model with normal hydrogen atom capping and QCP capping methods and the energy differential between the two methods.

Order	H-Capping (kJ/mol)	Si^{QCP}-Capping (kJ/mol)	Adsorption Energy Differential
SiCN1	-397.7	-383.5	3.6%
SiNC1	-365.0	-351.8	3.6%
ClCN2	-202.0	-193.4	4.3%
ClCN1	-44.4	-32.1	27.7%
TS1	-20.9	-8.6	59.1%

Table IV-4. Calculated adsorption energy of the ClCN adsorption configurations as well as the dissociation derivatives on the single silicon cluster model with normal hydrogen atom capping and QCP capping methods and the energy differential between the two different methods.
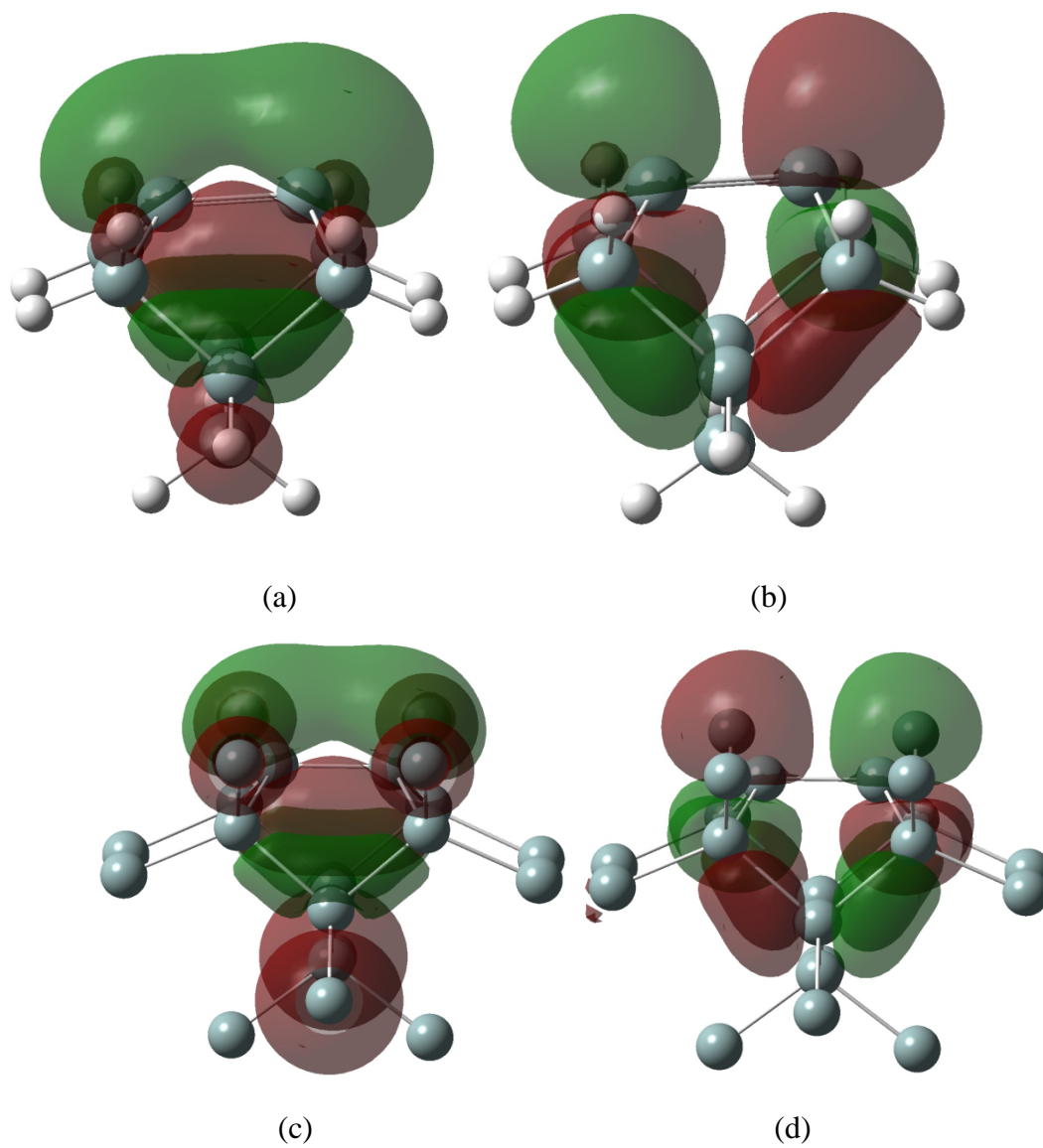
Figure VI-3. Pictures of (a) HOMO of the Hydrogen-capped bare single cluster (b) LUMO of the Hydrogen-capped bare single cluster (c) HOMO of the QCP-capped bare single cluster (d) LUMO of the QCP-capped bare single cluster
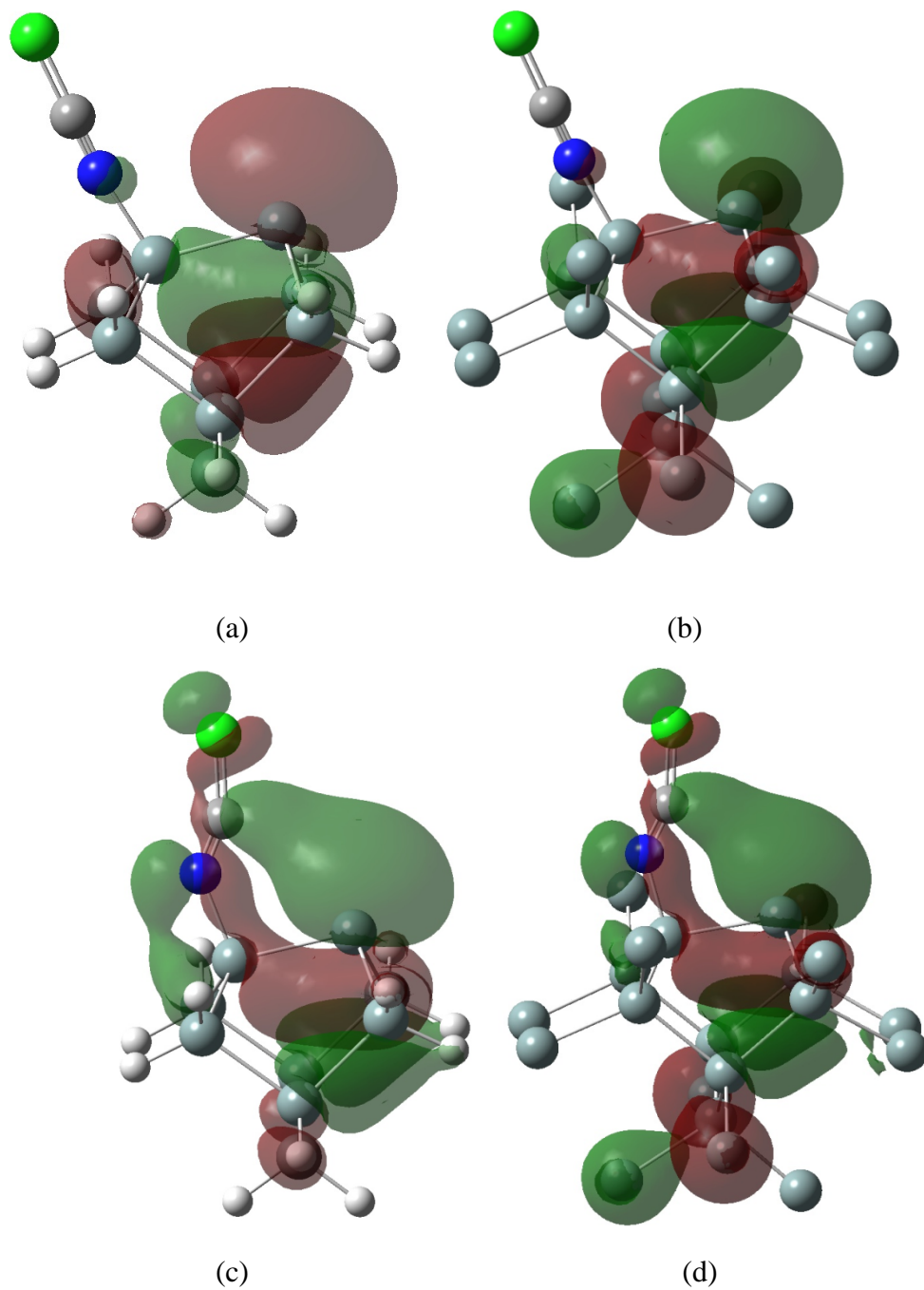
Figure IV-4. Pictures of (a) HOMO of the ClCN1 configuration in Hydrogen-capped single cluster (b) HOMO of the ClCN1 configuration in the QCP-capped single cluster (c) HOMO of the TS1configuration in Hydrogen-capped single cluster (d) HOMO of the TS1 configuration in the QCP-capped single cluster

conventional hydrogen capped models. Our calculation of the adsorption energy of the ClCN molecule and the phenanthrene molecules have also indicated that the QCP models have worse performance than the conventional hydrogen capped models. The analysis of the molecule orbital shape of the bare cluster models shows the electron density on the surface of the QCP models is more compact than that of the conventional hydrogen capped models. On the cluster models with molecule adsorbing on them, the electron density of the QCP models has become more delocalized. However, the QCP approach delocalizes the electron density into the bottom layer of the dimer cluster model instead of the neighbor dimers as that of the bigger cluster models. This unphysical redistribution of electron density has weakened the bond strength between the absorbate and the substrate and resulted with less favorable adsorption energies, which is in contradict with the behavior of the larger cluster models. Thus, we can conclude that the QCP approach brings in unphysical change to the electrical environment and gives worse results than the conventional hydrogen capped method.

REFERENCE

(1)   Moore, G. E. *Electronics* **1965**, *38*.

(2)   Wang, Y.; Shi, M.; Rabalais, J. W. *Phys Rev B* **1993**, *48*, 1678.

(3)   Weidenbruch, M. *in The Chemistry of Organic Silicon Compounds*, *Volume 3, Z. Rappoport, Y. Apeloig, Eds. (Wiley, Chichester, UK,* **2001***),* chap. 5.

(4)   Redondo, A.; Goddard, W. A. *Journal of Vacuum Science & Technology* **1982**, *21*, 344.

(5)   Jung, Y. S.; Akinaga, Y.; Jordan, K. D.; Gordon, M. S. *Theoretical Chemistry Accounts* **2003**, *109*, 268.

(6)   Shoemaker, J.; Burggraf, L. W.; Gordon, M. S. *J Chem Phys* **2000**, *112*, 2994.

(7)   Gordon, M. S.; Shoemaker, J. R.; Burggraf, L. W. *J Chem Phys* **2000**, *113*, 9355.

(8)   Jung, Y. S.; Shao, Y. H.; Gordon, M. S.; Doren, D. J.; Head-Gordon, M. *J Chem Phys* **2003**, *119*, 10917.

(9)   Bokes, P.; Stich, I.; Mitas, L. *Chem Phys Lett* **2002**, *362*, 559.

(10)   Paz, O.; da Silva, A. J. R.; Saenz, J. J.; Artacho, E. *Surf Sci* **2001**, *482*, 458.

(11)   Konecny, R.; Doren, D. J. *J Chem Phys* **1997**, *106*, 2426.

(12)   Yang, C.; Kang, H. C. *J Chem Phys* **1999**, *110*, 11029.

(13)   Penev, E.; Kratzer, P.; Scheffler, M. *J Chem Phys* **1999**, *110*, 3986.

(14)   Hess, J. S.; Doren, D. J. *J Chem Phys* **2000**, *113*, 9353.

(15)   Healy, S. B.; Filippi, C.; Kratzer, P.; Penev, E.; Scheffler, M. *Phys Rev Lett* **2001**,

8701.

(16)   Kondo, Y.; Amakusa, T.; Iwatsuki, M.; Tokumoto, H. *Surf Sci* **2000**, *453*, L318.

(17)   Yokoyama, T.; Takayanagi, K. *Phys Rev B* **2000**, *61*, R5078.

(18)   Le Lay, G.; Cricenti, A.; Ottaviani, C.; Perfetti, P.; Tanikawa, T.; Matsuda, I.; Hasegawa, S. *Phys Rev B* **2002**, *66*.

(19)   Hata, K.; Sainoo, Y.; Shigekawa, H. *Phys Rev Lett* **2001**, *86*, 3084.

(20)   Hata, K.; Yoshida, S.; Shigekawa, H. *Phys Rev Lett* **2002**, *89*.

(21)   Matsumoto, M.; Fukutani, K.; Okano, T. *Phys Rev Lett* **2003**, *90*.

(22)   Mitsui, T.; Takayanagi, K. *Phys Rev B* **2000**, *62*, R16251.

(23)   Steckel, J. A.; Phung, T.; Jordan, K. D.; Nachtigall, P. *J Phys Chem B* **2001**, *105*, 4031.

(24)   Perdew, J. P.; Chevary, J. A.; Vosko, S. H.; Jackson, K. A.; Pederson, M. R.; Singh, D. J.; Fiolhais, C. *Phys Rev B* **1992**, *46*, 6671.

(25)   Rajasekar, P.; Kadossov, E. B.; Materer, N. F. *Surf. Sci.* **2002**, *515*, 421.

(26)   Kadossov, E. B.; Rajasekar, P.; Materer, N. F. *Chem. Phys. Lett.* **2003**, *370*, 548.

(27)   Nunzi, F.; Sgamellotti, A.; Re, N. *J Phys Chem C* **2007**, *111*, 1392.

(28)   Jung, Y. S.; Gordon, M. S. *J Am Chem Soc* **2005**, *127*, 3131.

(29)   Shimomura, M.; Munakata, M.; Honma, K.; Widstrand, S. M.; Johansson, L.; Abukawa, T.; Kono, S. *Surf Rev Lett* **2003**, *10*, 499.

(30)   Lee, J. Y.; Cho, J. H. *Phys Rev B* **2005**, *72*.

(31)   Hofer, W. A.; Fisher, A. J.; Lopinski, G. P.; Wolkow, R. A. *Phys Rev B* **2001**, *6308*.

(32)   Nisbet, G.; Lamont, C. L. A.; Polcik, M.; Terborg, R.; Sayago, D. I.; Kittel, M.;

Hoeft, J. T.; Toomes, R. L.; Woodruff, D. P. *J Phys-Condens Mat* **2008**, *20*.

(33)   Zhou, X. J.; Leung, K. T. *Surf Sci* **2006**, *600*, 3285.

(34)   Fedor, Y., Naumkin; Polanyi, J. C.; Rogers, D. *Surf. Sci.* **2003**, *547*, 335.

(35)   Naumkin, F. Y.; Polanyi, J. C.; Rogers, D.; Hofer, W.; Fisher, A. *Surf Sci* **2003**, *547*, 324.

(36)   Zhou, X. J.; Leung, K. T. *J Phys Chem B* **2006**, *110*, 9601.

(37)   Taguchi, Y.; Fujisawa, M.; Takaoka, T.; Okada, T.; Nishijima, M. *J Chem Phys* **1991**, *95*, 6870.

(38)   Borovsky, B.; Krueger, M.; Ganz, E. *Phys Rev B* **1998**, *57*, R4269.

(39)   Witkowski, N.; Hennies, F.; Pietzsch, A.; Mattsson, S.; Fohlisch, A.; Wurth, W.; Nagasono, M.; Piancastelli, M. N. *Phys Rev B* **2003**, *68*.

(40)   Kim, Y. K.; Lee, M. H.; Yeom, H. W. *Phys Rev B* **2005**, *71*.

(41)   Lopinski, G. P.; Fortier, T. M.; Moffatt, D. J.; Wolkow, R. A. *J Vac Sci Technol A* **1998**, *16*, 1037.

(42)   Wolkow, R. A.; Lopinski, G. P.; Moffatt, D. J. *Surf Sci* **1998**, *416*, L1107.

(43)   Gokhale, S.; Trischberger, P.; Menzel, D.; Widdra, W.; Droge, H.; Steinruck, H. P.; Birkenheuer, U.; Gutdeutsch, U.; Rosch, N. *J Chem Phys* **1998**, *108*, 5554.

(44)   Gutdeutsch, U.; Birkenheuer, U.; Kruger, S.; Rosch, N. *J Chem Phys* **1997**, *106*, 6020.

(45)   Silvestrelli, P. L.; Ancilotto, F.; Toigo, F. *Phys Rev B* **2000**, *62*, 1596.

(46)   Bent, S. F. *Surf. Sci.* **2002**, *500*, 879.

(47)   Wolkow, R. A. *Annu. Rev. Phys. Chem.* **1999**, *50*, 413.

(48)   Yates, J., Jr. *Science* **1998**, *279*, 335.

(49)   Leftwich, T. R.; Teplyakov, A. V. *Surf. Sci. Rep.* **2008**, *63*, 1.(50)   Yoshinobu, J. *Prog. Surf. Sci.* **2004**, *77*, 37.

(51)   Cao, X.; Coulter, S. K.; Ellison, M. D.; Liu, H.; Liu, J.; Hamers, R. J. *J. Phys. Chem. B* **2001**, *105*, 3759.

(52)   Mui, C.; Filler, M. A.; Bent, S. F.; Musgrave, C. B. *J. Phys. Chem. B* **2003**, *107*, 12256.

(53)   Kadossov, E. B.; Rajasekar, P.; Materer, N. F. *J. Phys. Chem. B* **2004**, *108*, 303.

(54)   Mezhenny, S.; Lyubinetsky, I.; Choyke, W. J.; Wolkow, R. A.; Yates, J. T., Jr. *Chem. Phys. Lett.* **2001**, *344*, 7.

(55)   Teague, L. C.; Boland, J. J. *J. Phys. Chem. B* **2003**, *107*, 3820.

(56)   Hovis, J. S.; Liu, H.; Hamers, R. J. *J. Phys. Chem.* **1998**, *102*, 6873.

(57)   Hofer, W. A.; Fisher, A. J.; Bitzer, T.; Rada, T.; Richardson, N. V. *Chem. Phys. Lett.* **2002**, *355*, 347.

(58)   Lopinski, G. P.; Fortier, T. M.; Moffatt, D. J.; Wolkow, R. A. *J. Vac. Sci. Technol., A* **1998**, *16*, 1037.

(59)   Bacalzo-Gladden, F.; Lu, X.; Lin, M. C. *J. Phys. Chem. B* **2001**, *105*, 4368.

(60)   Bacalzo-Gladden, F.; Musaev, D. G.; Lin, M. C. *J. Chin. Chem. Soc. (Taipei)* **1999**, *46*, 395.

(61)   Bu, Y.; Ma, L.; Lin, M. C. *J. Phys. Chem.* **1993**, *97*, 7081.

(62)   Bu, Y.; Ma, L.; Lin, M. C. *J. Phys. Chem.* **1995**, *99*, 1046.

(63)   Qu, Y.-Q.; Wang, Y.; Li, J.; Han, K.-L. *Surf. Sci.* **2004**, *569*, 12.

(64)   Bu, Y.; Lin, M. C. *J. Phys. Chem.* **1994**, *98*, 7871.

(65)   Wang, J.-H.; Lin, M. C. *Surf. Sci.* **2005**, *579*, 197.

(66)   Romero, A. H.; Sbraccia, C.; Silvestrelli, P. L.; Ancilotto, F. *J. Chem. Phys.* **2003**, *119*, 1085.

(67)   Carreon-Macedo, J. L.; Harvey, J. N. *J Am Chem Soc* **2004**, *126*, 5789.

(68)   Carreon-Macedo, J.; Harvey, J. N.; Poli, R. *Eur J Inorg Chem* **2005**, 2999.

(69)   Cho, J.-H.; Kleinman, L. *J. Chem. Phys.* **2003**, *119*, 6744.

(70)   Cho, J.-H.; Kleinman, L. *J. Chem. Phys.* **2004**, *121*, 1557.

(71)   Becke, A. D. *J Chem Phys* **1993**, *98*, 5648.

(72)   Lee, C.; Yang, W.; Parr, R. G. *Phys. Rev.* **1988**, *B 37*, 785.

(73)   Francl, M. M.; Pietro, W. J.; Hehre, W. J.; Binkley, J. S.; Gordon, M. S.; Defrees, D. J.; Pople, J. A. *J Chem Phys* **1982**, *77*, 3654.

(74)   Frisch, M. J.; Trucks, G. W.; Schlegel, H. B.; Scuseria, G. E.; Robb, M. A.; Cheeseman, J. R.; Montgomery, J., J. A.; Vreven, T.; Kudin, K. N.; Burant, J. C.; Millam, J. M.; yengar, S. S.; Tomasi, J.; Barone, V.; Mennucci, B.; Cossi, M.; Scalmani, G.; Rega, N.; Petersson, G. A.; Nakatsuji, H.; Hada, M.; Ehara, M.; Toyota, K.; Fukuda, R.; Hasegawa, J.; Ishida, M.; Nakajima, T.; Honda, Y.; Kitao, O.; Nakai, H.; Klene, M.; Li, X.; Knox, J. E.; Hratchian, H. P.; Cross, J. B.; Bakken, V.; Adamo, C.; Jaramillo, J.; Gomperts, R.; Stratmann, R. E.; Yazyev, O.; Austin, A. J.; Cammi, R.; Pomelli, C.; Ochterski, J. W.; Ayala, P. Y.; Morokuma, K.; Voth, G. A.; Salvador, P.; Dannenberg, J. J.; Zakrzewski, V. G.; Dapprich, S.; Daniels, A. D.; Strain, M. C.; Farkas, O.; Malick, D. K.; Rabuck, A. D.; Raghavachari, K.; Foresman, J. B.; Ortiz, J. V.; Cui, Q.; Baboul, A. G.; Clifford, S.; Cioslowski, J.; Stefanov, B. B.; Liu, G.; Liashenko, A.; Piskorz, P.; Komaromi, I.; Martin, R. L.; Fox, D. J.; Keith, T.; Al-Laham, M. A.; Peng, C. Y.;

Nanayakkara, A.; Challacombe, M.; Gill, P. M. W.; Johnson, B.; Chen, W.; Wong, M. W.; Gonzalez, C.; Pople, J. A. *Gaussian 03, Revision C.02*; Gaussian Inc.: Wallingford CT, 2004.

(75)   Widjaja, Y.; Musgrave, C. B. *J. Chem. Phys.* **2004**, *120*, 1555.

(76)   Rodriguez-Reyes, J. C. F.; Teplyakov, A. V. *Phys. Rev. B: Condens. Matter* **2007**, *76*, 075348.

(77)   Rodriguez-Reyes, J. C. F.; Teplyakov, A. V. *Phys. Rev. B: Condens. Matter* **2008**, *78*, 165314.

(78)   Cho, J.-H.; Kleinman, L.; Chan, C. T.; Kim, K. S. *Phys. Rev. B: Condens. Matter* **2001**, *63*, 073306/1.

(79)   Di Felice, R.; Pignedoli, C. A.; Bertoni, C. M.; Catellani, A.; Silvestrelli, P. L.; Sbraccia, C.; Ancilotto, F.; Palummo, M.; Pulci, O. *Surf. Sci.* **2003**, *532-535*, 982.

(80)   Hofer, W. A.; Fisher, A. J.; Wolkow, R. A. *Surf. Sci.* **2001**, *475*, 83.

(81)   Silvestrelli, P. L.; Toigo, F.; Ancilotto, F. *J. Chem. Phys.* **2001**, *114*, 8539.

(82)   Dean, J. A. *Lange's Handbook of Chemistry*; 14 ed.; McGraw-Hill, 1992.

(83)   Hess, J. S.; Doren, D. J. *J Phys Chem B* **2002**, *106*, 8206.

(84)   Truhlar, D. G.; Garrett, B. C.; Klippenstein, S. J. *J Phys Chem-Us* **1996**, *100*, 12771.

(85)   Hellman, A. *Surf Sci* **2009**, *603*, 173.

(86)   Fan, X. L.; Zhang, Y. F.; Lau, W. M.; Liu, Z. F. *Phys Rev Lett* **2005**, *94*.

(87)   Kato, K.; Uda, T.; Terakura, K. *Phys Rev Lett* **1998**, *80*, 2000.

(88)   Harvey, J. N. *Physical Chemistry Chemical Physics* **2007**, *9*, 331.

(89)   Bernardi, F.; Olivucci, M.; Robb, M. A. *Chemical Society Reviews* **1996**, *25*, 321.

(90) Blancafort, L.; Jolibois, F.; Olivucci, M.; Robb, M. A. *J Am Chem Soc* **2001**, *123*, 722.

(91) Zener, C. *Proceedings of the Royal Society of London Series a-Containing Papers of a Mathematical and Physical Character* **1932**, *137*, 696.

(92) Landau, L. D. *Physikalische Zeitschrift Sowjetunion* **1932**, *2*, 46.

(93) Stueckelberg, E. C. G. *Helvetica Physica Acta* **1932**, *5*, 370.

(94) Desouterlecomte, M.; Lorquet, J. C. *J Chem Phys* **1979**, *71*, 4391.

(95) Lee, C. T.; Yang, W. T.; Parr, R. G. *Phys Rev B* **1988**, *37*, 785.

(96) Harvey, J. N.; Aschi, M.; Schwarz, H.; Koch, W. *Theoretical Chemistry Accounts* **1998**, *99*, 95.

(97) Bearpark, M. J.; Robb, M. A.; Schlegel, H. B. *Chem Phys Lett* **1994**, *223*, 269.

(98) Schmidt, M. W.; Baldridge, K. K.; Boatz, J. A.; Elbert, S. T.; Gordon, M. S.; Jensen, J. H.; Koseki, S.; Matsunaga, N.; Nguyen, K. A.; Su, S. J.; Windus, T. L.; Dupuis, M.; Montgomery, J. A. *J Comput Chem* **1993**, *14*, 1347.

(99) Bofill, J. M.; Pulay, P. *J Chem Phys* **1989**, *90*, 3637.

(100) Pulay, P.; Hamilton, T. P. *J Chem Phys* **1988**, *88*, 4926.

(101) Wolinski, K.; Pulay, P. *J Chem Phys* **1989**, *90*, 3647.

(102) Himpsel, F. J.; Fauster, T. *Journal of Vacuum Science & Technology a-Vacuum Surfaces and Films* **1984**, *2*, 815.

(103) Himpsel, F. J.; Eastman, D. E. *Journal of Vacuum Science & Technology* **1979**, *16*, 1297.

(104) Hamers, R. J.; Kohler, U. K. *Journal of Vacuum Science & Technology a-Vacuum Surfaces and Films* **1989**, *7*, 2854.

(105) Chabal, Y. J.; Christman, S. B.; Chaban, E. E.; Yin, M. T. *Journal of Vacuum Science & Technology a-Vacuum Surfaces and Films* **1983**, *1*, 1241.

(106) Monch, W.; Koke, P.; Krueger, S. *Journal of Vacuum Science & Technology* **1981**, *19*, 313.

(107) Lundberg, M.; Siegbahn, P. E. M. *Chem Phys Lett* **2005**, *401*, 347.

(108) Ruiz, R.; Mayer, A. C.; Malliaras, G. G.; Nickel, B.; Scoles, G.; Kazimirov, A.; Kim, H.; Headrick, R. L.; Islam, Z. *Appl Phys Lett* **2004**, *85*, 4926.

(109) Ruiz, R.; Choudhary, D.; Nickel, B.; Toccoli, T.; Chang, K. C.; Mayer, A. C.; Clancy, P.; Blakely, J. M.; Headrick, R. L.; Iannotta, S.; Malliaras, G. G. *Chem Mater* **2004**, *16*, 4497.

(110) Nickel, B.; Barabash, R.; Ruiz, R.; Koch, N.; Kahn, A.; Feldman, L. C.; Haglund, R. F.; Scoles, G. *Phys Rev B* **2004**, *70*.

(111) Li, Q.; Leung, K. T. *J Phys Chem B* **2005**, *109*, 1420.

(112) Yeo, W. C.; Tan, G. K.; Koh, L. L.; Leung, P. H. *Eur J Inorg Chem* **2005**, 4723.

(113) Hughes, G.; Roche, J.; Carty, D.; Cafolla, T.; Smith, K. E. *J Vac Sci Technol B* **2002**, *20*, 1620.

(114) Weidkamp, K. P.; Hacker, C. A.; Schwartz, M. P.; Cao, X. P.; Tromp, R. M.; Hamers, R. J. *J Phys Chem B* **2003**, *107*, 11142.

(115) Kasaya, M.; Tabata, H.; Kawai, T. *Surf Sci* **1998**, *406*, 302.

(116) Lopinski, G. P.; Moffatt, D. J.; Wolkow, R. A. *Chem Phys Lett* **1998**, *282*, 305.

(117) Ryan, P. M.; Teague, L. C.; Boland, J. J. *J Am Chem Soc* **2009**, *131*, 6768.

(118) Lopinski, G. P.; Moffatt, D. J.; Wayner, D. D. M.; Wolkow, R. A. *J Am Chem Soc* **2000**, *122*, 3548.

(119) Liu, H. B.; Hamers, R. J. *J Am Chem Soc* **1997**, *119*, 7593.

(120) Naumkin, F. Y.; Polanyi, J. C.; Rogers, D. *Surf Sci* **2003**, *547*, 335.

(121) Craig, B. I. *Surf Sci* **1993**, *280*, L279.

(122) Schmidt, M. W.; Gordon, M. S. *Annu Rev Phys Chem* **1998**, *49*, 233.

(123) Lu, X. *J Am Chem Soc* **2003**, *125*, 6384.

(124) Warshel, A.; Levitt, M. *J Mol Biol* **1976**, *103*, 227.

(125) Field, M. J.; Bash, P. A.; Karplus, M. *J Comput Chem* **1990**, *11*, 700.

(126) Eurenius, K. P.; Chatfield, D. C.; Brooks, B. R.; Hodoscek, M. *Int J Quantum Chem* **1996**, *60*, 1189.

(127) Thery, V.; Rinaldi, D.; Rivail, J. L.; Maigret, B.; Ferenczy, G. G. *J Comput Chem* **1994**, *15*, 269.

(128) Monard, G.; Loos, M.; Thery, V.; Baka, K.; Rivail, J. L. *Int J Quantum Chem* **1996**, *58*, 153.

(129) Gorb, L. G.; Rivail, J. L.; Thery, V.; Rinaldi, D. *Int J Quantum Chem* **1996**, *60*, 1525.

(130) Assfeld, X.; Rivail, J. L. *Chem Phys Lett* **1996**, *263*, 100.

(131) Maseras, F.; Morokuma, K. *J Comput Chem* **1995**, *16*, 1170.

(132) Shoemaker, J. R.; Burggraf, L. W.; Gordon, M. S. *J Phys Chem A* **1999**, *103*, 3245.

(133) Gao, J. L.; Amara, P.; Alhambra, C.; Field, M. J. *J Phys Chem A* **1998**, *102*, 4714.

(134) Reuter, N.; Dejaegere, A.; Maigret, B.; Karplus, M. *J Phys Chem A* **2000**, *104*, 1720.

(135) Zhang, Y. K.; Lee, T. S.; Yang, W. T. *J Chem Phys* **1999**, *110*, 46.

(136)   DiLabio, G. A.; Hurley, M. M.; Christiansen, P. A. *J Chem Phys* **2002**, *116*, 9578.

(137)   DiLabio, G. A.; Wolkow, R. A.; Johnson, E. R. *J Chem Phys* **2005**, *122*, 44708.

(138)   Igelmann, G.; Stoll, H.; Preuss, H. *Mol Phys* **1988**, *65*, 1321.

(139)   Moon, S.; Christiansen, P. A.; DiLabio, G. A. *J Chem Phys* **2004**, *120*, 9080.

VITA

Qing Zhu

Candidate for the Degree of

Doctor of Philosophy

Dissertation: THEORETICAL INVESTIGATION OF MOLECULE ADSORPTION
AND DISSOCIATION MECHANISMS ON THE SILICON SURFACE

Major Field: Chemistry

Biographical:

Date and place of birth:

September 02, 1985 in Huaian, China

Education:

Completed the requirements for the Bachelor of Science in Materials Science and Engineering at University of Science and Technology of China, Hefei, China in July, 2005.

Experience:

Employed as a teaching and research assistant in the Department of Chemistry at Oklahoma State University; Worked as a undergraduate research assistant in the Department of Materials Science and Engineering at University of Science and Technology of China